Probing the regulatory mechanisms of the actomyosin system in motile cells

Dissertation

zur Erlangung des akademischen Grades

"doctor rerum naturalium"

(Dr. rer. nat.)

in der Wissenschaftsdisziplin "Biologische Physik"

eingereicht an der

Mathematisch-Naturwissenschaftlichen Fakultät

der Universität Potsdam

von Eva Katharina Barbosa Pfannes

Potsdam, den 22.08.2011

Published online at the
Institutional Repository of the University of Potsdam:
URL http://opus.kobv.de/ubp/volltexte/2012/5781/
URN urn:nbn:de:kobv:517-opus-57812
http://nbn-resolving.de/urn:nbn:de:kobv:517-opus-57812

Table of contents

Summary 1

Zusammenfassung 3

1 Introduction

1.1 *Dictyostelium discoideum* biology 6

1.2 Signaling and chemotaxis in *Dictyostelium discoideum* 7

1.3 Cyclic AMP 9

1.4 The actin cytoskeleton 10

1.5 Actin interacting proteins 12

1.5.1 DdLimE 12

1.5.2 Arp2/3 complex 13

1.5.3 WASP (Wiskott–Aldrich syndrome protein) 14

1.6 Myosin II 18

1.7 cGMP signal transduction 21

1.8 Phospholipid signaling 25

1.9 Cytoskeleton-disrupting drugs 28

1.10 Cell mechanics and microfluidics 30

1.11 Caged compounds 31

The goal 33

2 Materials and Methods

2.1 Solutions and media 35

2.2 Other chemicals 36

2.3 Cell culture 37

2.4 Transformation and Electroporation 37

2.5 Cell lines 37

2.6 Microfluidics – Fluidic cell squeezer 38

2.7 Cell motility assays 41

2.8 Fluorescence microscopy and photouncaging 43

2.8.1 Confocal microscopy 43

2.8.2 Photouncaging 44

2.8.3 TIRFM – Total internal reflection fluorescence microscopy 47

2.9 PI and FDA assay – Cell vitality assay 47

2.10 Cell recovery (reversibility assay) 48

2.11 Total protein assay 49

2.12 F-actin quantification assay 50

2.13 Cell adhesion assay.....50

2.14 PH-$_{CRAC}$ translocation 51

2.15 Calculation of error 52

3 Results

3.1 Impact of drug induced WASP-inhibition on motile cells.....53

3.1.1 Wiskostatin treatment alters cell morphology and pseudopod formation 53

3.1.2 Wave formation and endocytosis are affected by Wiskostatin treatment 57

3.1.3 Wiskostatin treatment affects the mechanical stability of cells 60

3.1.4 Wiskostatin treatment does not affect the amount of F-actin in *D. discoideum* cells.....63

3.1.5 Substrate adhesion is increased by Wiskostatin treatment 65

3.1.6 Motility is reduced by Wiskostatin treatment 65

3.1.7 Chemotaxis is negatively affected by Wiskostatin treatment 67

3.2 Cytoskeletal dynamics in response to intracellular release of cGMP.....72

3.2.1 The influence of scattered light on photouncaging experiments 72

3.2.2 Caged cGMP experiments: actin and myosin responses in starvation developed cells 73

3.2.3 Caged cGMP experiments: actin and myosin responses in vegetative cells.....77

3.2.4 Micropipette aspiration controls.....80

3.3 The impact of Polyphosphoinositide-Binding Peptide (PBP10) on cell shape and dynamics 84

3.3.1 PBP10 suppresses pseudopod formation in *D. discoideum* cells.....84

3.3.2 Cells treated with PBP10 are still able to translocate PH domains to the membrane.....86

3.3.3 Cell-substrate adhesion is reduced by PBP10 89

3.3.4 Random cell motility is impaired by PBP10.....90

3.3.5 Chemotaxis is affected by PBP10.....93

4 Discussion

4.1 Wiskostatin treatment influences mechanical stability, adhesion, and dynamics of motile cells.....96

4.2 Intracellular cGMP induces myosin II association with the cytoskeleton and elicits an actin response 100

4.3 Polyphosphoinositide binding peptide (PBP10) affects cell shape and motility but does not suppress PIP_3 formation in response to chemoattractant stimuli 105

4.4 Conclusion and future experiments 106

5 References 110

6 Acknowledgements.....119

List of abbreviations

ABI	Abl (Abelson-interacting protein)-interactor
AC	Adenylyl cyclase
ACA	Adenylyl cyclase for aggregation
ADP	Adenosine 5'-(trihydrogen diphosphate)
Akt	PKB, from thioma of the AKR mouse strain
Arp2/3	Actin-related protein-2/3 complex
ArpC2	Actin-related protein 2/3 complex subunit 2
ArpC4	Actin-related protein 2/3 complex subunit 4
ATP	Adenosine 5'-(tetrahydrogen triphosphate)
cAM	Calmodulin
cAMP	3'-5'-cyclic adenosine monophosphate
cAR	Cyclic AMP receptor
Cdc42	Cell division cycle 42, RhoGTPase
cGMP	3'-5'-cyclic guanosine monophosphate
CR16	Corticosteroid and regional expression-16
CRAC	Cytosolic regulator of adenylyl cyclase
CRIB domain	CDC42/Rac-interactive binding domain
Crk	Chicken tumor virus regulator kinase
CRP	Cysteine-rich protein
DAG	Diacylglycerol
DMACM	[7-(dimethylamino)coumarin-4-yl]methyl
Ena domain	N-terminus domain of the Drosophila protein Enabled
EVH1 domain	Ena/VASP homology 1

GBD	GTPase-binding domain
Gbp	cGMP-binding protein
GCA	guanylyl cyclase A
GRAM domain	Glucosyltransferases, Rab-like GTPase activators and myotubularins
GTP	Guanosine triphosphate
HSPC300	Haematopoietic stem-cell progenitor
IP_3	Inositol 1,4,5-triphosphate
IQGAP	Rac and Cdc42 mediator
IRSp53	Insulin-receptor substrate p53
LatA	Latrunculin A
MHC	Myosin II heavy chain
MHCK	Myosin heavy chain kinase
NAP1	Nucleosome assembly protein 1
NAP125	Nck-associated protein 125kDa
Nck	Non-catalytic region of tyrosine kinase adaptor protein
NFP	Nucleation promoting factor
PakA	p21-activated protein kinase A
PBD	Rac/Cdc42 (p21) binding domain
PBP10	Polyphosphoinositide- Binding Peptide, Rhodamine B-QRLFQVKGRR
PDE	Phosphodiesterase
PDMS	Poly(dimethylsiloxane)
PH	Pleckstrin homology
PhdA	PH-domain-containing protein A

PIR121	p53-inducible mRNA
PI3K	Phosphatidylinositol 3-kinase
PIP_3	Phosphatidylinositol 3,4,5- triphosphate
PIP_2	Phosphatidylinositol 4,5-biphosphate
PKB	Protein kinase B
PKG	Protein kinase G
PLA2	Phospholipase A2
PPIs	Phosphoinositides
PTEN	Phosphatase and tensin homolog
Rac	Ras-related C3 botulinum toxin substrate
Rap1	Ras-related protein 1
Ras	Rat sarcoma protein subfamily
RLC	Regulatory light chain
SCAR	Suppressor of cyclic AMP receptor protein
sGC	Soluble guanylyl cyclase
SH3	Src-homology-3
SHIP	SH2 domain-containing inositol phosphatase
SRA1	Specific Rac1-associated protein 1
StmF	Streamer F mutants
TORC2	Target of rapamycin complex 2
VASP	Vasodilator-stimulated phosphoprotein
VCA domain (in WASP)	Verprolin-homology domain, cofilin-homology domain and acidic domain
WASP	Wiskott-Aldrich syndrome protein
WAVE	WASP-family verprolin-homologous protein

WCA domain	WASP-family verprolin-homologous protein
WH1 domain	WASP homology 1 domain
WH2 domain	WASP homology 2 domain
WICH	CR16-homologous protein
WIP	WASP interacting protein

Summary

Actin-based directional motility is important for embryonic development, wound healing, immune responses, and development of tissues. Actin and myosin are essential players in this process that can be subdivided into protrusion, adhesion, and traction. Protrusion is the forward movement of the membrane at the leading edge of the cell. Adhesion is required to enable movement along a substrate, and traction finally leads to the forward movement of the entire cell body, including its organelles. While actin polymerization is the main driving force in cell protrusions, myosin motors lead to the contraction of the cell body.

The goal of this work was to study the regulatory mechanisms of the motile machinery by selecting a representative key player for each stage of the signaling process: the regulation of Arp2/3 activity by WASP (actin system), the role of cGMP in myosin II assembly (myosin system), and the influence of phosphoinositide signaling (upstream receptor pathway). The model organism chosen for this work was the social ameba *Dictyostelium discoideum*, due to the well-established knowledge of its cytoskeletal machinery, the easy handling, and the high motility of its vegetative and starvation developed cells.

First, I focused on the dynamics of the actin cytoskeleton by modulating the activity of one of its key players, the Arp2/3 complex. This was achieved using the carbazole derivative Wiskostatin, an inhibitor of the Arp2/3 activator WASP. Cells treated with Wiskostatin adopted a round shape, with no of few pseudopodia. With the help of a microfluidic *cell squeezer device*, I could show that Wiskostatin treated cells display a reduced mechanical stability, comparable to cells treated with the actin disrupting agent Latrunculin A. Furthermore, the WASP inhibited cells adhere stronger to a surface and show a reduced motility and chemotactic performance. However, the overall F-actin content in the cells was not changed. Confocal microscopy and TIRF microscopy imaging showed that the cells maintained an intact actin cortex. Localized dynamic patches of increased actin polymerization were observed that, however, did not lead to membrane deformation. This indicated that the mechanisms of actin-driven force generation were impaired in Wiskostatin treated cells. It is concluded that in these cells, an altered architecture of the cortical network

leads to a reduced overall stiffness of the cell, which is insufficient to support the force generation required for membrane deformation and pseudopod formation.

Second, the role of cGMP in myosin II dynamics was investigated. Cyclic GMP is known to regulate the association of myosin II with the cytoskeleton. In *Dictyostelium,* intracellular cGMP levels increase when cells are exposed to chemoattractants, but also in response to osmotic stress. To study the influence of cyclic GMP on actin and myosin II dynamics, I used the laser-induced photoactivation of a DMACM-caged-Br-cGMP to locally release cGMP inside the cell. My results show that cGMP directly activates the myosin II machinery, but is also able to induce an actin response independently of cAMP receptor activation and signaling. The actin response was observed in both vegetative and developed cells. Possible explanations include cGMP-induced actin polymerization through VASP (vasodilator-stimulated phosphoprotein) or through binding of cGMP to cyclic nucleotide-dependent kinases.

Finally, I investigated the role of phosphoinositide signaling using the Polyphosphoinositide-Binding Peptide (PBP10) that binds preferentially to PIP_2. Phosphoinositides can recruit actin-binding proteins to defined subcellular sites and alter their activity. Neutrophils, as well as developed *Dictyostelium* cells produce PIP_3 in the plasma membrane at their leading edge in response to an external chemotactic gradient. Although not essential for chemotaxis, phosphoinositides are proposed to act as an internal compass in the cell. When treated with the peptide PBP10, cells became round, with fewer or no pseudopods. PH-$_{CRAC}$ translocation to the membrane still occurs, even at low cAMP stimuli, but cell motility (random and directional) was reduced. My data revealed that the decrease in the pool of available PIP_2 in the cell is sufficient to impair cell motility, but enough PIP_2 remains so that PIP_3 is formed in response to chemoattractant stimuli. My data thus highlights how sensitive cell motility and morphology are to changes in the phosphoinositide signaling.

In summary, I have analyzed representative regulatory mechanisms that govern key parts of the motile machinery and characterized their impact on cellular properties including mechanical stability, adhesion and chemotaxis.

Zusammenfassung

Aktin-basierte gerichtete Motilität ist von großer Bedeutung für zahlreiche biologische Prozesse, wie zum Beispiel Embryonalentwicklung, Wundheilung, Immunantwort und Entwicklung von Geweben. Aktin und Myosin sind entscheidende Komponenten in diesem Prozess, der in drei Phasen aufgegliedert werden kann: Ausstülpung der Membran, Adhäsion und Kontraktion. Die Ausstülpung der Membran findet in Bewegungsrichtung an der Vorderseite der Zelle statt (*leading edge*). Die Adhäsion verbindet die Membran mit dem Substrat und ist für die Zellbewegung über das Substrat erforderlich. Die Kontraktion an der Hinterseite der Zelle schließlich führt zur Verschiebung der gesamten Zelle in Bewegungsrichtung. Während Aktinpolymerisation die wichtigste Antriebskraft zur Ausstülpung der Membran darstellt, ist Myosin für die Kontraktion der Zelle verantwortlich.

Das Ziel der Arbeit war es, die regulatorischen Mechanismen der Zellmotilität zu untersuchen. Dazu habe ich für jedes Stadium dieses Prozesses einen repräsentativen regulatorischen Schritt ausgewählt und genauer untersucht: Die Regelung des Arp2/3 Komplexes durch WASP (Aktinsystem), die Rolle von cGMP in der Myosin II-Regulation (Myosinsystem) und der Einfluss von Phosphoinositiden im intrazellulären Signalprozess (Rezeptor-Signalweg). Die soziale Amöbe *Dictyostelium discoideum* wurde als Modellorganismus für diese Arbeiten gewählt. Gründe für diese Wahl waren die bereits vorliegenden detaillierten Kenntnisse über das Zytoskelett dieser Zellen, ihre einfache Handhabbarkeit im Labor, und die hohe Motilität der Zellen im vegetativen und entwickelten Zustand.

Als Erstes analysierte ich die Dynamik des Aktin-Zytoskeletts durch Modulation der Aktivität des Arp2/3-Komplexes. Dafür benutzte ich das Carbazol-Derivat Wiskostatin, ein Inhibitor des Arp2/3-Aktivators WASP. Zellen, die mit Wiskostatin behandelt wurden, zeigten eine runde Form mit wenigen oder keinen Pseudopodien. Mit Hilfe des mikrofluidischen *cell squeezer device* konnte ich zeigen, dass Wiskostatin-behandelte Zellen eine geringere mechanische Stabilität aufweisen, vergleichbar mit Zellen unter dem Einfluss des Aktin-depolymerisierenden Wirkstoffes Latrunculin A. Darüber hinaus zeigen Wiskostatin behandelten Zellen eine erhöhte Substratadhäsion und eine verringerte Motilität und chemotaktische Effizienz. Der F-Aktingehalt der Zelle insgesamt blieb jedoch unverändert. Konfokal-

und TIRF-mikroskopische Aufnahmen zeigten, dass die Zellen einen intakten Aktinkortex aufweisen. Es konnten lokalisierte dynamische Regionen erhöhter Aktinpolymerisation beobachtet werden, die jedoch nicht zur Ausbildung von Membrandeformationen führten. Daraus kann man rückschließen, dass die Mechanismen der Krafterzeugung im Aktin-Zytoskelett in WASP-inhibierten Zellen beeinträchtigt sind. Vermutlich liegt in diesen Zellen eine veränderte Mikroarchitektur des kortikalen Netzwerks vor, die zu einer verminderten Steifigkeit der Zelle führt, so dass die zur Bildung von Pseudopodien erforderlichen Kräfte nicht entfaltet werden können.

Als Zweites wurde die Rolle von cGMP in der Myosin II-Dynamik untersucht. Es ist bekannt, dass cGMP die Assoziation von Myosin II mit dem Zytoskelett reguliert. In *Dictyostelium* steigt die intrazelluläre Konzentration von cGMP in Gegenwart von chemoattraktiven Lockstoffen sowie in Antwort auf osmotischen Stress. Um den Einfluss von cGMP auf die Aktin und Myosin II -Dynamik zu untersuchen, benutzte ich laserinduzierte Photoaktivierung von DMACM-caged-Br-cGMP, um cGMP lokal innerhalb der Zelle freizusetzen. Meine Ergebnisse zeigten, dass intrazelluläres cGMP direkt zur Aktivierung von Myosin II führt, jedoch auch Aktinantworten unabhängig vom cAMP-Rezeptorsignalweg induzieren kann. Die Aktinreaktion wurde sowohl in vegetativen als auch in entwickelten Zellen beobachtet. Eine mögliche Erklärung könnte die cGMP-induzierte Aktinpolymerisation über VASP (vasodilator-stimulated phosphoprotein) sein oder über die Bindung von cGMP an Nukleotid-abhängige Proteinkinasen.

Als dritten Punkt meiner Arbeit untersuchte ich die Rolle der Phosphoinositide mit Hilfe des Phosphoinositide-bindenden Proteins PBP10, das bevorzugt an PIP_2 bindet. Phosphoinositiden können Aktin-bindende Proteine zu definierten subzellulären Orten rekrutieren und ihre Aktivität verändern. Sowohl Neutrophile als auch entwickelte *Dictyostelium* Zellen produzieren PIP_3 in der Plasmamembran an ihrer *leading edge* in Antwort auf externe Gradienten chemischer Lockstoffe. Obwohl Zellen auch ohne PIP_3 chemotaktisches Verhalten zeigen, werden Phosphoinositide im Allgemeinen mit dem inneren chemotaktischen Kompass der Zelle in Verbindung gebracht. Mit dem Peptid PBP10 behandelte Zellen nahmen eine runde Form an, mit wenigen oder keinen Pseudopodien. $PH\text{-}_{CRAC}$ -Translokation zur Membran konnte in PBP10-behandelten Zellen selbst bei geringen cAMP-Stimuli weiterhin beobachtet

werden. Ungerichtete wie auch gerichtete Zellmotiliät waren jedoch beeinträchtigt. Meine Daten zeigen, dass die Abnahme des PIP_2-Pools in der Zelle durch PBP10 ausreicht, um die Zellmotilität zu beeinträchtigen, dass jedoch genug PIP_2 erhalten bleibt um in Folge einer Rezeptorstimulation PIP_3 zu produzieren. Die Ergebnisse demonstrieren daher, wie empfindlich Zellmotilität und -morphologie gegenüber Modifikationen im Phosphoinositid-Signalweg sind.

Zusammenfassend habe ich mehrere repräsentative Beispiele für regulatorische Mechanismen der Zellmotilität untersucht und deren Auswirkung auf Eigenschaften der Zelle wie mechanische Stabilität, Zelladhäsion und Chemotaxis charakterisiert.

1 Introduction

1.1 Dictyostelium discoideum biology

Dictyostelium discoideum is a cellular slime mold (or social ameba) that feeds on bacteria. It has been classified into the Mycetozoa kingdom, before Metazoa, Microsporidia and Fungi (1). *D. discoideum* is a eukaryotic unicellular microorganism that undergoes multicellular morphogenesis when food is exhausted. Growing cells chemotax toward folic acid and factors from bacteria, and starved cells in a developmental process chemotax toward cAMP (2). In response to starvation, the cells can form microcysts (two layers of cellulose coating each cell, dormancy); macrocysts (three layers of cellulose, requires the presence of two mating types, sexual cycle); or fruiting bodies (production of spores, with three layers of cellulose but more complex) (3).

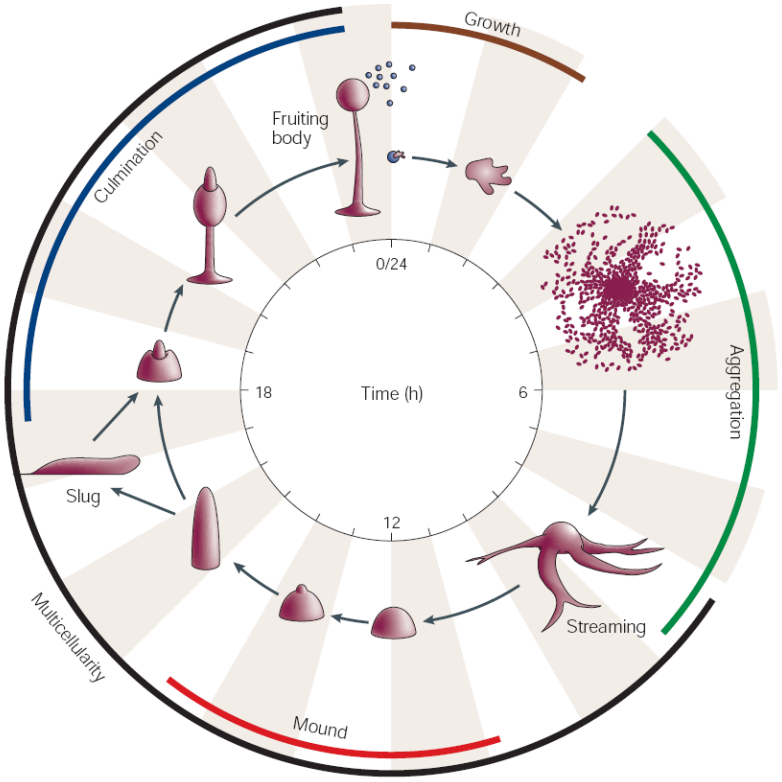

Figure 1 - *Dictyostelium discoideum* developmental morphogenesis, starting from single, vegetative amebae until the formation of the mature fruiting body, which contains a sorus of spore cells on top of a stalk that is composed of vacuolated stalk cells. A transition between growth and aggregation occurs, which is mediated by the chemotaxis of cells towards cyclic AMP to form a multicellular aggregate. During this process, cells can be seen streaming towards a central domain or aggregation center. Aggregation results in the formation of a multicellular structure, known as a mound, in which the precursors of the mature spore and stalk cells — prestalk and prespore cells — differentiate and sort, forming a tipped aggregate or tipped mound. As development proceeds, the tip extends and an anterior–posterior axis forms, which is maintained through the slug and early culminant stages. Culmination, the formation of the fruiting body, completes morphogenesis. During this stage, the precursor populations differentiate, producing a sorus on top of a stalk. The entire process from starvation of vegetative cells to the formation of a mature fruiting body takes 24 hours. Taken from (4).

Cells enter a developmental mode, producing the chemoattractant cyclic AMP (Figure 1), and in 24h they evolve into a fruiting body consisting of stalk and a spore head with spores (5). Their ability to synthesize, release, detect, and degrade cAMP is essential for the formation of aggregates that can have more than 100000 cells.

In nature, dispersion is essential for surviving, and balls of spores are usually picked up by the carapaces of arthropods or annelids. Competitors and predators of ameba are nematodes that compete for the bacteria but can also feed on ameba. *Dictyostelium* cells are haploid, have 6 chromosomes and aggregates are not always genetically homogeneous. They can have extra-chromosomal plasmids, important for long-term maintenance (3).

Dictyostelium discoideum has several advantages as a model organism, for example, the genetic and biochemical accessibility (2), the recently sequenced genome, and the inexpensive and relatively easy growing (5). A public database with genomic and biological information is also available (6).

1.2 Signaling and chemotaxis in *Dictyostelium discoideum*

Pulsatile cAMP signaling can induce the expression of early genes in *Dictyostelium*. The expression of chemoattractant receptors, G protein subunits and adenylyl cyclase requires periodic activation of the transduction machinery (2). Extracellularly, cAMP acts as a chemoattractant, and also on gene regulation inducing phenotype differentiation. Inside the cell, cAMP triggers initiation of development, maturation of spores, maintenance of spore dominancy, resistance to osmotic stress and orientation in chemotatic gradients. (7).

Dictyostelium discoideum cells sense extracellular cAMP via cARs (cAMP receptors). Cyclic AMP binds to the cAR on the outside, and activates G proteins on the inside of the cell. G protein activates PI3K (PI3-kinase) which induces the production of PIP_3 (phosphatidylinositol (3,4,5)- triphosphate). PIP_3 binds to CRAC (cytosolic regulator of adenylyl cyclase). CRAC is essential for adenylyl cyclase (AC) activation, and AC, when activated, produces intracellular cAMP (8).

Chemotaxis is the process by which an external chemical signal, detected by cell membrane receptors, is translated into movement of the cell toward or away from the chemical source (9). Four cAMP receptors (cAR1- cAR4) are found, and cAR1 is considered the most important. cAR1 is uniformly distributed along the cell membrane, and G protein dissociation mirrors receptor occupancy when cAMP is present (2). As mentioned before, *Dictyostelium discoideum* senses cAMP and migrates in response to the gradient, when developed under starvation (10). In summary, a gradient of cAMP results in a receptor-activation gradient that leads to G-protein cascade activation. This results in the activation of small G proteins of the Ras family that recruit PI3 kinases (PI3K) to the leading edge of the membrane, to convert PIP_2 to PIP_3, in a localized manner. PIP_3 production results in the recruitment of PIP_3-specific pleckstrin homology (PH)-domain proteins to the leading edge (9).

Chemotaxis can be divided into directional sensing, polarization, and migration (motility). Directional sensing is the ability of a cell to detect concentration differences in the extracellular medium and generate an amplified internal response. Directional sensing occurs within the first 10s after stimulation. The external signal is amplified in the pathway after G protein activation and before the accumulation of PIP_3 (11). During the process of polarization, the cell body elongates and forms a distinct front (leading edge) and back. Specific proteins localize in each pole (time scale 10-45s) (10). Involved molecules include actin binding proteins, SCAR, WASP, filopodin, cofilin and coronin (11). Front and tail of the cell can be distinguished by molecular markers, showing that actin is polymerized at the front and myosin at the tail of the cell (10, 12). PIP_3 is produced at the high side and is also a marker for sensing (10). Two to three seconds after the cAMP stimulus, actin polymerization increases in the cell cortex. Seconds after, actin starts to disassembly even if cAMP is still rising, and cellular responses subside during constant receptor occupancy, a process called adaptation (figure 2) (10, 12). After cytoskeletal rearrengements and asymmetric protein translocations, cells show directed migration towards the chemical source. New pseudopods are more frequently projected in direction of the gradient, and the actin polymerization pushes the leading edge forward.

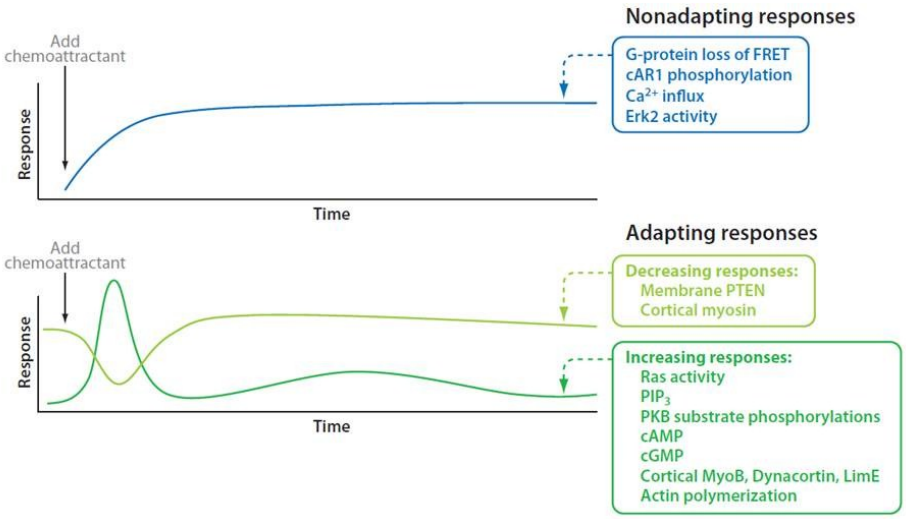

Figure 2 - The biochemical responses triggered by cAMP can be divided into two groups on the basis of whether or not they adapt to constant stimuli. Some responses, such as G-protein activation, are nonadapting and persist as long as the stimuli are maintained. The adapting responses, such as PIP_3 production, transiently increase, whereas others, such as membrane-localized PTEN, transiently decrease. From reference (13).

Overall, *Dictyostelium discoideum* chemotaxis also resembles neutrophilic motility. In both, cells signals are separated downstream after the receptor activation (14). Cancer cells can disseminate from the primary tumor as individual cells using ameboid- or mesenchimal-type movement. Cell motility has turned out to be unexpectedly durable and difficult to block pharmacologically (15). The social ameba has thus become a powerful model system for investigating the mechanisms of eukaryotic chemotaxis, due to its simplicity.

1.3 Cyclic AMP

Four cAMP receptors (cAR1-4) that differ in their affinity for cAMP and in their developmental expression were described for *Dictyostelium discoideum*. In addition, there are cAMP-receptor-like proteins that participate in growth and development. The cAMP receptor cAR1 is uniformly distributed in *Dictyostelium* cells, but components like F-actin, phosphatidylinositol 3-kinase (PI3K), phosphatidylinositol trisphosphate (PIP_3), and pleckstrin homology (PH) domain-proteins are found in the

front; PI 3-phosphatase (PTEN), adenylyl cyclase (ACA) and myosin II in the back (2, 16).

Heterotrimeric G proteins (with α, β, and γ subunits) bind to chemotactic receptors and later the βγ subunits forward this signal. When receptor occupancy is constant, *D. discoideum* cells adapt, responding again if the stimulus is removed or if there is an increase in receptor occupancy. The cell can sense cAMP gradients independent of the mean concentrations and chemotax independently of the distance of the chemoattractant source. Cells are able to chemotax even if the absolute difference in occupied cAR receptors at the front and back of the cell goes down to 10 to 20 molecules (17).

Occupied receptors repeatedly elicit G-protein activation, and regulators of G-protein signaling influence the steady-state of active and inactive G-proteins (18). Differences in receptor dissociation result from altered interactions between receptors and their coupled G-proteins rather than receptor phosphorylation. The differences in the rates of cAMP binding indicate a faster intermediate state of the receptor and the G-protein in the front than in the back of the cell (19).

Intracellular and extracellular cyclic nucleotide phosphodiesterases (PDEs) are divided in three functional groups: 1) PDE1 and PDE4, degrade extracellular cAMP; 2) PDE2/regA and PDE6/GbpB/PdeE degrade intracellular cAMP; and 3) PDE3, PDE5/GbpA/PDED and PDE6/GbpB degrade intracellular cGMP (2). The adenylyl cyclase for aggregation (ACA) is a 12-transmembrane domain protein similar to mammalian adenylyl cyclases, and is expressed during aggregation, producing cAMP in response to cAMP induction.

1.4 The actin cytoskeleton

Actin-based directional motility is important for embryonic development, wound healing, immune responses and development of tissues. Actin is one of the most abundant proteins in eukaryotic cells (20), and is found in two forms: monomeric G-actin and filamentous F-actin (figure 3). When the concentration of monomeric G-actin is above a critical value, it spontaneously polymerizes to form filamentous F-actin. But G-actin is also sequestered by other proteins which prevents spontaneous

polymerization of actin in the cell (21). Actin polymerizes into semi-flexible filaments, which then crosslink into a gel. The growth of this gel leads to the formation of cellular protrusions with different shapes (22). The protrusions at the leading edge can be explained by the dendritic nucleation treadmilling hypothesis. Treadmilling is a mechanism that drives actin dynamics in eukaryotes: In the presence of ATP, free actin-monomers add to the barbed end, also called 'plus-end' of the filament, while at the same time monomers detach from the 'pointed-end', the so called 'minus end' of the filament (23). During treadmilling, the plus-end of the actin filament then grows, while the minus-end shrinks (24).

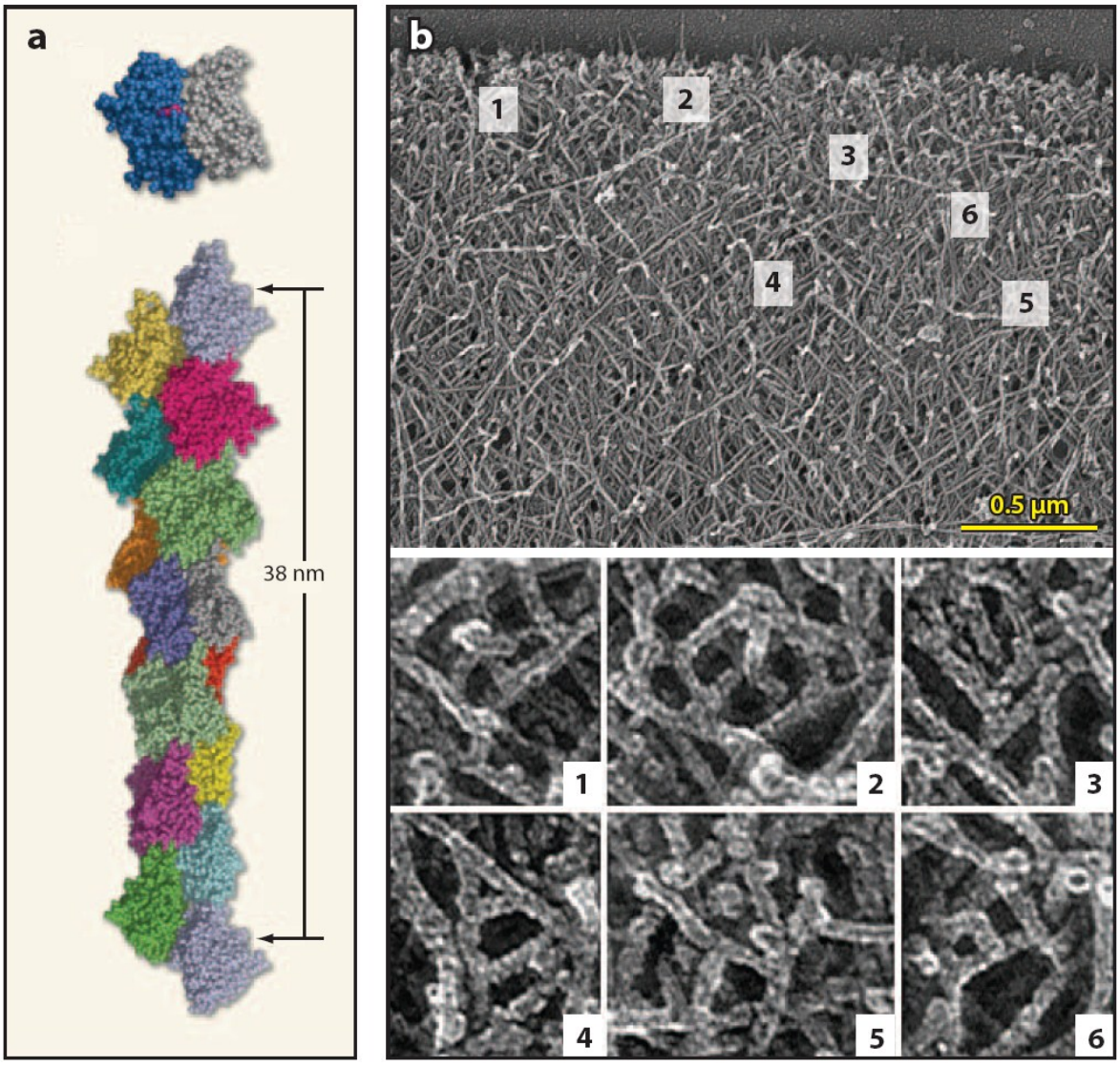

Figure 3 - (a) Structure of an F-actin filament based on electron microscopy. Total length of filament is about 38nm. Based on (25). (b) Branched network structure in keratocyte lamellipodium, immumo-electron microscopy, from original research article (26). Width of field in top frame is about 3µm. Close-ups are from indicated boxes in top frame. The picture in the format showed was taken from (22).

Actin-driven cellular locomotion can be divided into protrusion, adhesion, and traction. Protrusion is the forward movement of the membrane at the leading edge of the cell. Adhesion is required to enable movement along a substrate, and traction at the rear end finally leads to the forward movement of the entire cell body, including its organelles (27). There are three different types of membrane protrusions: Filopodia, lamellipodia, and pseudopodia (27). Filopodia are thin, finger-like structures with a core of actin filaments that form at the leading edge of migrating cells. Lamellipodia are flat cellular protrusions containing a network of actin filaments that mediate the protrusion of the leading edge. Pseudopodia are large cellular protrusions with a network of actin that drive the protrusion of the leading edge of an amoeboid cell or phagocyte (28). The dense assemblies of filamentous actin are also generated beneath the substrate-attached cell surface in the form of short-lived foci and traveling waves (29).

1.5 Actin-interacting proteins

The survival of *Dictyostelium* depends on the ability to sense, track, and consume bacteria based on chemotaxis and phagocytosis. The repertoire of actin-binding proteins in *Dictyostelium* is most similar to metazoan followed by fungi. Apart from exceptions like the Arp2/3 complex, most of the proteins of the actin cytoskeleton are encoded by two or more genes. There are 138 known actin-interacting proteins in *Dictyostelium*. They are divided in the following categories: Monomeric (G-actin) binding, actin capping and/or severing, actin capping and nucleating, actin cross-linking, lateral actin-binding, membrane-associated and motor proteins (30). In the next sections I describe some actin-interacting proteins that play an essential role for the understanding of the experimental work presented later.

1.5.1 DdLimE

DdLimE is a member of the cysteine-rich protein (CRP) family of the zinc ion-binding LIM domain family of proteins. LIM proteins are often associated with G-protein signaling pathways. In *Dictyostelium* DdLimE is recruited to dynamic protrusions like those at the leading edge and at phagocytic cups, and it is a component of a GTP-rac1 protein complex (31). DdLimE has three domains: an N-terminal LIM domain, a glycine-rich region, and a C-terminal coiled-coil domain. DdLimE is recruited to the cell cortex similarly to actin, the Arp2/3 complex, and

regulatory proteins of the cytoskeleton like coronin and Aip1. In DdLimE-null cells, the microtubules are longer than normal and the spindle persists for a longer time in mitotic cells (32). In the present study, cells expressing DdLimE (LimEΔcoil)-GFP or DdLimEΔ-mRFP were used to visualize F-actin dynamics. DdLimE is a common marker for visualizing F-actin (29, 33). The final LimEΔcoil GFP fusion protein consists of amino acids 1 to 145 of LimE, a threonine and serine residue and the complete S65T GFP protein (32, 34). The AX2 cell line expressing LimE-GFP was kindly provided by G. Gerisch.

1.5.2 Arp2/3 complex

Arp2/3 (actin-related protein 2/3) is a complex localized at the leading edge of motile cells that caps the minus-end of actin filaments *in vitro* and stabilizes the free plus-end (26, 35, 36). Nucleation and branching by the Arp2/3 complex are involved in lamellipodial protrusions and in the generation of forces that remodel or transport membranes during trafficking. Coordinated nucleation and branching by Arp2/3 play an important role in genetics (viability of unicellular and multicellular organisms), cell migration and adhesion, moving membranes and diseases (37). In mammalian cells, N-WASP, cortactin and the Arp2/3 complex localize to sites of chlatrin-mediated endocytosis (38).

Actin polymerization in the presence of Arp2/3 complex is autocatalytic, and it is proposed that filament nucleation and branching are tightly coupled (20, 35). There are two models that link nucleation and branching: one proposes that branching occurs from the sides of existing filaments. The other proposes that it occurs from the barbed ends of filaments (38). The Arp2/3 complex is activated by nucleation promoting factor (NPF) proteins, to initiate a new daughter filament that emerges from a mother filament in a y-branch configuration (38). Examples of NFPs from the eukaryotic class I are proteins of the WASP (Wiskott–Aldrich syndrome protein) family (21). The Arp2/3 complex is a stable assembly of Arp2 and Arp3, two actin-related proteins (37). In the cytoplasm of human leukocytes it is present in concentrations higher as 10μM. Activation of the complex is assumed to require a significant conformational change. Arp2 and Arp3 interact with the pointed end of the daughter filament; ArpC2 and ArpC4, subunits of the Arp2/3 complex, make contacts with the mother filament (36). Arp2 and Arp3 bind to ATP, and nucleotide binding and hydrolysis influence their structure and function (39).

Actin organization is determined by the branching mediated by the Arp2/3 complex. Plasma membrane-associated proteins control the activation of the Arp2/3 complex and regulate the elongation and turnover of the nucleated filaments, also determining actin organization (40). Extracellular stimuli, like cAMP in *Dictyostelium*, activate membrane receptors leading to signal transduction activating Rho GTPases and PIP_2. The activated molecules then induce actin polymerization and activation of WASP, which in turn activates the Arp2/3 complex. It is generally assumed that the complex is intrinsically inactive and depends on extrinsic activators (20).

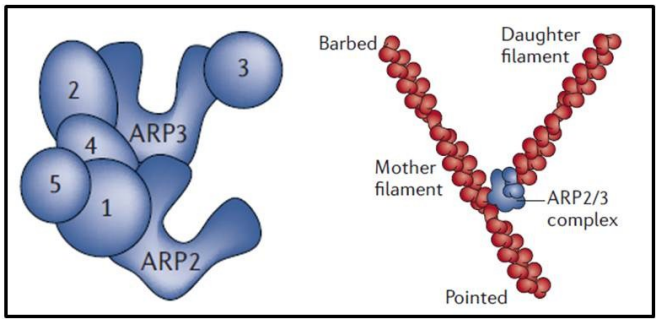

Figure 4 – The organization of the subunits Arp complex 1(ArpC1) to ArpC5 of the Arp2/3 complex from an inactive actin-related protein-2/3 (Arp2/3) complex is shown on the left. On the right, a diagram of the binding of Arp2/3 to the mother and daughter filaments is depicted. Modified from reference (41).

1.5.3 WASP (Wiskott–Aldrich syndrome protein)

WASP was initially identified as the causative gene of the Wiskott-Aldrich syndrome (WAS). WAS is a X-linked recessive disease. Without treatment, most patients die by 10 years of age due to infections, hemorrhage, and autoimmune diseases. Neural (N-) WASP was first identified in neural tissue, but is also present in other tissues (42). WASP and N-WASP are found in animals, fungi, and protists. The first members of the WASP family were identified in humans, but yeast, *Drosophila*, and *Dictyostelium* also possess proteins of this family. *Dictyostelium* has a WASP homologue with the conventional domain topology (named WASP A). Two other proteins are found in *D. discoideum*, and were recently named WASP B and WASP C (figure 5). WASP B and WASP C do not have a WH1 domain, but have a PBD and a VCA domain. Both have functions in clathrin-mediated endocytosis, targeting coated pits. WASP C is also visible as long strands, similar to actin-filament bundles (43).

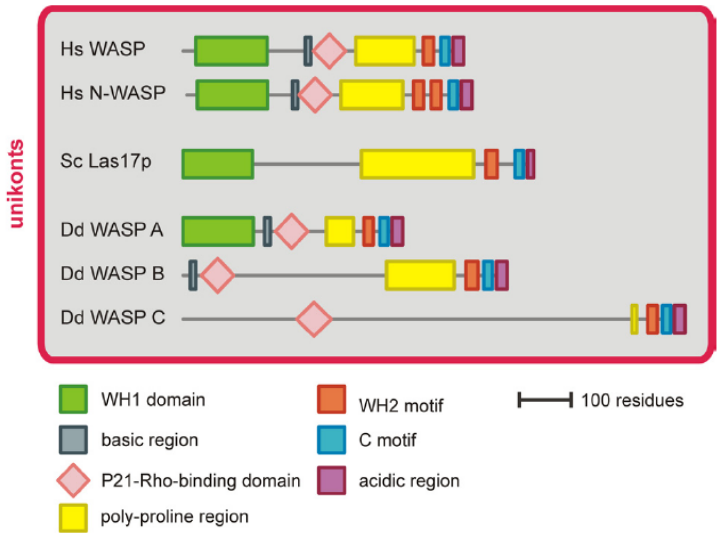

Figure 5 - Domain topology diagrams of WASP orthologues from unikonts. Hs: *Homo sapiens*, Sc: *Saccharomyces cerevisiae*, Dd: *Dictyostelium discoideum*. Modified from reference (43).

WASP proteins have a proline rich domain that interacts with profilin, an actin-binding protein, as well as with SH3 domain containing proteins. Profilin participates in the regulation of filament polymerization, and the knockout mutant for the two profilin isoforms in *Dictyostelium* has more F-actin, less motility, bigger size and alterations in development and cytokinesis (21).

Mammalian WASP is expressed specifically in haematopoietic cells, and its mutation results in defective cell migration, phagocytosis and T-cell signalling. N-WASP deletion results in neurological and cardiac defects in mice, and can also be lethal in mice embryos (44). WASP family members function as scaffold proteins, transducers of signals from proteins or membranes that mediate changes in the cytoskeleton. They lack intrinsic catalytic activity and have a common modular structure to interact with distinct binding proteins (45).

N-WASP induced activation of Arp2/3 is thought to be essential for actin cytoskeleton activation associated with protrusion of podosomes and invadopodia in macrophages and some invasive cancer cell types. N-WASP and WASP binds to adaptor proteins including Crk at immunological synapses and Nck in kidney (42). Tyrosine phosphorylation of WASP leads to an increase in its ability to activate the Arp2/3 complex, without the need of Cdc42 or $PI(4,5)P_2$, and serine/threonine phosphorylation can stimulate actin polymerization in vitro (46).

WASP and N-WASP contain a WH1 (WASP homology 1) domain, also known as the Ena/VASP homology 1 (EVH1) domain. It also has a CRIB domain, which binds to Cdc42 (figure 6). WH1 domains interact with the WIP (WASP-interacting protein) family, and this interaction suppresses the activity of WASP or N-WASP. (46). WASP and N-WASP possess a VCA region, composed of 3 domains: the C-terminal verprolin-homology domain (also called WH2 domain), the cofilin-homology domain, and the acidic domain. In the VCA region, the V domain binds to an actin monomer, and the CA domain binds to the Arp2/3 complex, leading to a burst of actin polymerization (42).

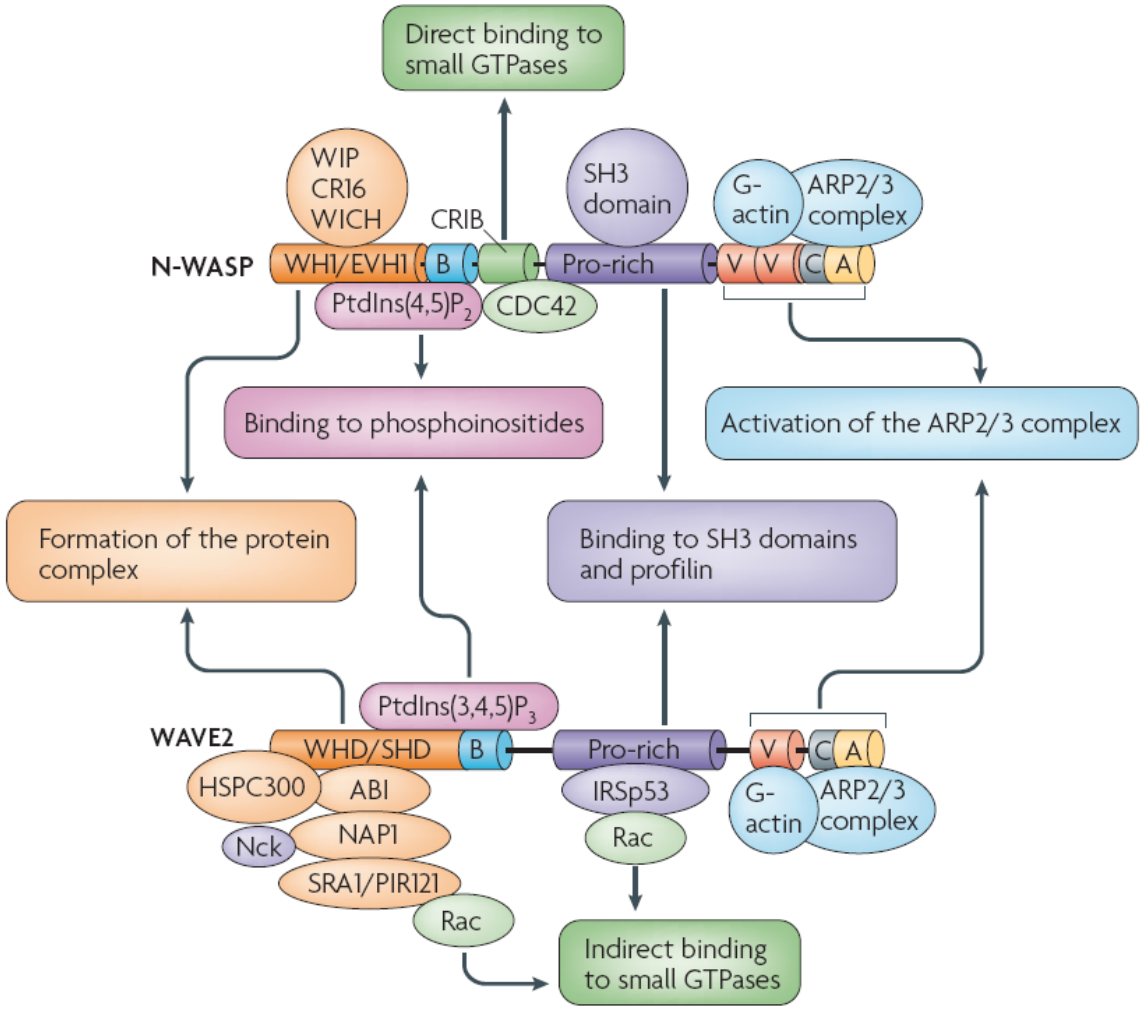

Figure 6- Domains and binding partners of N-WASP and WAVE2. Taken from Takenawa and Suetsugu (42).

The autoinhibtion of WASP is released by the binding of Cdc42 and PIP_2 (46). The WH1 domain binds to a proline-rich sequence of the WASP-interacting protein (WIP) family. The interaction with WIP suppresses the activity of WASP or N-WASP,

but also has the function to act as a scaffold, linking WASP to adaptor proteins. Phosphoinositides interact with the WASP basic region, and the CRIB region binds to Cdc42. Under resting conditions, WASP and N-WASP are folded and inactive because the VCA region cannot be accessed, since the VCA region interacts with a hydrophobic pocket in the GTPase-binding domain (GBD) (45). When molecules bind to the CRIB or surrounding regions, autoinhibition is released. N-WASP is involved in filopodium formation together with Arp2/3.

Homologous of WASP are SCAR (suppressor of cAMP receptor) in *Dictyostelium* and WAVE [WASP (Wiskott–Aldrich syndrome protein)-family verprolin homology protein] in mammals. SCAR/WAVE proteins belong to the class I of nucleation promoting factors (NPFs), like WASP. SCAR was first cited in 1998 as a new family of the WASP family in *Dictyostelium discoideum* (47). Class I NPFs have a diverse domain organization, but all possess a WCA domain (WH2 – WASP homology 2 – domain, also called verprolin-homology domain, together with a central and acidic region). The WCA domain is sufficient for the activation of the Arp2/3 complex in vitro. The current model for class I NPF is that the acidic region mediates binding to Arp2/3, the central region initiates an activating conformational change in the complex and the WH2 together with the central region present an actin monomer to the complex, facilitating the polymerization of the daughter filament (38).

SCAR/WAVE proteins are activated and bind to the Arp2/3 complex, initiating new filaments. The barbed ends grow and the filaments age. Profilin exchanges ADP to ATP in actin and a pool of ATP-actin is formed (20). It was shown that SCAR plays a role in regulating actin polymerization and participates in the pathway connecting the cAR receptor to the cytoskeleton (47). SCAR/WAVE proteins are directly involved in the protrusion of both lamellipodia and filopodia. There is evidence that different mammalian SCAR isoforms (usually called WAVE), have specific functions and may be regulated differentially (48). Under resting conditions SCAR forms a complex with four other proteins: PIR121 (p53-inducible mRNA), NAP125 (Nck-associated protein), ABI (Abl-interactor) and HSPC300 (haematopoietic stem-cell progenitor). Upon stimulation, GTP-bound Rac bind to PIR121 leading to SCAR/WAVE activation (38).

1.6 Myosin II

Myosins are a superfamily of proteins that walk along, propel the sliding of, or produce tension on actin filaments. The required energy is provided by the hydrolysis of ATP at its catalytic site with ATPase activity. Class II myosins form the biggest group of myosins, and are also present in all non-muscle eukaryotic cells. Myosin (figure 7) rapidly hydrolyzes ATP in the absence of actin, but rapid hydrolysis product release requires interaction with actin. Once phosphate and ADP have been released, ATP rebinds to the actin-bound myosin, causing rapid dissociation from actin (49). Non-muscle myosin II molecules are comprised of three pairs of peptides: two heavy chains (230kDa), two regulatory light chains (RLC, 20kDa) and two essential light chains (17kDa) (50).

Actin-driven membrane protrusions together with myosin II-based contractility generate the force necessary for locomotion of the cell body and the disassembly of cell adhesions at the posterior of the cell. Myosin II also contributes to cell polarity by positioning the nucleus and the microtubule-organizing center away from the leading edge (51, 52), and to the persistence of migration by suppressing the formation of lateral membrane protrusions (52). Myosin II is required for F-actin anterograde flow in the cell body and retrograde flow in the lamella, but it is absent from the lamellipodium in mammalian cells. It is proposed to mediate cell contractility and provides coupling between microtubules and the actomyosin system (53). In *Dictyostelium*, 12 different myosin heavy chain genes have been identified, representing 6 different myosin classes, including a single-conventional myosin II, seven single-headed class I myosins, and four unconventional myosins (54). Approximately 0.7% of the total protein of *Dictyostelium* in the growth phase is myosin II. Myosin II null cells are unable to complete cytokinesis when grown in suspension, cannot crawl efficiently over adhesive surfaces, have a reduced cortical stiffness and fail to proceed past the mound stage of development (55).

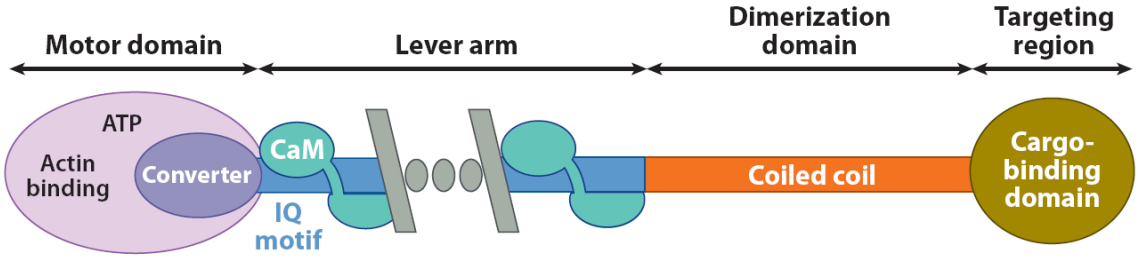

Figure 7 - Schematic organization of the myosin molecule. All myosin sequences contain a motor domain with conserved elements able to bind ATP as well as more variable regions involved in actin binding. The C-terminal sequence of the motor domain folds in a converter subdomain that plays a critical role in amplifying structural rearrangements of the motor domain and transmitting them to the adjacent region (the lever arm). This elongated region is composed of a variable number of IQ motifs (IQ-Calmodulin binding motif) that form a helix that is the target for binding of calmodulin or specialized light chains of this superfamily. The rest of the sequence is more variable, depending on the myosin class, but can contain coiled-coil sequences for dimerization. Most of the C-terminal regions play a role in targeting the myosin to specific cargos in the cell. The N-terminal motor domain also plays a role in targeting for a number of myosins. From reference (49).

Myosin II exists in a dynamic equilibrium between a cytoplasmic pool of monomers and a cytoskeleton-associated assembly of bipolar filaments (56). Signaling pathways governing cell polarity, pseudopod extension, and the control of myosin II localization are tied into the sensing of the extracellular gradients. Rapid application of 10^{-6}M or more cAMP to starved *Dictyostelium* cells results in a rapid (25s) translocation of myosin II to the cortical cytoskeleton (12). In response to activation of G protein-coupled chemoattractant receptors, myosin II is dephosphorylated in the cytosolic region of the cell, and then assembles into filaments. Translocation to the cortex requires an intact motor domain and an intact actin cytoskeleton (50).

The ability of *Dictyostelium* myosin II to assemble into filaments is inhibited by phosphorylation of three threonine residues near the carboxyl terminus of the myosin II heavy chain (MHC). These phosphorylation sites are sites for the enzyme myosin heavy chain kinase A (MHCK A). Myosin II filament assembly is regulated via MHC phosphorylation trough the combined activities of an MHC phosphatase and a group of MHC kinases (56). MHCK A is expressed throughout the growth and developmental phases of the *Dictyostelium* life cycle, and has a role in recycling cortical myosin II filaments back to the cytoplasm. It is found in the cytoplasm but can be enriched at the leading edge of migrating, polarized cells, and in actin-rich

extensions involved in phagocytosis and endocytosis. Stimulation of cells with cAMP results in the translocation of MHCK A to the cell cortex within 15s. MHCK A may function to disrupt myosin filaments at sites where new pseudopodia are being formed (57). The *Dictyostelium* MHCK family also comprises MHCK B and MHCK C (55). MHKC B is mostly cytosolic with enrichment in the cleavage furrow of dividing cells. MHKC C is enriched in the cleavage furrow as well as in the posterior of cells migrating under agarose. A third protein not yet fully described was named MHCK D (57).

Exposure of resting, aggregation competent cells to a pulse of exogenous cAMP produces a 2-6 fold increase in the amount of myosin II associated with the Triton-insoluble cytoskeleton within 30s, followed by a return to basal levels within 80-120s. Some studies suggest that resting, aggregation competent cells contain a pool of cytoplasmic myosin II filaments, other suggest that filament assembly from a monomeric pool is the primary mechanism for relocating myosin II to the cell cortex (54). The assembly of *Dictyostelium* myosin II involves the formation of a parallel dimer with monomers staggered by 98 residues (14.3nm). Subsequently, two parallel dimmers bind end-to-end to form an antiparallel tetramer which then grows thicker by the lateral addition of parallel dimmers (55). Myosin has two modes of action: One is stabilization of the actin cytoskeleton by myosin filament association and the other is ATP-powered contraction that also requires the stabilization of the actin cytoskeleton. Myosin II motor activity is regulated by the phosphorylation of RLC serine 13 by MLCKs (myosin light chain kinases). Stimulation with cAMP induces a transient increase in serine 13 phosphorylation, leading to a four to six-fold increase in myosin motor activity (57).

The study of mutants was essential to characterize the effect of different modulators on myosin II activity. KI-8 and KI-10 (non-chemotactic mutants isolated from the parental strain XP55, see reference (58)) are two chemotaxis deficient mutants that do not produce cGMP in response to chemoattractants, do not recruit myosin II into the cytoskeleton and have no increase in the RLC phosphorylation. Streamer F (StmF) mutants, that have a defect in cGMP specific phosphodiesterase (59) and accumulate increased amount of cGMP in response to cAMP, display a persistent and elongated morphology, a prolonged association of myosin II with the cytoskeleton and a delay in the phosphorylation of MHC and RLC (55). Cyclic GMP is

an important intracellular signal in the control of chemotaxis and the regulation of myosin II. Wild-type aggregation competent *Dictyostelium* cells respond to a pulse of extracellular cAMP with a spike of intracellular cGMP that peaks at 10s (54). Cells lacking soluble guanylyl cyclase (sGC) activity or the cGMP target proteins do not recruit myosin II to the cytoskeleton in response to cAMP, form more lateral pseudopods, display less persistent movement and cannot maintain a polarized morphology (55). In the next section a more detailed view of cGMP signal transduction in *Dictyostelium* is presented.

1.7 cGMP signal transduction

In 1960, cGMP was synthesized for the first time, and at about the same time the existence of endogenously produced cGMP was confirmed. In 1969, guanylyl cyclases activity was confirmed and it became clear that some of them were bound to the cytoskeleton (60). In starvation developed *Dictyostelium* cells, receptor binding of the chemoattractant cAMP induces an increase in the innositol phosphates, cyclic GMP, cyclic AMP, calcium influx, phosphorylation of myosin II, and actomyosin association to the cytoskeleton (61).

The formation of the second messenger cGMP from GTP is catalyzed by guanylate (or guanylyl) cyclases. The two families of guanylyl cyclases are *soluble* (cytoplasmic enzymes, sGC) and *receptor* (GCA) types. One isozyme is a membrane spanning form that is activated by extracellular ligands (GCA), the other one is a soluble heme-containing enzyme (sGC), found in many tissues (62). *Dictyostelium* guanylyl cyclase A (GCA) has 12 membrane spanning domains, whereas conventional membrane-bound GCs have only one transmembrane region (57). Because most drugs or mutations that interfere with signal transduction alter the magnitude but not the timing of the cGMP response, the kinetics is considered robust (63).

In 1975, Putnam and Pedersen (64) described the discovery of a 3‘,5‘-guanosine monophosphate stimulating factor in *Dictyostelium*. Later, Mato and co-workers showed that folic acid also stimulates cGMP accumulation, and that cGMP function and hydrolysis is mainly intracellular. This was the first description of a

cGMP phosphodiesterase (PDE) activity in *Dictyostelium* (65). Cyclic GMP formation was shown to be dependent on the concentration of cAMP added to starved cells. Within 2s after the addition of cAMP, the cellular cGMP concentration increased 3-6 fold and reached a peak at 10s, recovering in 30s the pre-stimulating levels (66, 67). Further, the addition of ATP (0.2mM) caused a 2-3 fold activation of guanylyl cyclase, additive to that induced by cAMP (67). The estimated number of cGMP receptors (binding proteins) per cell is sufficient to mediate the transduction of a physiological cAMP signal (68).

The first studies of the role of cGMP reported that, during chemotaxis, cGMP regulates the association of myosin II with the cytoskeleton. The KI-10 (chemotaxis defective) mutants show less regulation by cGMP (58, 61) and the streamer F mutant (stmF) NP368 (cGMP-specific phosphodiesterase deficient) shows a delay in the phosphorylation of myosin II light chain (69), suggesting that cGMP regulates the myosin response (70). Myosin II phosphorylation could also be dependent on the action of Ca^{2+}-calmodulin, which would induce an increase in myosin heavy chain (MHC) accumulation in the cytoskeleton (71). In metazoans, cGMP can bind to cGMP-dependent protein kinases (PKGs), cGMP gated ion channels, cAMP/cGMP-regulated Ras, and cGMP-regulated phosphodiesterases.

Four cGMP-binding proteins were identified in *Dictyostelium* and named GbpA-D (72). GbpA and GbpB were shown to encode cGMP-stimulated PDEs and have a cNB domain that mediates activation by cAMP or cGMP, and a Zn^{2+}-hydrolase domain. GbpC and GbpD are cGMP target proteins with Ras-homologous domains, a protein kinase and a Ras-GEF. GbpD is homologous to the C-terminal part of GbpC and also contains a Ras-GEF domain, a GRAM domain, and two cNBDs (73).

In *Dictyostelium*, cGMP is synthetized by guanylyl cyclase A (GCA) and soluble guanylyl cyclase (sGC) (55). Both GCA and sGC are activated *in vivo* by folic acid and cAMP (74). Cells lacking sGC activity do not recruit myosin II to the cytoskeleton in response to cAMP and cannot maintain a polarized morphology (55). The sCG protein is localized in the pseudopodia and at the leading edge, while cGMP supresses pseudopod formation in the back and sides of the cell (75). The *Dictyostelium* guanylyl cyclase regulates the magnitude but not the timing of cGMP response, and is strongly inhibited by Ca^{2+} ions (63). Guanosine triphosphate (GTP)

is not only a substrate but also a regulator of guanylyl cyclase activity (76). At least three phosphodiesterases (PDEs) degrade cGMP: PDE3, cGMP-binding protein A (GbpA) and GbpB, a dual specificity PDE that can be activated by cAMP and cGMP (55). Altogether, there are six known PDEs enconding genes in *Dictyostelium* (74), the first characterized was named DdPDE3. DdPDE3 is not activated by cGMP and shows similarity to mammalian PDE9 (77). DdPDE1 (PdsA) is a PDE that degrades extracellular cAMP and cGMP. DdPDE2 (regA) is a cAMP-specific PDE in the cytosol that degrades intracellular cAMP. DdPDE4 is a PDE mainly expressed in the multicellular stage of development, and is involved in the degradation of cAMP. DdPDE5 (also called GbpA or PDED) is a cGMP-stimulated cGMP-specific PDE. Finally, DdPDE6 (also GbpB or PDEE) degrades cAMP and to a minor extent also cGMP inside the cell. DdPDE7 is a close homologue to DdPDE1 with different kinetics (78).

After stimulation, intracellular cGMP can reach a concentration of 3μM. DdPDE5 is the predominant enzyme involved in cGMP degradation. At 0.03μM cGMP (basal level), both DdPDE3 (40%) and DdPDE5 (60%) contribute to cGMP degradation, and at very high levels DdPDE6 becomes increasingly more important (78). Different than in other organisms, no cGMP-binding protein is known to be associated to protein kinase stimulation in *Dictyostelium*, excluding that protein kinase G (PKG) is a target of cGMP (79). Cyclic GMP production appears to be regulated by Ras subfamily GTPases and the small GTPase Rap1 promotes cGMP production under osmotic stress. Rap1 is known to control cell adhesion in mammalian cells. It was shown that in *Dictyostelium* it also regulates cell polarity and motility by controlling myosin II function (80). Phosphorylation of myosin is probably not the only target of intracellular cGMP, because cells with a deletion in the myosin heavy chain display normal chemotaxis and mutants with impaired cGMP synthesis show no chemotaxis (63).

In *Dictyostelium*, osmotic stress induces the activation of guanylyl cyclase and leads to myosin phosphorylation and filament redistribution (81). Cyclic GMP peaks 10s after chemotactic stimulation, and after 10min under osmotic stress. Chemoattractant receptors and G protein mediate guanylyl cyclase for chemotaxis but not for osmotic stress (82). Thus, osmo-regulation and chemotaxis use different detectors, but share the same cGMP pathways (63). It was shown that in response to

hyperosmotic stress, actin structures are reorganized and contract into bundles, a process controlled by cofilin in a myosin II-independent manner (83).

The non-chemotactic mutants KI-4 and KI-7 have an aberrant cGMP binding activity, and an altered cGMP response. This suggested that chemoattractants stimulate guanylyl cyclase that further binds to a cGMP-binding protein, activating even more the guanylyl cyclase and transducing the signal downstream to myosin (84). A model for cGMP signaling in *Dictyostelium* has been proposed by Bosgraaf and co-workers (73). There, cAMP stimulation transiently activates the guanylyl cyclases sGC and GCA, leading to an increase in cytosolic cGMP. Cyclic GMP binds to GbpC, a high affinity cGMP binding protein, and is degraded by the PDEs GbpA and GbpB. The increase of cGMP is transient, and cGMP binding reaches a maximum at 15s after stimulus, with a half-time complex dissociation at 90s. Activated GbpC contributes to myosin RLC (regulatory light chain) phosphorylation, necessary for myosin II motor activity. Binding of cGMP to GbpC also induces MHC (myosin heavy chain) phosphorylation, which is essential for myosin II filament assembly. This maintains cell shape and polarization in a gradient of chemoattractant. Recently, the same group concluded that GbpC and GbpD have different functions in *Dictyostelium* chemotaxis and act via different signal transduction pathways (34). GbpC is regulated by cGMP and is needed for myosin translocation and cell polarisation, whereas GbpD does not depend on intracellular cyclic nucleotides and induces surface-attached lateral pseudopodia. GbpD could then act in a signal transduction pathway that influences actin polymerization. This is supported by the observation that cAMP induced actin polymerization in GbpD overexpressing cells has a delayed recovery compared to that of wild-type cells (34).

Cyclic GMP enhances cAMP-induced Ca^{2+} influx, but those results are still controverse since they were shown only for stmF mutants (85). In PDE knock out cells, elevated cGMP concentrations inhibited Ca^{2+} influx (85). Cyclic GMP binds to a bovine cyclic-nucleotide-Ca^{2+}-gated channel and it is hypothesized that a similar channel could exist in *Dictyostelium discoideum* (86).

Persistent movement is observed if cells extend a series of pseudopodia in the same direction. When a cell is exposed to a gradient of chemoattractant, it shows actin polymerization in the front region and recruitment of filamentous myosin II in the tail. After the stimulus, the assembly of myosin II in the cell cortex takes around 20s

and since cGMP peaks at 10s, filamentous myosin from the cytoplasm is probably shuttled to the cell cortex downstream of cGMP (12). Calculating the contribution of signaling pathways to persistence and orientation showed that PLA2 (phospholipase A2) and cGMP modulate persistence (87). Only a small amount of the produced cGMP is secreted, the major part is degraded by a cGMP specific phosdiesterase. Effects of extracellular cGMP in *Dictyostelium discoideum* cells are not known (88).

1.8 Phospholipid signalling

Phosphoinositides (PPIs) are important second messengers that can recruit actin-binding proteins to defined subcellular sites and alter their activity (89). Chemotaxing neutrophils and *Dictyostelium* amebae produce in their plasma membrane gradients of phosphatidylinositol 3,4,5-triphosphate (PIP_3), which are orientated with the external chemotactic gradient. PPIs have been proposed to act as an internal compass, guiding the movement of the cell (11). PIP_3 gradients in the plasma membrane are formed by the receptor-driven redistribution and activation of the corresponding metabolic enzymes. Type 1 phosphoinositide 3-kinase (PI3K), converting phosphatidylinositol 4,5-bisphosphate (PIP_2) into PIP_3, is recruited to the front region of the cell (90-92), whereas the PTEN (phosphatase and tensin homolog) phosphatase is located at the back of the cell (93). The production of PIP_3 is regulated by PI3K, whereas its dephosphorylation is mediated by PTEN and SH2 domain-containing inositol phosphatase (SHIP) (94). PIP_2 is hydrolized by phospholipase C to generate two important second messengers, inositol 1,4,5-triphosphate (IP_3) and diacylglycerol (DAG) (89). It is not known how phosphoinositides change actin dynamics, but most likely changes in the levels of cellular PPIs alter the function of actin binding proteins and signalling pathways regulated by GTPases, ion channels, and protein kinases (95).

One of the largest groups of PIP_3-binding proteins are the pleckstrin-homology (PH) domain-containing proteins. PH domain-containing proteins that bind to PIP_3, for example the cytosolic regulator of adenylyl cyclase (CRAC), AKT/protein kinase B (PKB), and PH-domain-containing protein A (PhdA), are highly localized at the front of chemotaxing cells. The PH domain has seven stranded β-sandwiches formed from two near-orthogonal β-sheets. There are around 100 PH domain-containing proteins in *D. discoideum* (94).

Translocation of PH-$_{CRAC}$-GFP to the membrane of *Dictyostelium* cells has two phases: a transient translocation to the entire membrane followed by continuous translocation to smaller areas of the cell (8). Receptor-stimulated PI3K activity leads to the formation of the PH-$_{CRAC}$ patches, and they are supposed to enhance chemotactic movement by increasing the cAMP sensitivity and amplitude of cAMP-induced pseudopod extensions. Low concentrations of cAMP can still induce the patches, but the concentration does not affect the size and fluorescence intensities of the patches. Those patches are thought to be self-organizing structures (8). Cyclic AMP can induce PH-$_{CRAC}$ patches even in cells treated with Latrunculin A, an F-actin disrupting agent (96). Because the receptor-mediated PIP_3 response does not fully adapt to constant cAMP levels, this partial adaptation, together with the cGMP-mediated myosin filaments, could be enough to inhibit pseudopod formation in the back of the cell. The advantage of such an adaptation would be the temporal and spatial information provided by the PI3K pathway, that could make the cell change the direction of the movement when the direction of the chemoattractant also changes (8).

PIP_3 diffuses about 100 times more slowly than intracellular second messengers like cGMP, cAMP and IP_3. Because of that, high local concentrations can be maintained (8). PIP_3 is thought to participate in a positive-feedback loop (figure 8), comprising GTPase Ras, PI3K, PIP_3 and F-actin. This positive feedback loop is a regulatory pathway used by cells to modulate the cytoskeleton, with or without the activation of an extracellular stimulus (97, 98). *Dictyostelium* amebae can extend pseudopodia in the absence of PI3K activity, but a pseudopodium is preferentially formed at a region of the cell with a PH-$_{CRAC}$ patch (8, 96).

A quintuple PI3K knockout mutant, of all *Dictyostelium* PI3Ks (PI3K 1-5^{-}), and a sextuple mutant with PTEN knocked out in addition (PI3K1-5^{-}, PTEN^{-}), show a similar increase in F-actin content after global stimulation of the cells and a polarized overall distribution of F-actin at the front and rear when in a cAMP gradient. Cells of the sextuple mutant can still chemotax efficiently towards a micropipette releasing cAMP. The speed of random motility, which is the movement without externally applied chemotactic gradients, is severely impaired in those mutants, suggesting a role for PIP_3 in basal motility. PIP_3 is most likely involved in regulating the rate of pseudopod formation and in maintaining their subsequent stability (91).

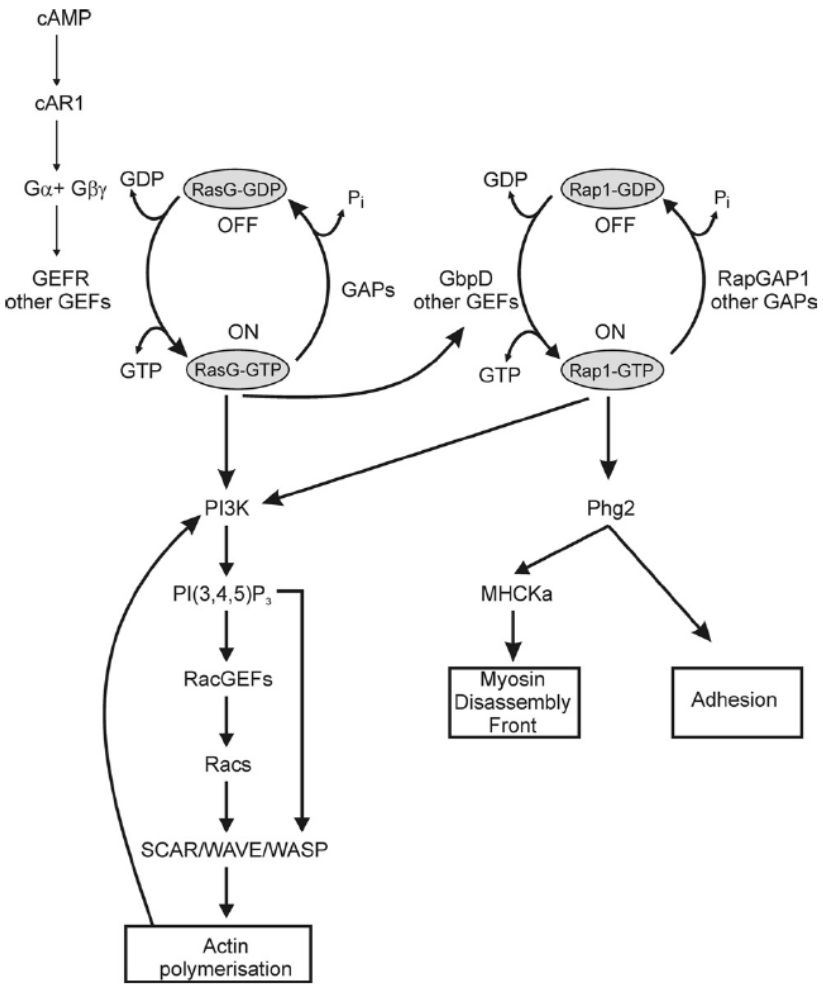

Figure 8 - Phosphoinositide signaling and the role of RasG proteins (Ras proteins activated by cAMP). RasG activation is essential for the regulation of PIP_3 signaling, and also for the amplification of the initial signal, the initiation of cell polarity, and actin polymerization. Rap1 interacts with PI3K, and its activation in response to cAMP occurs downstream of RasG. Figure taken from (98).

The protein N-WASP, normally in an inactive state, binds PIP_2 and exposes the binding sites for actin and the Arp2/3 protein complex. The Arp2/3 complex then nucleates the assembly of actin filaments and forms branches between the actin filaments. The ATP-consuming polymerization of actin does mechanical work that produces forces sufficient to propel the cell membrane forward (99).

There are three models for the PPI regulation of actin-binding proteins. The most simple one is that an actin-binding protein site coincides with a PIP_2-binding site and targeting of the protein to PPI-rich membranes dissociates actin competitively. Another model is that the binding to PIP_2 causes a rearrangement of actin-binding domains or a local unfolding of polypeptide within these domains, deranging the

surface required to bind actin. The third mode of binding would be when the protein docks to the membrane in a manner that disrupts interactions between domains that mask binding sites for actin or membrane anchors (89). PIP_2 is produced locally at the plasma membrane and recruited to the negatively charged inner leaflet in response to an external signal.

1.9 Cytoskeleton-disrupting drugs

Many actin-targeting natural products are known, and they provide a valuable tool to manipulate the cytoskeleton in living cells. The actin-targeting natural products have usually common structural features such as a primarily hydrophobic component and complex side groups. They can be divided according to their function in either destabilizing (inhibitors) or stabilizing agents of actin assembly. Because actin filaments are dynamic, the filament-destabilizing compounds can be also divided in those that only sequester actin monomers after their dissociation from the filament, and those that actively sever the filaments by binding directly to them and disrupting the interactions between the actin monomers (100).

The latrunculins are the first class of marine natural products that were found to bind to actin and disrupt its organization (101). Latrunculin is purified from *Negombata magnifica*, a red sea sponge that exudes a fluid that can kill fishes in minutes. Latrunculin A and B, isolated from the fluid, were shown to depolymerize actin *in vitro* and *in vivo* (102). Latrunculin A (LatA, figure 9) binds within the interface between actin subdomains 2 and 4, above the ATP-binding site. It inhibits adenine nucleotide exchange on actin, limits the flexibility of the cleft, and traps nucleotides, resulting in the inhibition of nucleotide exchange. The effects of LatA on cells *in vivo* may be changed by the effect of the drug also on actin binding proteins, and not only simple monomer sequestration (103).

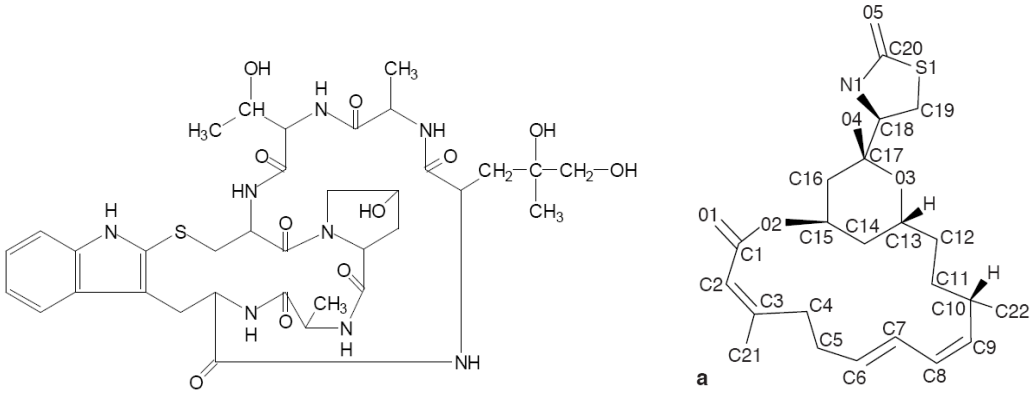

Figure 9 - Structure of the Phalloidin-conjugate (left) and of Latrunculin A (right) (102).

The fungal metabollite phalloidin was isolated in 1937 as one of the toxic peptides derived from the mushroom *Amanita genus*. Phalloidin induces the formation of microfilament-like structures *in vitro* and *in vivo*, and coupled to fluorescent dyes, was one of the first cell stains for F-actin used (104). In the present work, I used a fluorescent conjugate (figure 9) of phalloidin to quantify F-actin in cells exposed to Wiskostatin.

New molecules that target the actin system have been found with the help of combinatorial chemistry and high-throughput bioassay screening. Wiskostatin (figure 10), an inhibitor of N-WASP, was found in this way. Wiskostatin is a derivative of carbazole, with the carbazole backbone symmetrically brominated at the 3- and 6-positions, and an N-propyl side chain carrying a hydroxyl group at the 2-position and a dimethylamino function at the 3-position (105). It inhibits N-WASP by stabilizing its autoinhibited conformation, preventing subsequent activation of the Arp2/3 complex (104) by binding within a pocket in the GBD regulatory region. Wiskostatin inhibits actin assembly in response to PIP_2 in a dose-dependent manner. Both enantiomers are equally potent. Most likely, Wiskostatin can also target other components in a cell, in particular, other members of the WASP family (106).

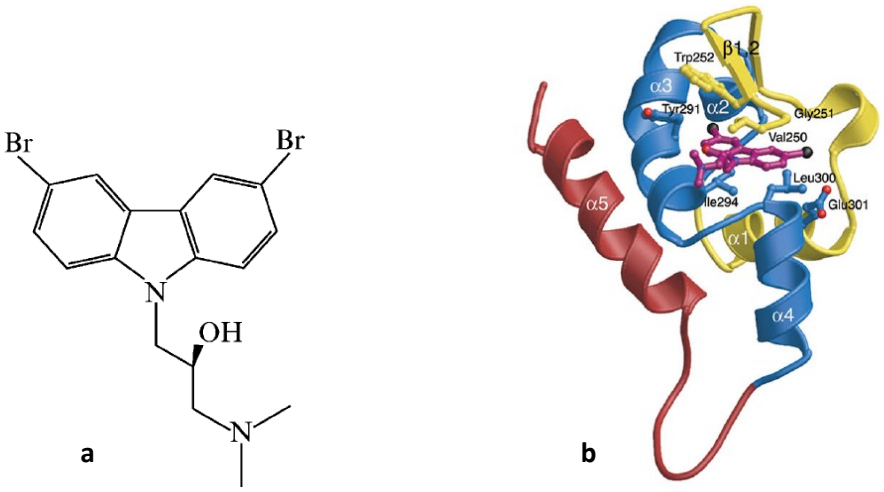

Figure 10 - (a) Structure of Wiskostatin and (b) structure of Wiskostatin bound to mini-WASP. From references (106) and (105).

Another way of severing actin filaments by drugs is by targeting phospholipids or the phospholipid production. Gelsolin is an actin-binding protein of the actin-severing gelsolin/villin superfamily, which severes actin filaments. It can be differentially activated by Ca^{2+} and polyphosphoinositides. Between the residues 150-169 of gelsolin, there is a PPI binding site regulating filament severing. Synthetic peptides based on this sequence bind tightly to PPIs. These peptides also bind with moderate affinity to F-actin (107). The amino acid sequence QRLFQVKGRR competes with intact Gelsolin for binding PPIs. A fluorescence derivative of this peptide with rhodamine B was synthesized and named PBP10. PBP10 is cell permeable, and besides binding to PPIs, also strongly stimulates the enzymatic activity of PI3K *in vitro* (108). I used PBP10 to study the effect of phospholipid signalling on cell motility and cytoskeleton dynamics.

1.10 Cell mechanics and microfluidics

The mechanical properties of a cell are determined by the cytoskeleton. In particular, the subcortical actin network contributes to the elastic response of cells and was studied by the use of modulators of actin polymerization (109). The cytoskeletal network is not only controlled by the amount of F-actin, but also by accessory proteins that bind to actin. Small changes in the concentration of actin-

binding proteins dramatically alter the elasticity of F-actin, that determines the stiffness of the network (110).

Depolymerization of actin filaments by drugs softens cells, and alters other physical properties, like cellular viscosity. The analysis of cell mechanics can predict complex cell characteristics, such as motility (109). Currently, cell mechanics is mostly studied by microrheology and atomic force microscopy. For global cell mechanics measurements micropipette aspiration, microplate manipulation, optical stretching and microfluidic deformation are used (109).

Microfluidics is a technology to manipulate fluids in networks of channels with dimensions of about 5-500µm. To construct microfluidic channels, soft litography based on poly(dimethylsiloxane) (PDMS) is used. PDMS is well suited for biological experiments, because it is soft, electrically insulating, flexible, transparent, unreactive, and permeable to gases. It has a surface that can be oxidized, allowing PDMS to seal to other surfaces, like glass (111). PDMS consists of repeating –$OSi(CH_3)_2$ units. The CH_3 groups are responsible for making the surface hydrophobic, but different techniques are available to readily change it to a hydrophilic surface (112). PDMS microfluidic systems have many applications in cell biology, including cytoskeleton research, the study of cell-substrate adhesion, cell sorting, and many more (113). In our microfluidic *cell squeezer* device, we quantify the deformation of cells exposed to Latrunculin A and Wiskostatin.

1.11 Caged compounds

Caged nucleotides like caged cAMP or caged cGMP are nucleotide analogs with an esterified phosphate terminal carrying a blocking group that makes the molecule biologically inactive (114). It is important that the caged analog is biologically inert and solvolytically stable. The uncaging reaction should be rapid and with a high quantum yield, without generating toxic side products. (115). Caged biomolecules can be introduced into living cells without evoking any biological response and are useful for *in situ* studies of cellular processes (116). Flash photolysis permits the release of the probes in a spatiotemporally controlled manner. Many caged compounds carry a nitrobenzyl group for the photochemical reaction, activated by light with a wavelength in the range of 300-400nm (117).

In contrast to cAMP and cGMP, 8-Br-cAMP and 8-Br-cGMP are poorly hydrolized by phosphodiesterases and display a higher biological efficacy and membrane permeability. DMACM ([7-(dimethylamino)coumarin-4-yl]methyl) and DEACM ([7-(diethylamino)coumarin-4-yl]methyl) esters of 8-Br-cAMP and 8-Br-cGMP combine high solvolytic stability and rapid photorelease with long wave length absorption and high extinction coefficients, enabling photorelease under non-damaging conditions (118). Here, I use photoactivation of DMACM-caged-8-Br-cGMP to study the effect of intracellular cGMP release on the cortical dynamics of actin and myosin II.

The goal

Ameboid cell motility is mediated by the actin cytoskeleton. In a chemotaxing *Dictyostelium* cell, membrane receptor signals transmit the chemoattractant stimulus to the actomyosin system, leading to actin-driven pseudopod formation at the leading edge and to myosin II-mediated contraction at the uropod of the cell, see figure 11.

It is the goal of this work to study the regulatory mechanisms that govern the different aspects of cell motility. For each stage of this process – actin dynamics, myosin II dynamics, and upstream receptor signaling – a key player of the pathway was chosen to exemplarily study the underlying regulatory mechanisms:

- the regulation of the Arp2/3 complex by WASP and its effects on the actin cytoskeleton;
- the role of cGMP on myosin II assembly;
- the role of the phosphoinositide signaling.

To achieve these objectives, drug exposure experiments and the photochemical release of signaling molecules were used:

- the carbazole derivative Wiskostatin, an inhibitor of the Arp2/3-activator WASP;
- DMACM-caged-8-Br-cGMP to release cGMP in a spatiotemporally controlled manner;
- the peptide PBP10, that binds to phosphoinositides.

Signal transduction in eukaryotic cells is highly complex, and often many parallel pathways exist. Because of that, *D. discoideum*, a well-established model organism for studies on the cytoskeleton and on cell motility, was chosen for my experiments. The solid existing knowledge about *Dictyostelium* and its life cycle provided a basis for my analysis of the regulatory mechanisms of cell motility.

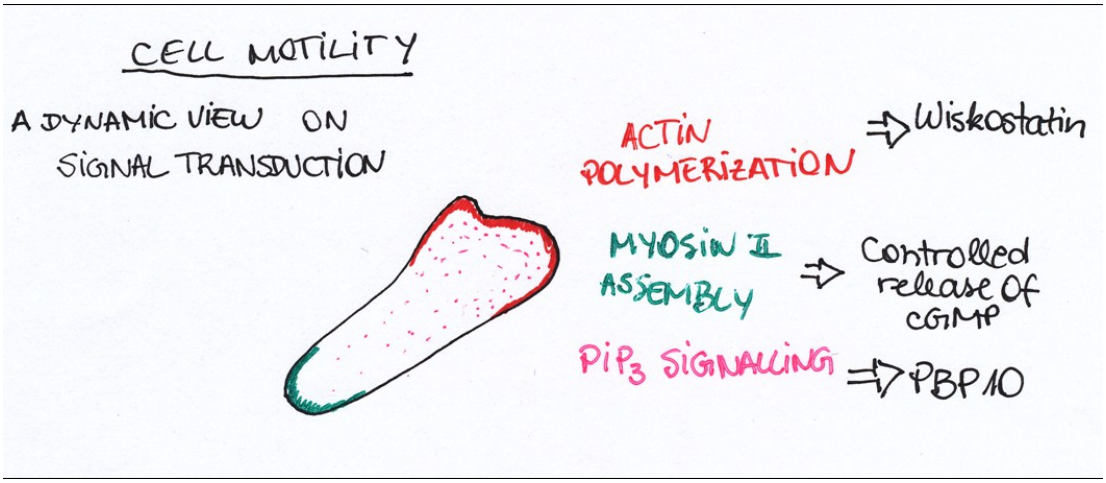

Figure 11 - A view on the three regulatory systems analyzed in this work: the actin dynamics, the myosin II dynamics, and the upstream receptor signaling by phosphoinositides. To investigate actin polymerization I used Wiskostatin, to study myosin II assembly cGMP was released in a controlled manner, and to analyze the phosphoinositide dynamics the peptide PBP10 was used.

To achieve my goal, I performed live-cell experiments using different techniques of optical microscopy, microfluidics, and customized data analysis tools, along with well-known biochemical assays to complement the results.

2 Materials and Methods

2.1 Solutions and media

Sørensen buffer: 14.6 mM KH_2PO_4 (Merck, Darmstadt, Germany), 2 mM Na_2HPO_4 (Merck, Darmstadt, Germany), pH 6.0.

HL-5 medium (Formedium, Hunstanton, UK): Nutrient medium for axenic cultures.

Cell Lysis buffer: 7M Urea (Sigma-Aldrich, Taufkirchen, Germany), 2M thiourea (Sigma-Aldrich Germany), 0.1% Triton X-100 (Applichem, Darmstadt, Germany), 10mM Tris base (Applichem, Darmstadt, Germany), 600µL protease inhibitor cocktail (Sigma-Aldrich, Taufkirchen, Germany) for 6mL total volume of buffer, 50mM Dithiothreitol (DTT, from Applichem, Darmstadt, Germany).

F-actin assay solutions: 6% paraformaldehyde

0.1% Triton X-100 (Applichem, Darmstadt, Germany)

1% BSA/phosphate buffer (Bio-Rad, München, Germany)

0.2µg/mL TRITC-phalloidin (Fluka, Sigma-Aldrich, Taufkirchen, Germany)

Methanol (Roth, Karlsruhe, Germany)

Bacteria transformation solutions:

Ψb-Medium: 5g yeast extract, 20g peptone, 5g $MgSO_4$, pH= 7.6.

TfbI: 30mM KAc, 100mM RbCl, 10mM $CaCl_2 \cdot 2H_2O$, 15% Glycerin, 50mM $MnCl_2 \cdot 4H_2O$, pH=5.8.

TfbII: 10mM MOPS, 75mM $CaCl_2 \cdot 2H_2O$, 10mM RbCl, 15% Glycerin, pH= 6.5.

(All reagents from: Applichem, Darmstadt, Germany).

Dictyostelium transformation solutions:

Electroporation buffer: 50mM sucrose (Applichem, Darmstadt, Germany), 10mM KH_2PO_4 (Merck, Darmstadt, Germany), pH= 6.1.

0.1M $CaCl_2$ and 0.1M $MgCl_2$ (Applichem, Darmstadt, Germany).

2.2 Other Chemicals

Adenosine 3‘,5‘-cyclic monophosphate, 99% (Sigma-Aldrich, Taufkirchen, Germany)

DMACM-caged-8-Br-cGMP (7 - Dimethylaminocoumarin- 4- yl)methyl- 8 bromoguanosine- 3', 5'- cyclic monophosphate), (Biolog, Bremen, Germany)

cGMP (Guanosine 3,5-cyclic monophosphate) (Sigma-Aldrich, Taufkirchen, Germany)

Br-cGMP (8-Bromoguanosine 3,5-cyclic monophosphate sodium salt), (Sigma-Aldrich, Taufkirchen, Germany)

DMAC (7-Dimethylamino-4-methyl-coumarin) (Sigma-Aldrich, Taufkirchen, Germany)

Dihydroethidium (for fluorescence) (Sigma-Aldrich, Taufkirchen, Germany)

Trypan blue (Applichem, Darmstadt, Germany)

G418 disulfate (Applichem, Darmstadt, Germany)

Bio-Rad Protein Assay (Bio-Rad, München, Germany)

Hygromycin B, 50mg/mL (Roth, Karlsruhe, Germany)

Wiskostatin (Calbiochem, Merck Chemicals, Nottingham, UK)

Polyphosphoinositide-Binding Peptide, PBP10 (Calbiochem)

Latrunculin A (Sigma-Aldrich, Taufkirchen, Germany)

PDMS (Dow Corning GmbH, Wiesbaden, Germany)

Sylgard 184 (Dow Corning GmbH, Wiesbaden, Germany)

Fluorescein (Acros Organics, Fisher Scientific GmbH)

Fluorescein diacetate (Sigma-Aldrich, Taufkirchen, Germany)

Propidium iodide (Sigma-Aldrich, Taufkirchen, Germany)

2.3 Cell culture

D. discoideum cells were cultivated in HL-5 medium (Formedium, Hunstanton, UK) at 21± 2^{o}C. For cell motility assays, cells were washed two times in Sørensen phosphate buffer or kept in cell medium (assays with vegetative cells). For pulsing, cells were shaken until a density of 1x10^{7} cells/mL and pulsed with a 21.5µM cAMP solution, with 3 drops every 6 minutes to create a 50nM cAMP pulse concentration in the shaking flask.

2.4 Transformation and Electroporation

SCAR-GFP and WASP-GFP vectors were kindly provided by Veltman and Insall (*Beatson Institute for Cancer Research, UK*). Competent *E. coli* cells were transformed and plasmid DNA isolated using the kit Nucleo Bond PC100 and Nucleo Spin Extract II (Macherey-Nagel, Düren, Germany). Bacteria were made competent in Ψb-Medium at 37^{o}C, incubated on ice, and resuspended in TfbI. After 5 minutes incubation on ice, cells were centrifuged and resuspended in cold TfbII. The frozen competent cells were incubated with 100ng DNA and heat-shocked at 42^{o}C for 90s. After the heat-shock, bacteria were shaken at 37^{o}C for 60 minutes (140 rpm) and subsequently plated in Ampicillin agar plates. For the electroporation of *Dictyostelium* cells, 5x10^{7} cells in total were cooled until 4^{o}C, centrifuged, and washed with Sørensen phosphate buffer. Afterwards, cells were washed in 10mL electroporation buffer, centrifuged, and resuspended in 700µL electroporation buffer. Approximately 15-30µg plasmid was added to a pre-cooled 4mm cuvette, together with the 700µL cells. The electroporation was done using the Gene Pulser Xcell System (Bio-Rad, München, Germany) equipment, at 3µF, 1.1kV, in 2 pulses, with 5s interval. The cell suspension was transferred to a microtube and incubated for 10 minutes at room temperature. 7µL of $CaCl_2$ and $MgCl_2$ solutions (from a 0.1M stock) were added, and cells gently shaked for 15 minutes. Cells were then plated in dishes with HL5 medium and selected with Hygromycin (50µg/mL). Fluorescence was checked using a confocal microscope (LSM 710, Carl Zeiss Microimaging, Jena, Germany).

2.5 Cell lines

In this work, several *Dictyostelium discoideum* cell lines were used (see next table).

Cell line	Construct	Origin	Marker
MyoII-GFP + mRFP-LimEΔ	Myosin II-GFP LimEΔ-GFP, AX2	G. Gerisch	B10/ G10
Wf38	PH-$_{CRAC}$, AX3	P. Devreotes	G10
AX2-WT	none	R. Gräf	none
SCAR-GFP	SCAR A, AX2	Veltman/Insall	Hyg
WASP A-GFP	WASP A, AX2	Veltman/Insall	Hyg
G=G418 (geneticin) - stock 20mg/ml B=Blasticidin - stock 10mg/ml, used 1µL/mL Hyg= Hygromycin, stock, used 1µL/mL			

2.6 Microfluidics – Fluidic cell squeezer

One of the main effects of cytoskeleton disrupting drugs in cells is the loss of their cellular mechanical stability. The cells get softer and can easily be deformed, not recovering from abrupt deformations. To compare the effect of mechanical deformations in non-treated and drug treated cells, I used a microfluidic device developed by Wegner C (119). The experiments were also performed with the help of Christian Wegner. The microfluidic structure is based on several studies (120-122). The angle of the channel wall is 45^{o} with respect to the flow, and 5 equal triangles were designed in order to have five constriction sites (see figures 12 and 13). At each constriction site the flow speed and, due to the no-slip boundary condition, also the shear stress on a passing object, increase. The width of the constriction sites are 20µm. The length, width, and height of the channel were l=400µm, w=100µm, and h=20µm, respectively. An automated syringe pump (Hugo Sachs Elektronik - Harvard Apparatus GmbH, March-Hugstetten, Germany) was used to maintain a steady flow of cells in buffer, or cells-buffer-Wiskostatin mixture.

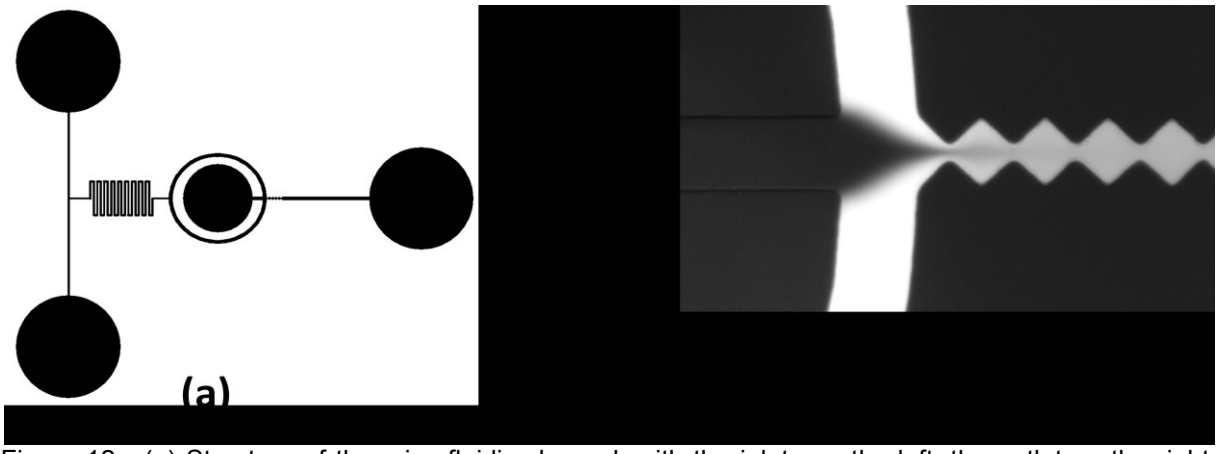

Figure 12 - (a) Structure of the microfluidic channel, with the inlets on the left, the outlet on the right and the folded channel for diffuse mixing. (b) Focused fluid stream (Fluorescein and buffer) showing the mixing of the solutions of the three inlets, and the entrance of the zig-zag channel imaged during the experiments. Adapted from (119).

Soft lithography, in order to get a master wafer, was done as stated in (123). In a laminar flow bench, the master wafer was cleaned with acetone, isopropanol, and deionized water. Afterwards, the wafer was dried with air. PDMS and curing agent (Sylgard 184, Dow Corning GmbH, Wiesbaden, Germany) were added, in a 10:1 proportion. Elastomer and curing agent were mixed and placed on the top of the master wafer, inside a weighting boat. Everything was put into a desiccator and evacuated for about 1h, until all air bubbles disappeared. Then the weighting boat was placed in an oven at 75^{o}C for 1h, and cooled back to room temperature. The PDMS around the microstructure was cut, peeled off, and the side with the structure protected with scotch tape. A clean polished needle was used to punch holes for the inlets and outlets. Together with a clean coverslip, the PDMS piece was placed inside a plasma cleaner. The plasma cleaner was evacuated and operated for 2.5 min, oxidizing the PDMS and the glass surface of the coverslip. Both were then put in contact with each other so that stable Si-O-Si bonds formed at the interface. The microchannel is sealed and ready for use. Two different experimental types were done, a) control experiments and b) Wiskostatin experiments. Solutions with a.1) buffer, a.2) buffer and cells or b.1) buffer and drug, and b.2) buffer and drug and cells, were prepared and filled into 250µL glass syringes (Hamilton Bonaduz AG). For the experiments with beads, polystyrene microspheres with 10µm diameter (Polysciences, Warrington, US) were used instead of cells. The Teflon tubing was

connected to those syringes. They were filled, and placed in the syringe pump (Hugo Sachs Elektronik - Harvard Apparatus GmbH, March-Hugstetten, Germany).

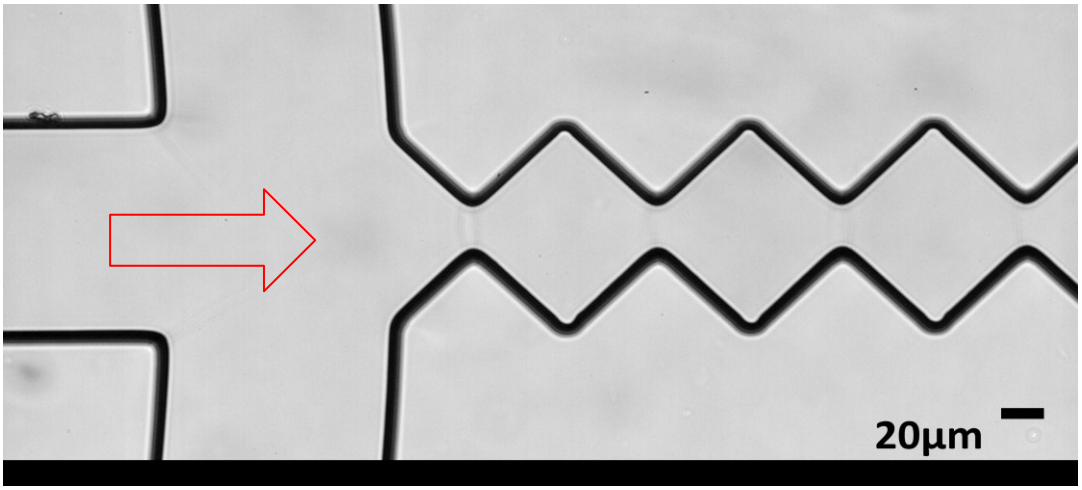

Figure 13 - Cutout of the microfluidic channel, and direction of cell flow (red arrow). At each bottleneck constriction, the enhanced shear stress squeezes the cells. Scale bar shows a length of 20µm.

The average flow speed was 1mm/sec in the wide sections and 4.1mm/sec at the narrow constriction sites of the channel. The folded channel before the main channel guaranteed a uniform flow and mixture of buffer and drug, and also centered the cells entering the channel. Images were recorded with a resolution of 1280 × 305 pixels at 800 frames/sec using a CMOS camera (EoSens MC1362, Mikrotron, Unterschleißheim, Germany) mounted on an inverted Olympus IX71 microscope. Images were analyzed with a custom-made MATLAB program to quantify the roundness of the cells based on the isoperimetric inequality, see also section 2.10.

The data for the isoperimetric quotient of all cells was averaged and then divided by the plateau (the beginning of each data set, about 6 to 8 data points, before the cell entered the first constriction site). Since there were four constriction sites, each response of the cell was divided by its preceding plateau value. The average of the four responses was calculated. In a control experiment, I repeated the analysis with non-deformable polystyrene beads. The resulting dataset was subtracted from the cell response curves. This was done to exclude a possible bias in the shape detection of the high speed objects that were recorded with too long exposure times. The curve obtained after the subtraction of the cell-curves minus the beads-curve is the subtracted or corrected data set.

2.7 Cell motility assays

For the random motility experiments, AX2-WT cells were incubated in medium (experiments with vegetative cells) or Sørensen buffer (experiments with developed cells). For the experiments with developed cells, cells were pulsed as stated in section 2.3. Control cells and drug-exposed cells were placed in an 8-well slide (Ibidi, Martiensried, Germany), and imaged in parallel using an IX71 inverted microscope (Olympus, Hamburg, Germany), with conventional brightfield illumination through a LUC PLAN FLN 20x/0.45 objective (Olympus, Hamburg, Germany). Images were recorded every 10 seconds for 4 hours with an Olympus F-VIEW Camera and transferred to a personal computer for further processing.

For the chemotaxis experiments, LimEΔ-GFP cells (AX2) were pulsed as described in section 2.3. Cells were plated in a glass bottom dish and imaged on a Zeiss LSM 710 microscope (Carl Zeiss Microimaging, Jena, Germany), with one image taken every 10s. A Femtotip pipette (Eppendorf, Hamburg, Germany) filled with 10^{-4}M cAMP was placed in the middle of the field of view.

The cell motility analysis was done together with Matthias Theves. To extract the cell centroid positions (figure 14) we segmented each image using *Sobel edge detection* and standard thresholding techniques (124, 125). From the binarized images, cell positions were calculated as the center of mass of every interconnected region.

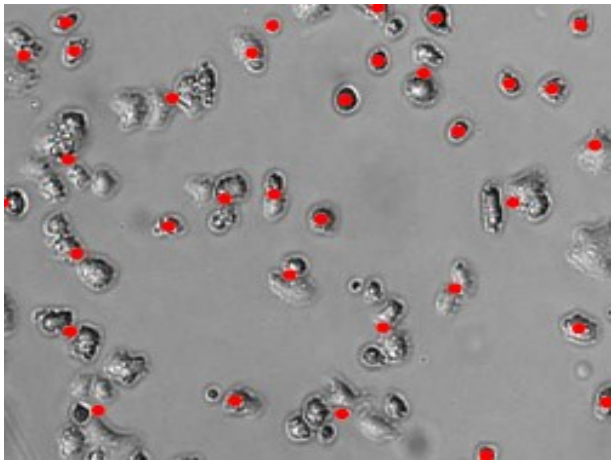

Figure 14 - Cell centroid positions in the original image (brightfield). Note that the code sometimes identifies more than one cell as a single cell. If too big, cell aggregates are excluded from the data analysis.

Positions of all cells on every image were then linked together to form trajectories in time using a customized version of the tracking algorithm written by Crocker and Grier (126), see figure 15. In this algorithm, the most probable set of two cell positions in two consecutive time frames is determined by minimizing a cost function Υ, which is the sum over all possible distances for a given set of cell links:

$$\Upsilon = \sum_{i=1}^{N}(r_{i,t} - r_{i,t+1})^2$$ Based on reference (126).

Here, $r_{i,t}$ is the location of the cells on an image with *N* cells at time *t*.

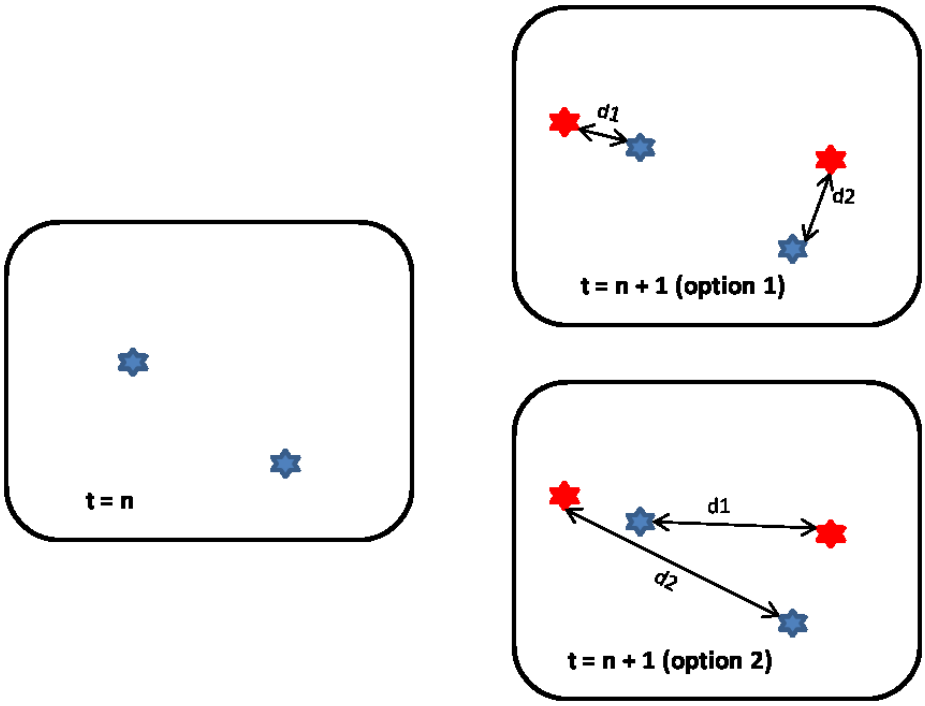

Figure 15 - A graphical explanation of the cost function. ∑*di* = *d1*+*d2* should be the minimum possible. The algorithm selects the lowest sum of the possible distances, here: Option 1.

The customized program is based on the work by Theves, M (125). The velocities were calculated from finite, euklidean distances. The average motility in a given experiment was defined as an ensemble and time average, the average velocity of all cells at all times during the whole observation period. The chemotactic index (CI), the distance a cell has moved in direction of the chemotactic stimulus, divided by the total distance travelled, was calculated for each cell trajectory longer than 5 minutes.

The average velocity was calculated as an ensemble- and time average over all single cell trajectories (see figure 16). To estimate the error on the measured average velocity we subdivided the region of interest into three equally sized bins. For each bin the average velocity was then calculated separately (in figure 16 indicated as v_1, v_2 and v_3). The error bars then indicate the range of the velocities observed in the three bins. It is important to note that they are prone to changes when cells start to aggregate and the number distribution across the bins becomes uneven. Furthermore, cell aggregates are recognized as single cells or if too big excluded from the statistics, as represented in figure 16.

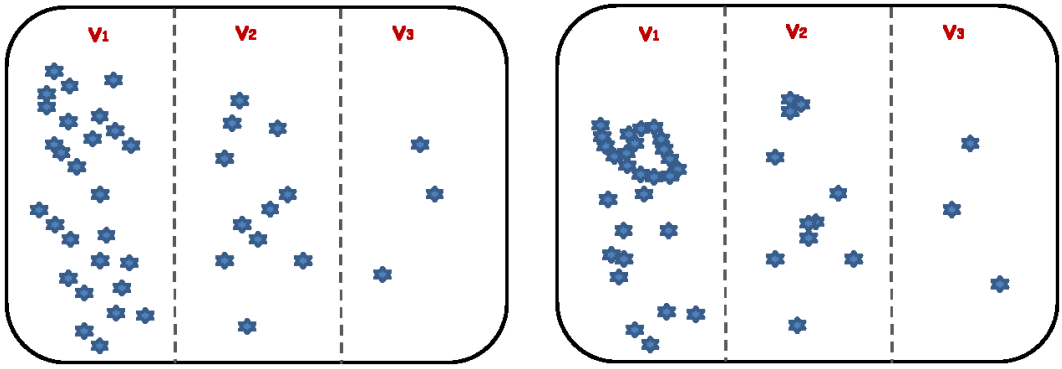

Figure 16 - Graphic showing how the error bars on the average velocity were calculated. Left: The region of interest is subdivided into three bins. The error on v, Δv then reads $\Delta v = \max\{v_1, v_2, v_3\} - \min\{v_1, v_2, v_3\}$. Right: As local aggregates form, the error estimate is biased.

All routines were programmed using MATLAB 7.5 (Mathworks, Ismaning, Germany) together with its image processing toolbox.

2.8 Fluorescence microscopy and photouncaging

2.8.1 Confocal microscopy:

Confocal microscopy imaging was done with a LSM 710 microscope. Access to the microscope and technical support was kindly provided by the group of Prof. Dr. Bernd Walz and apl. Prof. Dr. Otto Baumann (*Zoophysiologie, Universität Potsdam*). The lasers used had the following wavelengths: 488nm argon laser, 561nm DPSS laser, and a Diode 405-30 laser (405nm, photobleaching laser). (Microscope and lasers are from Carl Zeiss Microimaging, Jena, Germany).

For the cell morphology, cell recovery (reversibility assay), cell motility (chemotaxis pipette assay), and PH-$_{CRAC}$ translocation assay with WF38 cells, cells were imaged at the LSM710 confocal microscope using the 488nm line of an argon laser, with 0.5 to 1% of the maximum laser intensity. For the chemotaxis pipette assay, cells were also pulsed for 5 to 6h and incubated with the drug for 30min, before starting the image sequence. I kept the cells at all times exposed to the drugs, while control cells were kept in buffer. A pipette filled with 10^{-4}M cAMP was placed in the middle of the field of view and images were acquired every 20s. Fluorescence images were analyzed using a modified version of the next neighbor algorithm (as stated in section 2.7).

2.8.2 Photouncaging:

For the cGMP uncaging experiments, Myosin II-GFP + LimEΔ-mRFP cells were incubated in 10µM caged-cGMP diluted in Sørensen buffer, placed in a glass bottomed dish, and visualized using the 488nm and 561nm lasers, with a PlnApo 63x/1.4 Oil DicIII objective (Carl Zeiss Microimaging, Jena, Germany).

The DMACM-caged-8-Br-cGMP releases its cage, DMACM, together with the cyclic nucleotide cGMP, at a maxima at 386 ± 398 nm in the absorption, and with a molar extinction coefficient of 16000 - 17000 L M^{-1} cm^{-1} (118), see figure 17. I exposed the cells to a 405nm laser line (Diode 405-30, Carl Zeiss Microimaging, Jena, Germany). The uncaging experiments were performed in an area inside or outside the cell, see figure 17 B and C. A circle with 21 pixels was drawn inside or outside the cell, and with a 25.21 msec pixel dwell time at 100% laser intensity the area was bleached. Images were acquired every second. Two sets of images were taken simultaneously, one for each label.

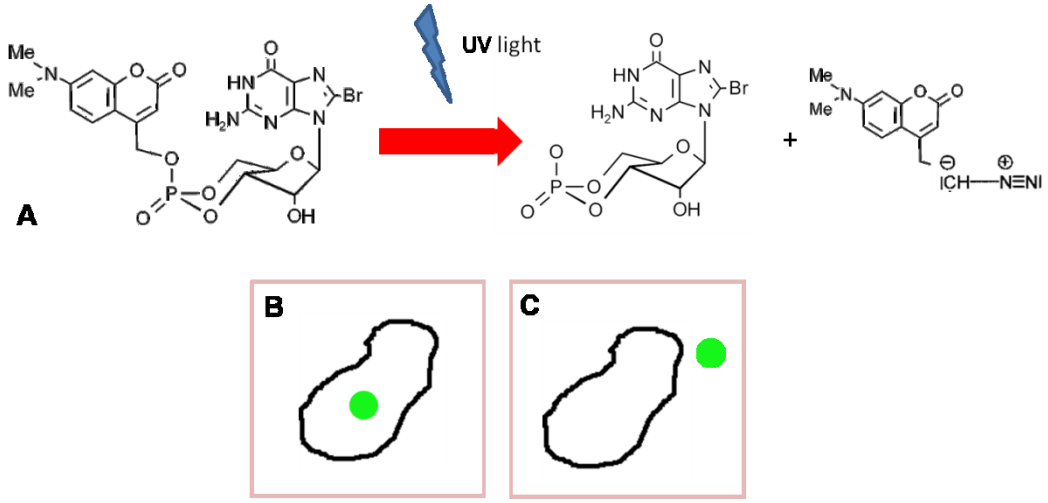

Figure 17 - Uncaging of DMACM-caged-8-Br-cGMP. In A, the structure of DMACM-caged-8-Br-cGMP, and the released Br/cGMP is shown. B + C show the setup for uncaging inside and outside the cell. Images based on reference (118).

For the Dihydroethidium control assay, cells (AX2-WT) were plated in individual dishes and incubated, protected from light, for 2 hours in 20µM Dihydroethidium (Sigma-Aldrich, Taufkirchen, Germany). Cells were exposed to a 355nm laser for 60s (Genesis 355-150, Coherent Deutschland, Dieburg, Germany); the fluorescence intensities of cells at 600nm before and after stimulation were measured and plotted as a function of the distance from the laser.

For the micropipette assay a pipette was filled with 10µM of DMAC, cGMP or Br-cGMP. Sørensen phosphate buffer was used as a control. The pipette was mounted on an Eppendorf Femtojet (Eppendorf, Hamburg, Germany). Cells were plated, the micropipette was positioned next to one chosen cell, and imaging started, using the LSM 710 microscope with a PlnApo 63x/1.4 Oil DicIII objective. Images were acquired every second and after 20s solutions were released from the pipette next to the cell for 10s, while imaging.

Every recorded sequence was converted into a 3D-array containing the stack of all images with dimensions x, y, t, with t being the number of the subsequent images. First, the background intensity was calculated by averaging over all images t, therefore calculating the temporal mean value of every pixel (x,y). From the resulting background image, a mean intensity and a maximum intensity value were calculated.

The images in the 3D-array were then smoothed by a 3D median filter with a 5 x 5 x 5 pixel cube mask. After this operation was performed on both color channels, the two channels (for the GFP and for the mRFP images), both being normalized by the maximum intensity from the background image, were added together. To determine the cytosol and cortex of the cell and to distinguish both from each other we generated two masks: The first one, to identify the cytosol, was generated by thresholding the filtered image with 40% of the mean intensity value retrieved from the background image. The second one, which should represent the cortex, was generated by eroding the binarized image with a diameter of 16 pixels, and subtracting the result from the cytosol image. Both masks were then applied to the sequence of original images. We then defined the mean fluorescence intensity, separately for the sequence of cell cortex images and the sequence of cytosol images. To characterize the cytoskeleton response, the ratio of both values over the time was plotted. In figure 18, a summary of this image analysis can be seen.

The image analysis was done with a custom-made MATLAB program (MATLAB 7.5, Mathworks, Ismaning, Germany) with the assistance of Alexander Anielski.

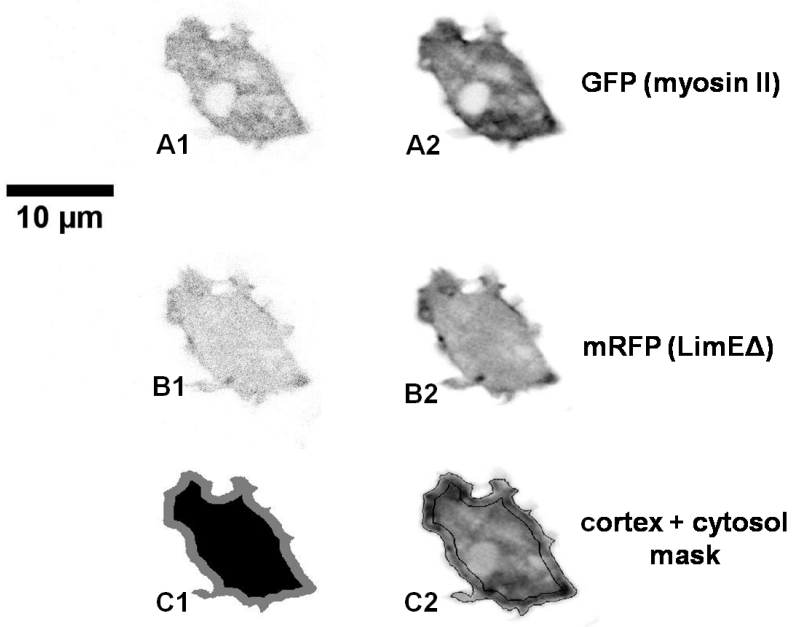

Figure 18 - Image processing of fluorescence measurement of the inner part of the cell and of the cell cortex. In A1 the original image, with its fluorescence intensity for the GFP channel (myosin II) is shown, and in A2 the same image after the 3D median filter is displayed; B1 and B2 show the corresponding images for the mRFP channel (LimEΔ). In C1, the masks for the cortex and for the cytosol of the cell are shown. C3 displays both masks together with the fluorescence channels of the original images. This customized Matlab code was applied to every frame from all image sequences.

2.8.3 TIRFM – Total internal reflection fluorescence microscopy:

To visualize SCAR and WASP A in the cortex, the two cell lines expressing each one of these proteins coupled to GFP (vector kindly provided by Veltman and Insall, see section 2.4) were imaged using a Olympus IX71 microscope, (Olympus, Hamburg, Germany), equipped with a TIRF condensor, a 491nm excitation laser (LAS/491/50), and a 100x oil immersion objective (UApoN TIRF). LimEΔ-GFP cells were also imaged with this setup. The light striking the interface between two media with different refractive indexes undergoes total reflection when focused at an angle greater than the critical angle. The refractive index of the first medium has to be bigger than the second medium (in this case the cell) so reflection can occur (figure 19). Although the light is reflected, the electromagnetic field of the incoming light still extends into the medium, in form of an evanescent wave that decreases exponentially. The electromagnetic field which constitutes the evanescent wave is usually 200nm thick. The portion of the cell within the evanescent wave, mostly the cell membrane and the cell cortex, can be excited and the fluorescence recorded.

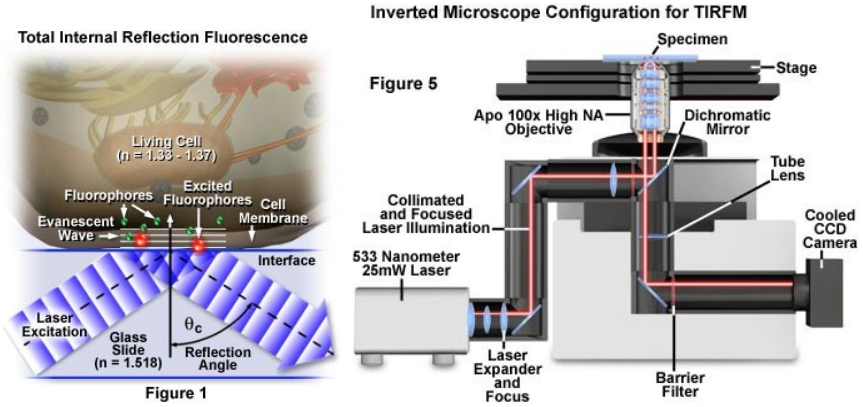

Figure 19 - On the left, the principle of TIRF microscopy is visualized. Light indergoes total internal reflection while the evanescent wave is exciting a 200nm thick layer in the interface. On the right, the configuration of the Olympus TIRF microscope is shown. Pictures taken from (127).

Image sequences were taken, with 1s interval and later on analyzed using Image J software (http://rsbweb.nih.gov/ij/).

2.9 PI and FDA assay – Cell vitality assay

To quantify the cell vitality, *Dictyostelium* AX2-WT cells were plated in 8-well slides (Ibidi, Martinsried, Germany) and exposed for 30 min to different concentrations of Wiskostatin and for 10 min or 3h to 0.02mM hydrogen peroxide. After the treatment, cells were incubated for 10 minutes in the dark with 4µM

propidium iodide (PI) and 0.05mg/mL fluorescein diacetate (FDA) in Sørensen buffer. This solution was always mixed freshly from separate propidium iodide and fluorescein diacetate stocks. Cells were then washed two times with buffer and observed under an LSM 710 confocal microscope, using a ECPln NeoFluar 20x/0.50 M27 objective (Carl Zeiss Microimaging, Jena, Germany), a 488nm excitation laser for FDA, and a 561nm excitation laser for PI.

2.10 Cell recovery (reversibility assay)

To quantify the large number of cells with morphological changes after drug treatment, we decided to focus on the rounding up of the cells after drug exposure and the decreased number of pseudopods. To quantify this, we used a geometric inequality called isoperimetric inequality (128). In curves enclosing a plane with a fixed perimeter, the curve that maximizes the area of its enclosed region is a circle with a closed curve of length L and an enclosed area A. The area A thus has to fulfill the inequality:

$$4\pi A \leq L^2.$$

Equality holds if and only if the curve is a circle. For a given closed curve, the isoperimetric quotient is defined as the ratio between its enclosing area and that of the area of a corresponding circle with the same perimeter:

$Q = \frac{4\pi A}{L^2}$, $For\ Q = 1, the\ cell\ shape\ is\ perfectly\ round\ and\ resembles\ a\ circle,$

$for\ all\ other\ cases\ Q < 1.$

For the experiment, LimEΔ-GFP cells (AX2) from a shaking culture were imaged with a LSM710 Zeiss confocal microscope, as follows: control aliquots were taken and imaged. The remaining cells were incubated with 6µM Wiskostatin for 30 minutes. An aliquot of the drug treated cells was taken and imaged, the rest of the cells washed twice with phosphate buffer and let in shaking culture with the buffer for 30 minutes (washing assay). The washed cells were then imaged. All images were analyzed with ImageJ (http://rsbweb.nih.gov/ij/) and a self-written MATLAB 7.5

program (Mathworks, Ismaning, Germany), based on the isoperimetric inequality. The program was written by Achim Quaas and Christian Wegner.

The closer the value of the quotient to 1, the less protrusions the cell has, the rounder it is and consequently the more affected by the drug. Isoperimetric quotient values were averaged and plotted as shown in the results section (sections 3.1.1 and 3.3.1).

2.11 Total protein assay

To quantify the total amount of protein in non-treated and Wiskostatin-treated cells, I used the Bio-Rad Protein Assay (Bio-Rad Laboratories GmbH), which is based on the method of Bradford (129). For that, cells were lysed with the Lysis Buffer (see recipe in section 2.1, based on reference (130)). Before, cells were grown in shaking culture until a density of 1 x 10^7 cells/mL, transferred to 1.5mL tubes (Sarstedt AG, Nümbrecht, Germany) and centrifuged (3 minutes, 1000rpm). Cells were washed two times with phosphate buffer, centrifuged again and 100µL of the lysis buffer was added.

The cell suspension was pipetted vigorously up and down, ensuring complete cell lysis and shearing of the DNA. After the cell lysis, the lysate was incubated for 10 minutes on ice and subsequently spun down at 20 000g, 4^{o}C. The supernatant was transferred to a microtube, since proteins are in the supernatant, and pipetted in wells of a 96 microwell plate (Sarstedt AG, Nümbrecht, Germany), together with BSA controls. Dye reagent concentrate (Bio-Rad, 500-0006) was prepared (1 part to 4 parts of deionized water) and filtered. Three dilutions of BSA were used as a control. 10µL of standard or sample were pipetted in the wells, and in sequence 200µL of the prepared reagent dye was added and mixed. The microplate was incubated for 5 minutes in room temperature and the absorbance was measured in a microplate reader (Imark Microplate Reader, Bio-Rad, München, Germany) at 595nm.

2.12 F-actin quantification assay

Since Wiskostatin is suppose to affect WASP, a major protein responsible for cellular signal transduction and actin dynamics, I decided to quantify the F-actin content of cells exposed to the drug. For that, I used tetramethylrhodamine (TRITC)-phalloidin (Sigma-Aldrich, Taufkirchen, Germany). Phalloidin binds specifically to F-actin, and can be quantified using a Fluorometer, thanks to the fluorescent dye (TRITC) bound to it.

For the F-actin quantification experiments, cells were prepared in 5 different parallel assays for control cells, cells exposed to 6µM Wiskostatin, and to 5µM Latrunculin A. Experiments were repeated two times. The cells were centrifuged (1000rpm, 3 min), washed with Sørensen buffer and counted. For each microtube I counted $0.5x10^7$ cells, in 1mL. Cells were incubated with the drug for at least 30 minutes, while control cells were kept in buffer. After the drug incubation period, cells were centrifuged and 200µL of cold 6% paraformaldehyde was added. I waited 15 minutes for cell fixation, and then washed the cells two times with buffer. After washing, 500µL of a 0.1% Triton X-100 solution was added for 3 minutes. Again, cells were washed with Sørensen buffer and then treated with a 1% BSA/ Sørensen buffer solution for 30 minutes. For the staining, 200µL of a 0.2µg/mL TRITC-phalloidin solution was added, and cells were incubated in the dark for 30 minutes. After washing, I added 1mL of pure methanol into each microtube, and extraction was performed in the dark for 1h. The fluorescence was determined at 550nm excitation, and emission between 560-650nm, recorded as a spectrum in a fluorometer (Fluorolog, Jobin Yvon Horiba Scientific, Unterhaching, Germany). Access to the equipment was kindly provided by Prof. Dr. Robert Seckler and Dr. Christian Fiedler (*Physikalische Biochemie, Universität Potsdam*).

2.13 Cell adhesion assay

Drugs can impair cell motility by affecting the strength of cell adhesion to the substrate. To quantify cell adhesion, I used a published protocol by Bosgraaf and co-workers (34). Cells (AX2-WT) were grown in six-well plates (Sarstedt AG, Nümbrecht, Germany) and the medium was replaced by fresh medium (or medium and drug) before starting the experiment. The plates were rotated on a shaker at

150rpm and samples were collected at different time points. The number of cells in the samples was determined, and the wells were always replenished by fresh medium after collecting samples. After the final time point, remaining cells were detached and counted. This number was added to the other cell countings (from the different time points) to calculate the total number of cells and the relative number of detached cells.

2.14 PH-$_{CRAC}$ translocation

To test the effect of PBP10 on PH-$_{CRAC}$, cells expressing the plasmid WF38 were used. This plasmid has an enhanced green fluorescent protein (eGFP) tagged to the N-terminal pleckstrin-homology (PH) domain of cytosolic regulator of adenylyl cyclase (CRAC), with an actin15 promoter (8, 131). To observe the translocation of PH-$_{CRAC}$ to the cell membrane, PH-$_{CRAC}$-GFP cells were starved and pulsed, as explained in section 2.3. Approximately 100µL of cells (density ~ $1x10^6$ cells/mL), were plated in each well of an 8-well µ-chamber (Ibidi, Martiensried, Germany) and allowed to attach to the glass substrate. PBP10 was added at least 30 minutes before imaging started, and cells were exposed to the drug during the whole experiment. Cyclic AMP drops of 100µL volume in total were added to control and drug-treated cells. With this, in a final volume of 200µL, the concentrations of 10nM, 100nM, 1µM, 10µM, 100µM and 1mM were achieved. PH-$_{CRAC}$-GFP translocation was observed in the LSM 710 microscope using the 63x oil immersion objective. Pictures (512x512 pixels) were taken every second, for 100 seconds. All other fluorescence microscopy settings resemble the settings described in section 2.8. To measure the fluorescence intensities in cortex and cytosol, a similar custom made Matlab program, as explained in section 2.8 for the cGMP data was used, but in the PBP10 data, a radius of 2 pixels for erosion to determine the cortex was used.

2.15 Calculation of error

The number of cells analyzed in the experiments is always referred to as n in all the graphics and results.

For the drug experiments, error was always calculated as the standard deviation, as follows:

$Sd = \sqrt{var}$, var being the variance

$$var = \frac{1}{n-1}\sum_{i}(x_i - \bar{x})^2,$$

$\bar{x}$ is the mean value.

When ratios between control experiments and drug experiments were taken (for example Wiskostatin 6μM/control), the ratio of the error (ratio y) was calculated as follows:

$$\text{If } y = \frac{x_1}{x_2}, \Delta y = \left(\frac{\Delta x_1}{x_2}\right) \pm \left(\frac{x_1 \Delta x_2}{(x_2)^2}\right).$$

For the cGMP data, the standard error (SEM, standard error of the mean), was used, which is the standard deviation of the sample mean.

$$SEM = \frac{Sd}{\sqrt{n}}$$

Sd is the standard deviation, n is the number of cells in the experiment.

3 Results

3.1 Impact of drug induced WASP-inhibition on motile cells

3.1.1 Wiskostatin treatment alters cell morphology and pseudopod formation

To find an adequate concentration of Wiskostatin (physiologically active but not lethal), I counted the ratio of living and dead cells after drug treatment using Trypan Blue as an exclusion dye (132). As shown in the next graphic (figure 20), the concentration closest to a median lethal dose was 6µM. This concentration was chosen for most of the following experiments.

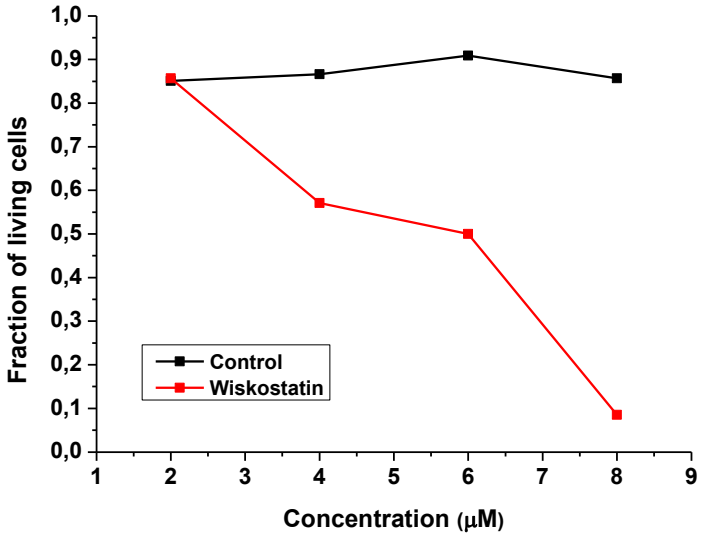

Figure 20 – Experiment to find the median lethal dose using the Trypan Blue method. Cells (AX2-WT) were incubated for at least 30 minutes with the drug. Using the exclusion dye Trypan Blue, dead and living cells were counted. For each data pint I used a minimum of 15 cells.

A complementary way of quantifying cell death in *Dictyostelium* is to label cells with propidium iodide (PI) and fluorescein diacetate (FDA) (132). Propidium iodide is a red fluorescent DNA-intercalating dye that cannot cross intact cell membranes. Cells thus fluoresce red only if the membrane has become permeable, a late sign of cell death. Fluorescein diacetate is a non-fluorescent, hydrophobic compound that enters the cell and becomes green fluorescent when it is cleaved by cytoplasmic lipases. Green fluorescing cells can be considered alive and metabolically active.

I used PI and FDA to quantify living and dead cells, after treatment with Wiskostatin (figures 21 and 22). The negative control for necrosis was done incubating cells in hydrogen peroxide for 10 minutes or 3h.

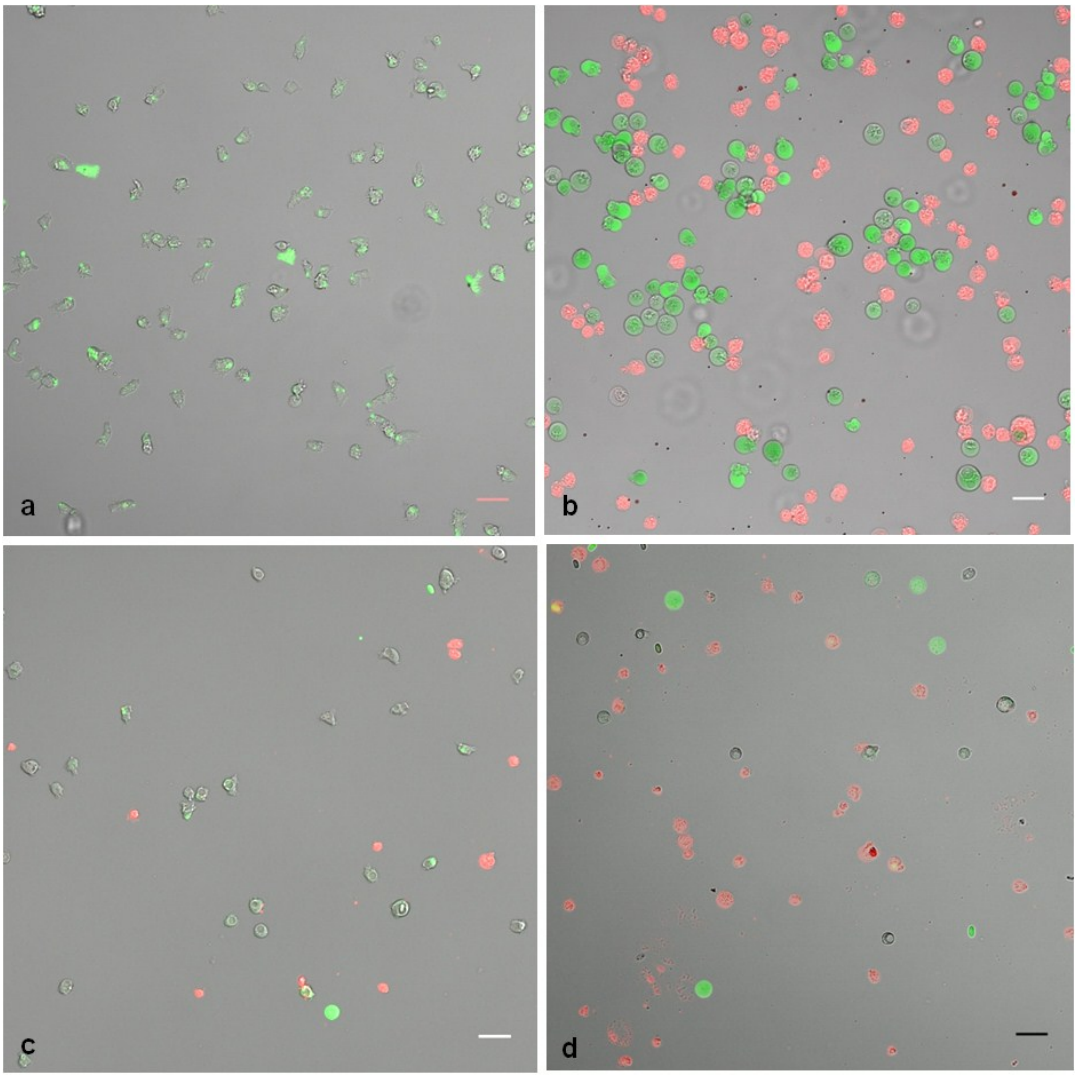

Figure 21 - Images of cells treated with PI and FDA. (a) Control cells in Sørensen buffer; (b) cells treated with hydrogen peroxide for 3h; (c) cells treated with 6µM Wiskostatin for 30 minutes before staining; (d) cells treated with 12µM Wiskostatin for 30 minutes before staining. Bars represent the length of 20µm. Images were taken using a 20x objective, 1668 x 1688, LSM 710 confocal microscope (Zeiss), and are an overlay of brightfield and fluorescence pictures.

For several frames taken, I counted the red (dead) and green (living) cells (figure 21). The results (in percentage) are shown in figure 22. The total number of cells for each example is: H_2O_2 10 min n=431, H_2O_2 3h n=609, Control n=501, 6µM Wiskostatin n=720, and 12µM Wiskostatin n=487.

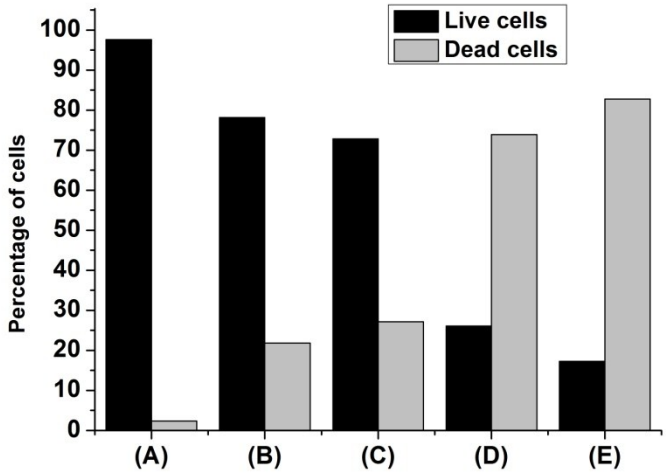

Figure 22 – Results of PI and FDA assay. For each treatment, the percentages of living cells (black) and dead cells (grey) are shown in the graphic. (A) Control cells in the absence of any drug (n=501); (B) cells incubated for 30 min in 6µM Wiskostatin (n=720); (C) cells incubated for 10 min in 0.02mM H_2O_2 (n=431); (D) cells incubated for 3h in 0.02mM H_2O_2 (n=609); and (E) cells incubated for 30 min in 12µM Wiskostatin (n=487).

A first assay to quantify the impact of Wiskostatin was to observe the changes in cell morphology of cells exposed to the drug. A concentration of 6µM Wiskostatin had a pronounced effect on the morphology of vegetative *Dictyostelium discoideum* cells. In figure 23, LimEΔ-GFP cells exposed to the drug were observed under a confocal microscope. In A and B, bright field images of control and Wiskostatin-treated cells are shown, respectively. The images C and D show the corresponding fluorescence images.

Cells exposed to the drug were round, with only few or no membrane protrusions. This suggests that Wiskostatin strongly affects the formation of pseudopods in *Dictyostelium* cells. However treated cells still maintained a cortical network, as can be seen from the increased fluorescence at the inner side of the plasma membrane (figure 23D). Spots and patches of LimEΔ-GFP indicate localized activity in the actin cortex, even after exposure to Wiskostatin.

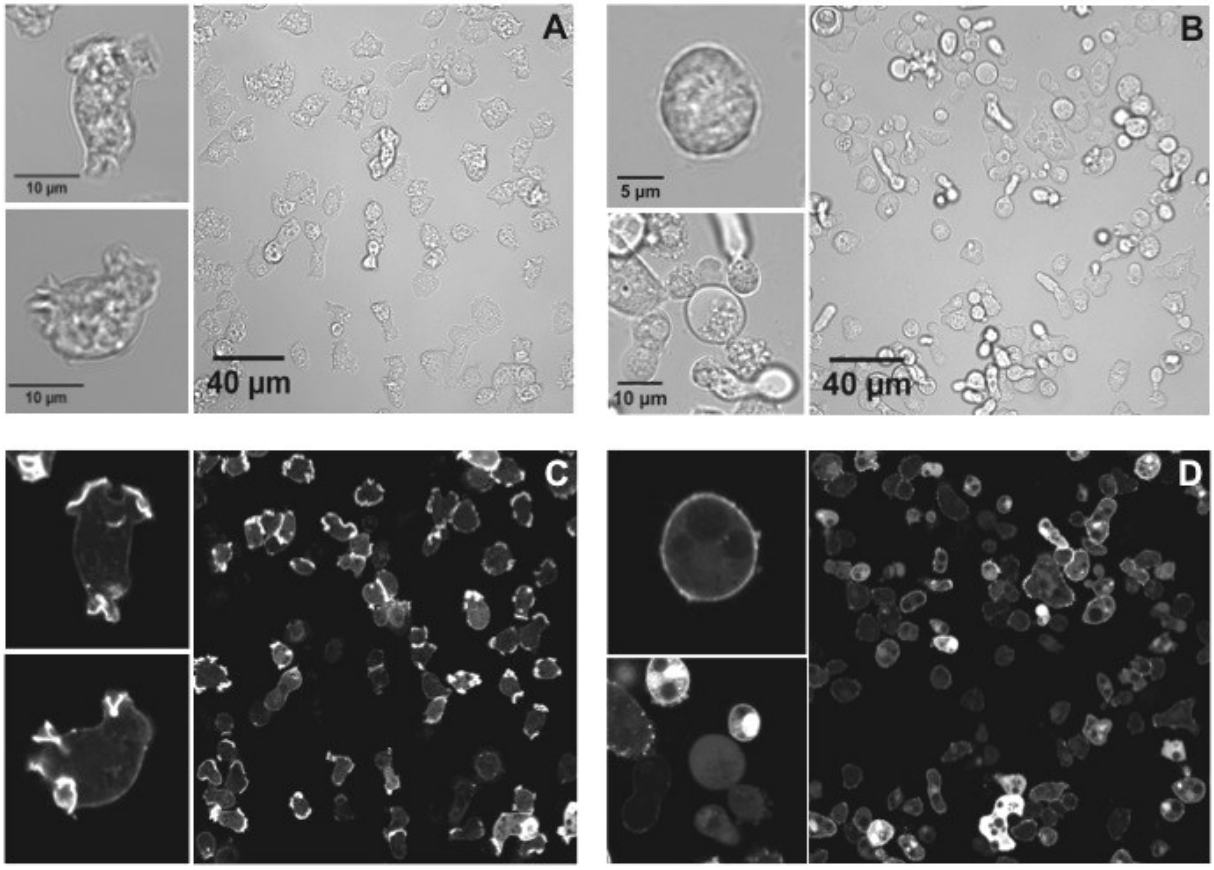

Figure 23 - Cell morphology, LSM 710 microscope (Zeiss). Vegetative LimEΔ-GFP cells (Ax2), before (A and C) and during (B and D) the drug treatment with 6µM Wiskostatin. Cells were exposed to the drug for at least 30 minutes.

The crucial step when studying changes in cell morphology is to quantify them, especially when morphological changes are due to cytoskeleton disruption and vary between cells in the same experiment. Because of that, I quantified the morphological changes using a measure of a cell's roundness. This measure is based on the isoperimetric inequality, and relates the area of a cell cross section to the area of a circle with the same perimeter. For arbitrary cell shapes the measure of the isoperimetric quotient is smaller than one and approaches unit for a circular cross section (for details see section 2.10).

The average roundness of a population of vegetative *Dictyostelium* cells (a) prior to drug exposure, (b) after exposure to 6µM, and (c) after washing cells with phosphate buffer was calculated using a custom-made MATLAB program. The

results are displayed in figure 24. As seen, the cell roundness increases by about 30%, and the morphological change is mostly reversible after cells have been washed with Sørensen buffer.

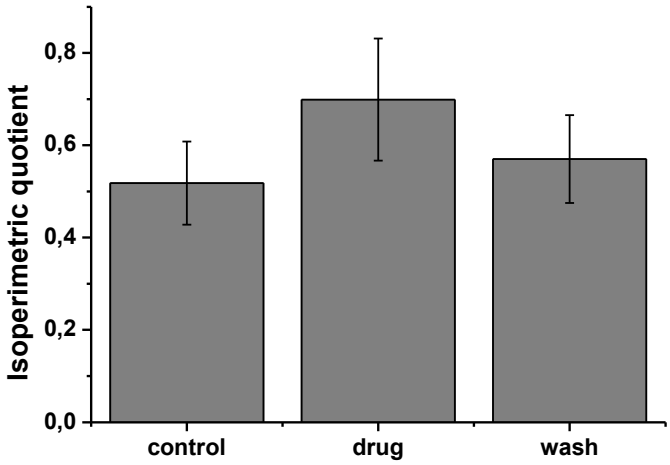

Figure 24 - Cell recovery assay. The mean isoperimetric quotient is plotted for control cells (n=11), drug treated cells (Wiskostatin 6μM, n=19), and washed cells (recovery, n=20). Cells were taken from the same shaking culture.

3.1.2 Wave formation and endocytosis are affected by Wiskostatin treatment

To study the subcellular dynamics of the actin cytoskeleton, I performed TIRF imaging with the following cell lines: LimEΔ-GFP, SCAR-GFP and WASP A-GFP. LimEΔ, as a marker for filamentous actin, is recruited to dynamic cellular protrusions, for example the leading edge and phagocytic cups (31). The LimEΔ-GFP label has been extensively used to visualize F-actin in *Dictyostelium* cells (32, 33). WASP A is the *Dictyostelium* WASP homologue that resembles most the mammalian N-WASP (43), and SCAR is a homologue protein of WASP proteins in *Dictyostelium*, and is associated to cell motility (47).

In figures 25 and 26, TIRF images of LimEΔ-GFP cells are displayed for different levels of drug exposure. In both the drug-treated cells and in the control cells small and localized spots in the actin cortex can be observed. They are usually associated with endocytosis (43). In control cells, the filamentous actin structures of

the cell cortex were clearly displayed, forming a dense network that is continuously rearranged (133). One has to consider that with TIRF imaging only bundles of several actin filaments can be resolved (33).

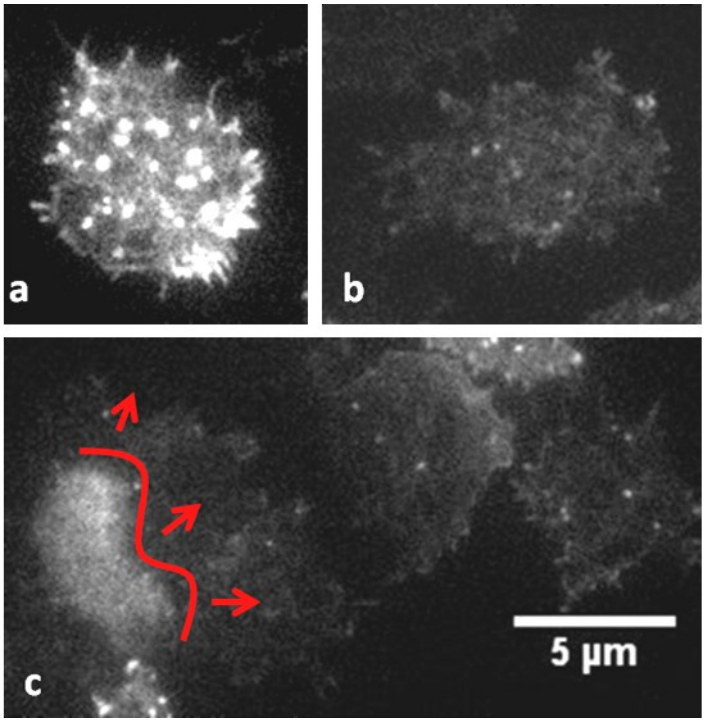

Figure 25 - TIRF images (100x objective, oil immersion, *Olympus*) of LimEΔ-GFP cells in phosphate buffer. It is possible to visualize localized spots (a) and (b) along the actin cortex and the formation of actin waves (c), highlighted with a red line and arrows. Scale bar holds for a, b and c.

After Wiskostatin treatment, LimEΔ-GFP cells get rounder and show less cortex activity, although it is still possible to visualize spots and localized areas of intense actin polymerization (fig. 26). The overall network structure of the actin cortex remained intact under the influence of Wiskostatin.

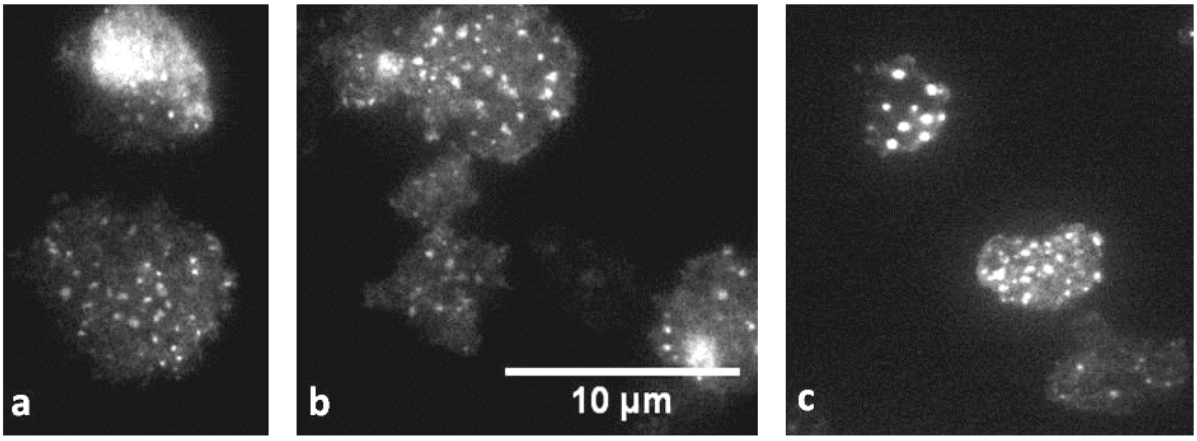

Figure 26 - TIRF images (100x objective, oil immersion, *Olympus*) of LimEΔ-GFP cells, in phosphate buffer and Wiskostatin. In (a) and (b), cells were incubated with 6µM Wiskostatin, in (c) cells were incubated with 12µM drug. Cells get rounder and have less protrusions, compared to the control pictures. Scale bar holds for a, b and c.

In order to visualize how Wiskostatin changed the subcellular SCAR distribution, SCAR-GFP cells were incubated with the drug and images were taken with a TIRF microscope. As seen in figure 27A, control SCAR-GFP cells are spread on the substrate and show episodes of wave formation. After drug treatment (figure 27 B and C), cells seem less spread on the substrate and the SCAR-GFP distribution along the cortex is more homogeneous with less or no wave activity.

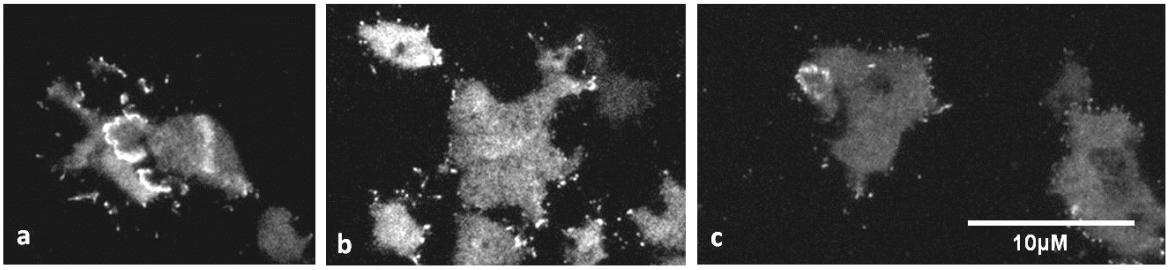

Figure 27 - TIRF images of SCAR-GFP cells (100x objective, oil immersion, *Olympus*). (a) Control cells in buffer, and (b), (c) cells in 6µM Wiskostatin. Note that in (a) cells clearly show wave formation, whereas in drug-treated cells (b and c), the cortex is more homogeneous. Scale bar holds for a, b and c.

It is known that mammalian N-WASP and *Dictyostelium* WASP A are involved in clathrin-mediated endocytosis (43). To investigate how Wiskostatin affects WASP activity in vivo, WASP A-GFP cells were imaged with TIRF. As expected from the experiments by Veltman et al. (43), localized WASP A spots appear and disappear

on the basal membrane of control cells, see figure 28A. Wiskostatin-treated cells show instead very few or no such spots of WASP A (figure 28B and C).

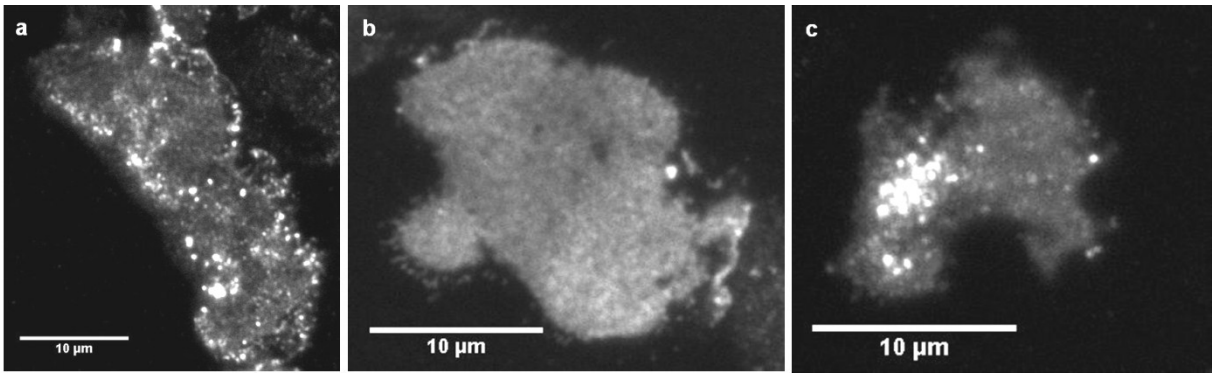

Figure 28 - WASP A-GFP cells imaged with a TIRF microscope (100x objective, oil immersion, *Olympus*). In (a), control cells in buffer show the typical spots that are related to endocytosis. After drug treatment with 6µM Wiskostatin, the distribution of WASP A inside the cell is more uniform, with no or few dots ((b) and (c)).

3.1.3 Wiskostatin treatment affects the mechanical stability of cells

The polymerization of actin filaments against the membrane exerts force that pushes the membrane to form protrusions. Since pseudopod formation is affected by WASP inhibition, the mechanical properties of the cell should be affected as well.

To analyze and quantify the mechanical changes of cells exposed to drugs, a microfluidic chip, as described in section 2.6, was used. Cells were injected into the channel with a continuous flow of buffer (or buffer + Wiskostatin). As the cells travel through the series of fluidic apertures, they experience an alternating sequence of maxima and minima in flow speed and shear stresses. This leads to a deformation as the cells pass through the narrow sections of the channel. In figure 29, cells exposed to 5µM Latrunculin A deform the most, and Wiskostatin-treated cells show a smaller deformation. It can be concluded that treatment of cells with Wiskostatin results in a reduction of mechanical stability. The isoperimetric quotient was calculated the same way as in section 3.3.1.

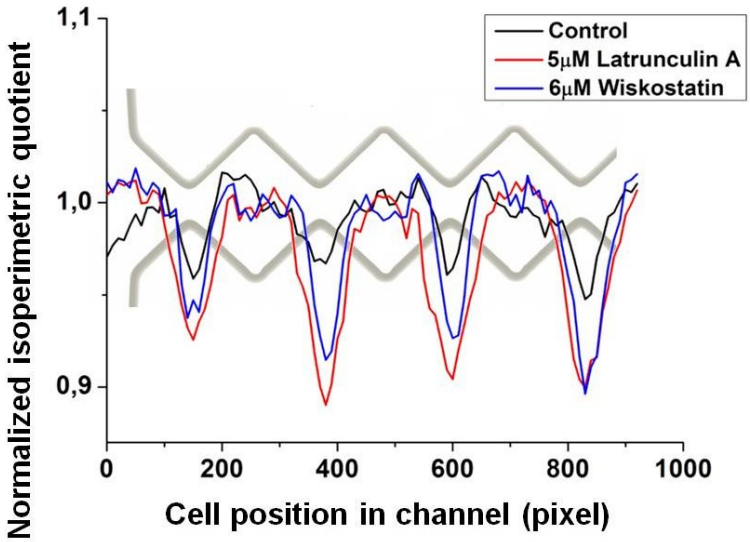

Figure 29 - Change of cell shape (average isoperimetric quotient) as a function of the cell position in the microfluidic channel. Note the large deformation when cells are treated with Latrunculin A or Wiskostatin, at the narrow constriction sites. (Control n=40, Latrunculin A n=33, and Wiskostatin n=50). Flow speed is 4.1mm/s.

The camera setup and the relatively long exposure times as compared to the high flow velocity can cause optical artifacts by blurring. This occurs because passing cells move while pictures are taken. To extract this source of error, non-deformable polystyrene beads were flushed through the channel, and the isoperimetric quotient was calculated as a control. The curve for the beads can be seen in figure 30.

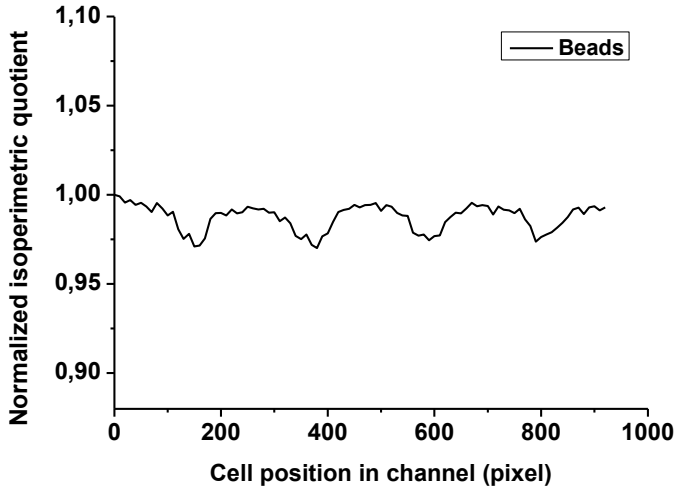

Figure 30 - Apparent change of polystyrene beads shape (average isoperimetric quotient) as a function of the bead position in the microfluidic channel.

In possession of this curve, one can then subtract it from the original data to correct the exposure time bias. The corrected data is plotted in figure 31.

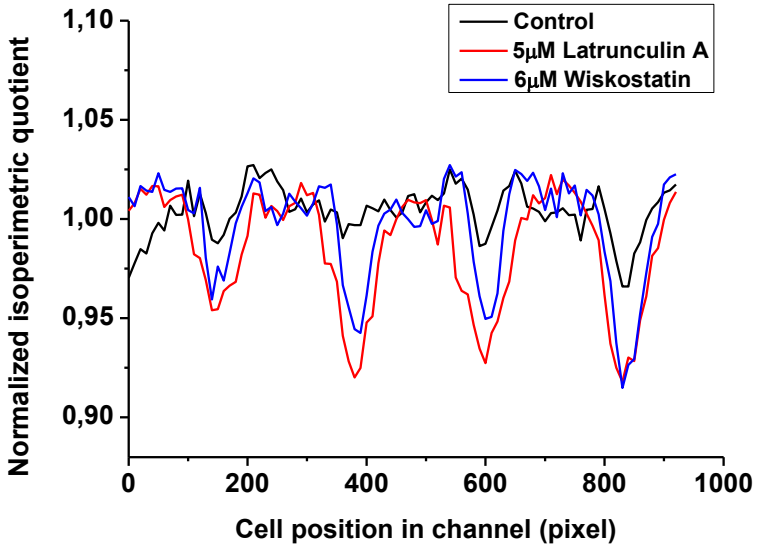

Figure 31 - Corrected curves of the change in the cell shape (average isoperimetric quotient) as a function of the cell position in the microfluidic channel. The curve for the beads deformation (figure 30) was substracted from the original curve (showed in figure 29), to give the corrected data. Details on error calculation are stated in section 2.6. (Control n=40, Latrunculin A n=33, and Wiskostatin n=50).

The cell deformation increases with higher flow velocity. In figure 32, the isoperimetric quotient of cells exposed to different flow velocities is shown. The deformation increases with the flow velocity. However in the data set of figure 32, cells exposed to a flow velocity of 4.1mm/s surprisingly show less deformation than cells exposed to 3.3mm/s. This could be due to variations of the cell batch. Since I used only one flow velocity in my data analysis (4.1mm/s), the variation between different flow velocities in not significant for the final results.

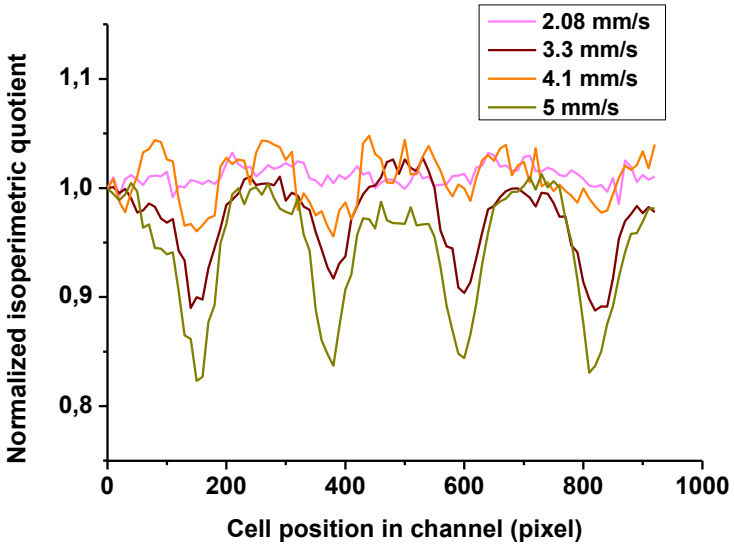

Figure 32 - Deformation of cells treated with 5µM Latrunculin A exposed to varying flow velocities. Note the trend to a bigger cell deformation with higher flow velocities. (2.08mm/s: n=20; 3.3 mm/s: n=21; 4.1 mm/s: n=14; 5 mm/s: n=19).

3.1.4 Wiskostatin treatment does not affect the amount of F-actin in D. discoideum cells

Drug treatment can affect the total protein content of a cell, or disrupt specific protein targets, when it binds to it or to related binding proteins. To investigate whether Wiskostatin-treated cells or LatA-treated cells show changes in protein content, I quantified the total amount of protein in cells exposed to different concentrations of the drug. I used the Bio-Rad Protein Assay (Bio-Rad, München, Germany), standardized for a 96-micro well plate. The kit is based on the method of Bradford (129), which states that the absorbance maximum for a solution of Coomassie Brilliant Blue G-250 dye shifts from 465nm to 595nm when proteins bind to it. The dye is acidic and binds primarily to basic and aromatic amino acid residues. No significant change in total protein content was measured in cells exposed to Wiskostatin or Latrunculin A, as shown in figure 33 A and B.

For Latrunculin A, it is known that a loss in mechanical stability is caused by depolymerization of F-actin rich structures in the cell cortex (103). To measure the F-actin content, I used a TRITC-phalloidin-based assay, taking advantage of the specific binding of phalloidin to F-actin. Cells exposed to Latrunculin have reduced F-actin content, but not cells exposed to Wiskostatin. Figure 34 shows the result of the

F-actin assay. It indicates that Wiskostatin does not affect the overall F-actin content directly, but probably only the nucleation and branching of actin by the proteins of the Arp2/3 complex. Other actin nucleators in the cell could compensate for the lowered nucleation by the Arp2/3 complex.

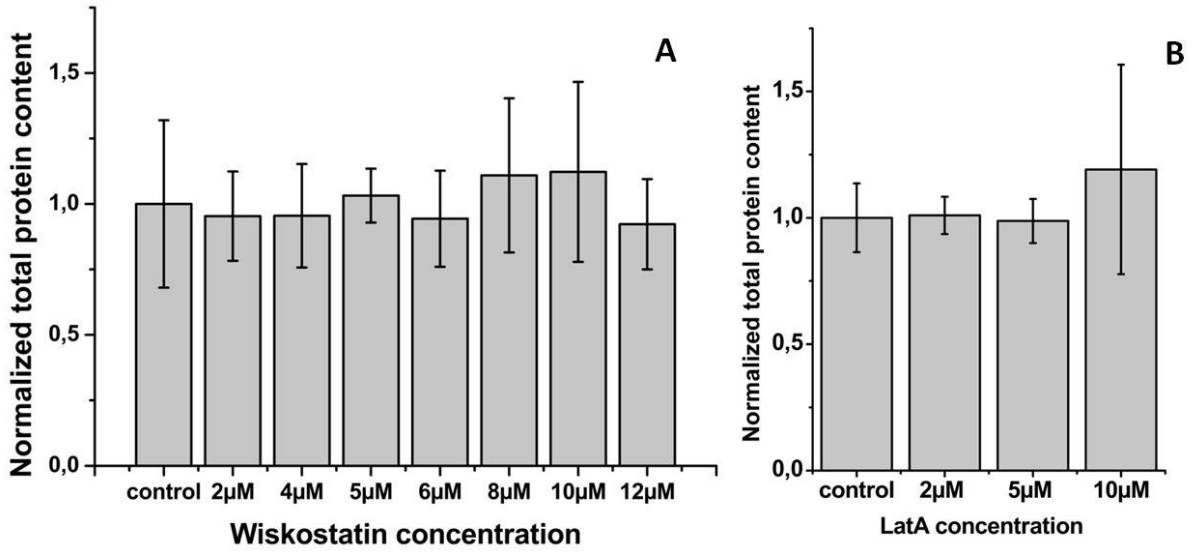

Figure 33 - Total protein content of cells treated with different concentrations of Wiskostatin (a) and Latrunculin A (b). All results were normalized by the control data.

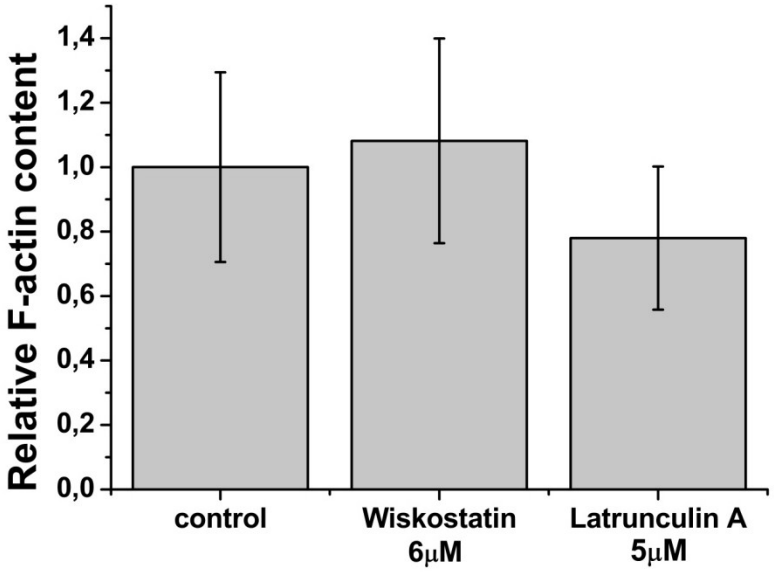

Figure 34 – Relative F-actin content of cells treated with Wiskostatin or Latrunculin A. Results were normalized by the control.

3.1.5 Substrate adhesion is increased by Wiskostatin treatment

The degree of attachment of cells to the substrate can be an *in vitro* marker of cell vitality (134). To analyze the degree of cell-substrate adhesion after Wiskostatin treatment I used a previously published protocol by Bosgraaf et al. (34). Surprisingly, my results showed an increase of cell adhesion for cells treated with the drug, especially in the first 30 minutes of the assay (figure 35). Fluctuations in cell adhesion might be also influenced by changes in cellular morphology (in my case, stated in the experiments of section 3.1.1) or in the polarization of the cell, and are not necessarily connected to cell death (134). My results on cell adhesion could thus point to changes in cell morphology and motility.

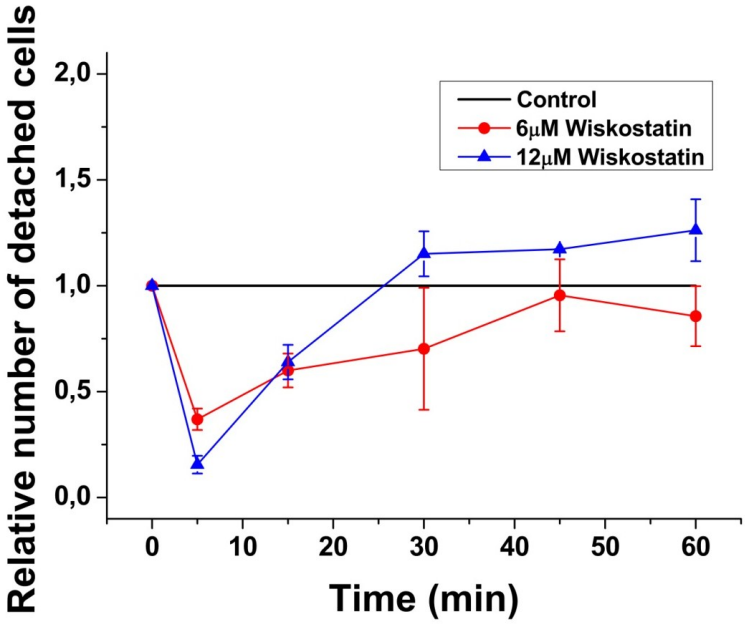

Figure 35 - Cell adhesion assay: number of detached cells relative to the control. Cells were incubated for 30 minutes with Wiskostatin before starting the experiment, control cells were maintained in phosphate buffer. The mean over samples from four different wells is shown (see methods part, section 2.13).

3.1.6 Motility is reduced by Wiskostatin treatment

Here, random cell motility of *D. discoideum* cells was quantitavely analyzed. Time-lapse movies were taken and cells were tracked (see section 2.7) The first observation when analyzing the cell tracks was that cell motility is indeed impaired when cells are incubated with Wiskostatin. This can be seen in figure 36, which shows tracks of control cells and Wiskostatin-treated cells.

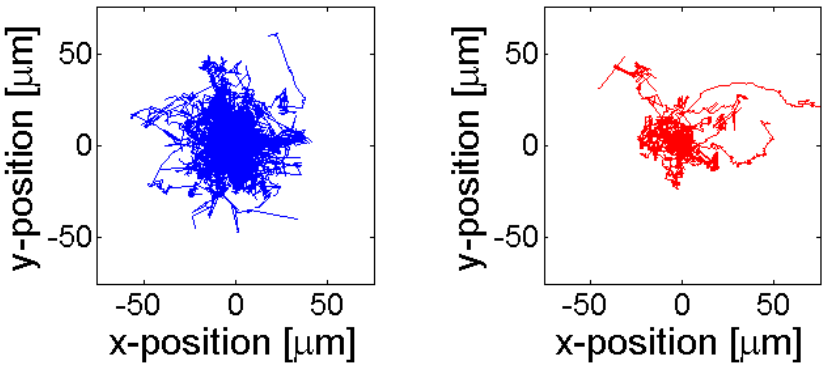

Figure 36 - Examples of tracks of random motility. In blue, control cells in HL-5 medium are shown. In red, cells incubated with 6μM Wiskostatin in medium are displayed. Experiments were performed on vegetative AX2-WT cells.

Throughout the experiment, cells were kept in HL-5 medium. The graph shows that motility is reduced with increasing Wiskostatin concentration (figure 37), but only by less than 25%. In the experiments with developed cells, cells were pulsed with cAMP as described, and kept in buffer during the image acquisition. As can be seen in figure 38, the motility of developed cells was much stronger affected by Wiskostatin treatment.

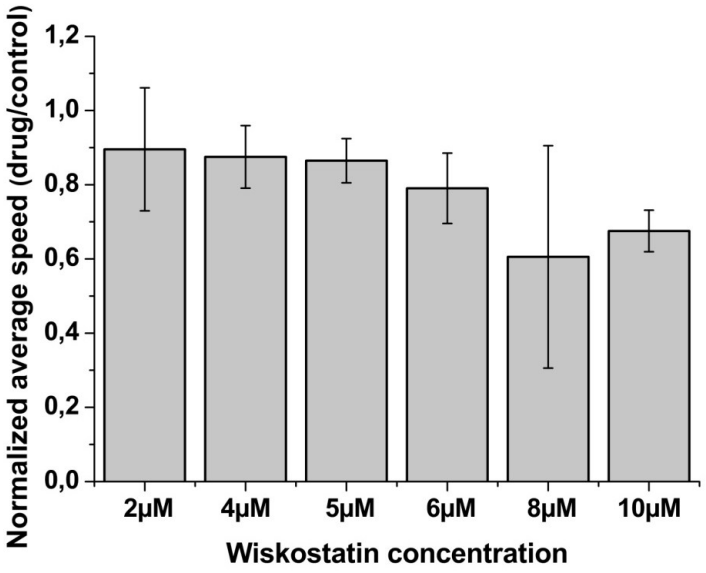

Figure 37 - Effect of different Wiskostatin concentrations on random motility of vegetative cells. Cells were incubated for one hour with the drug and images were taken every 10s, for a recording time of 4h. Velocity was calculated using a cell tracking program, as described in section 2.7. Cells (AX2-WT) were recorded in HL-5 medium, with the indicated concentrations of Wiskostatin.

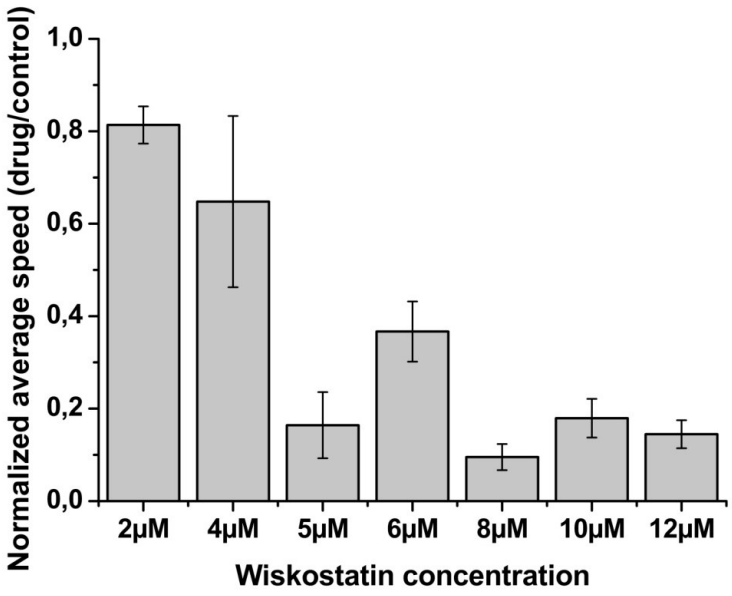

Figure 38 - Effect of different Wiskostatin concentrations on random motility of starvation developed AX2-WT cells. Cells were grown in shaking culture and pulsed with cAMP (see section 2.3). After 5h of pulsing, cells were incubated for 1h in phosphate buffer with the drug, and images were recorded as described.

3.1.7 Chemotaxis is negatively affected by Wiskostatin treatment

As seen in the previous results (figure 38), developed cells are much stronger affected by Wiskostatin than vegetative cells. Those cells move *per se* more rapidly than vegetative cells, but the effect on motility seems to be also related to a role of WASP during chemotaxis. To investigate chemotaxis, LimEΔ-GFP cells were pulsed and exposed to cAMP gradients generated by a pipette filled with a 10^{-4}M cAMP solution that was placed in the middle of the field of view of a LSM 710 confocal microscope.

I performed the chemotaxis assay in the presence of the following Wiskostatin concentrations: 2µM, 4µM, 5µM, 6µM, 8µM, 10µM and 12µM. For the concentration of 6µM I did four independent experiments. In most cases, a clearly reduced chemotactic performance was observed in the presence of the drug. However, no systematic trend of a change in the chemotactic index (CI) as a function of the applied Wiskostatin concentration could be observed, as shown in the following table:

Wiskostatin concentration	CI control (buffer only)	CI drug
2µM	0.34	0.15
4µM	0.13	0.23
5µM	0.14	0.024
6µM (1)	0.37	0.31
6µM (2)	0.37	0.048
6µM (3)	0.38	0.024
6µM (4)	0.28	0.15
8µM	0.22	0.26
10µM	0.17	0.17
12µM	0.31	0.17

Table 1- Chemotatic index of control cells in buffer and cells in different Wiskostatin concentrations are shown. In some cases, like for 4µM, 8µM, and 10µM Wiskostatin, the CI of drug-treated cells is bigger than the CI for control cells. This could be due to the different responsiveness of cells, and their stage of development.

The trajectories show that Wiskostatin-treated cells are differently sensitive to the drug. Some cells do not move at all, whereas others persistently move in the direction of the pipette. In the following images of trajectories (figure 39), a control experiment is displayed next to each drug experiment. Blue traces are trajectories of cells moving in the direction of the pipette (CI > 0), red traces belong to trajectories of cells moving away from the pipette (CI < 0). The position of the pipette tip is represented by an asterisk in the images.

A

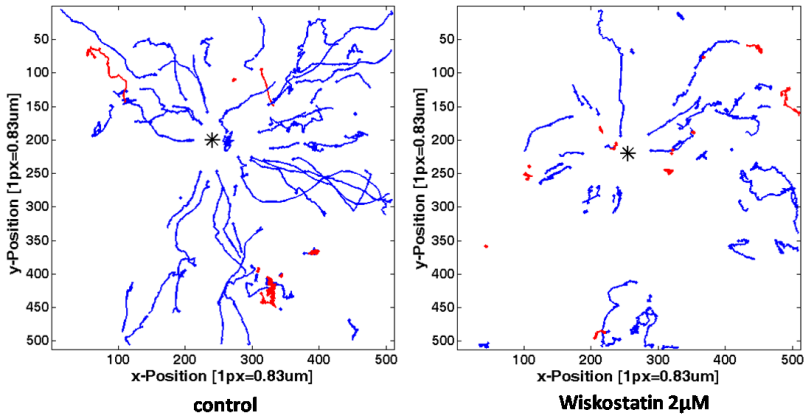

B

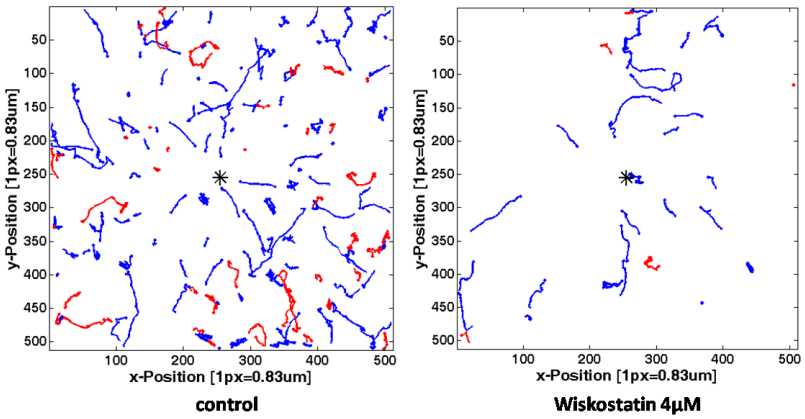
y-Position [1px=0.83um]
x-Position [1px=0.83um]
control
Wiskostatin 4µM

C

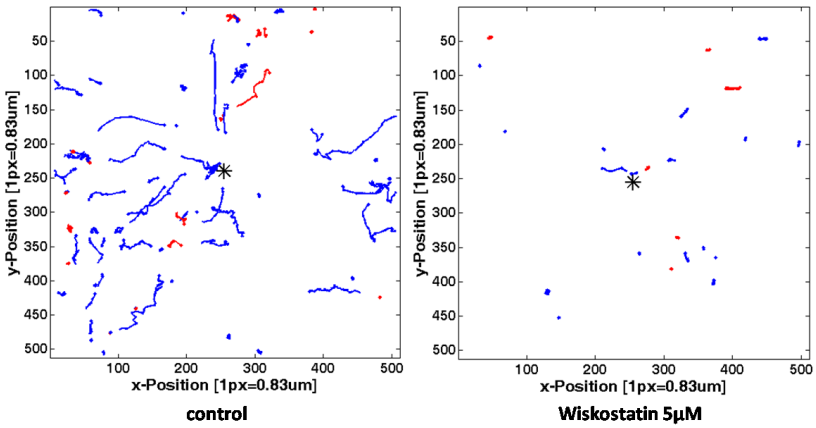
y-Position [1px=0.83um]
x-Position [1px=0.83um]
control
Wiskostatin 5µM

D

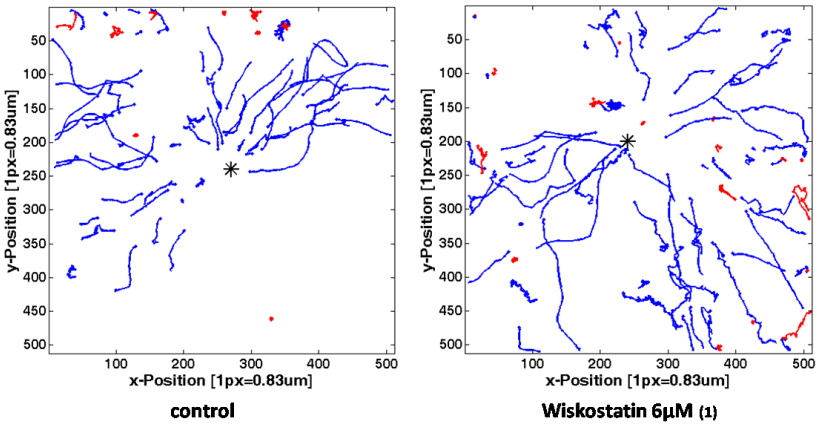
y-Position [1px=0.83um]
x-Position [1px=0.83um]
control
Wiskostatin 6µM (1)

E

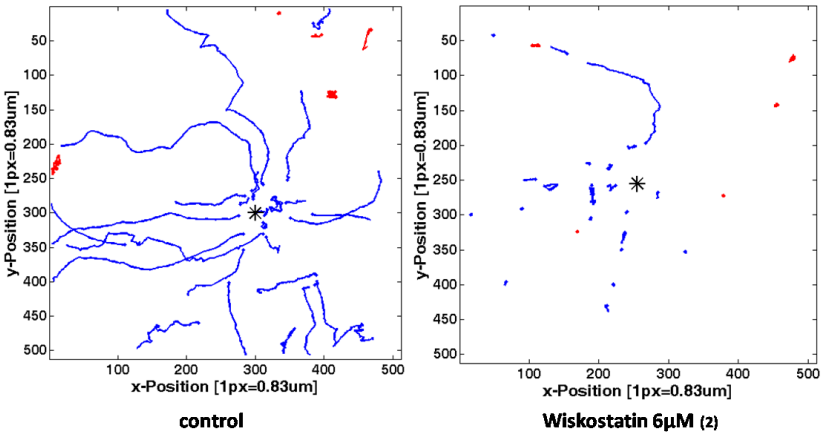
y-Position [1px=0.83um]
x-Position [1px=0.83um]
control
Wiskostatin 6µM (2)

F

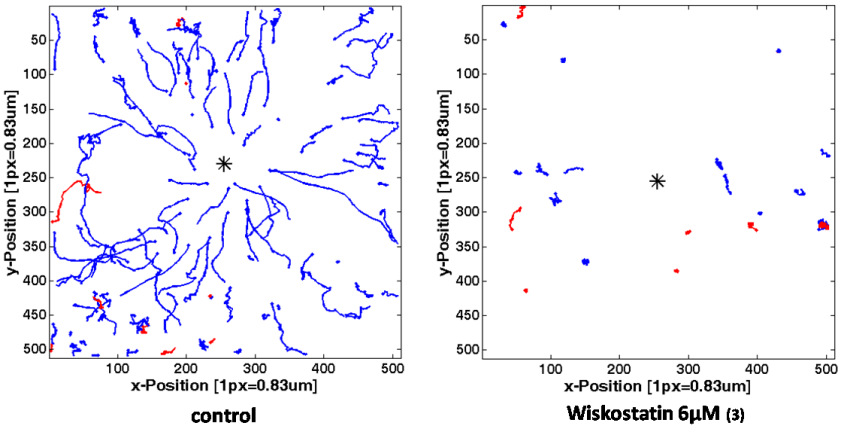
y-Position [1px=0.83um]
x-Position [1px=0.83um]
control
Wiskostatin 6µM (3)

G

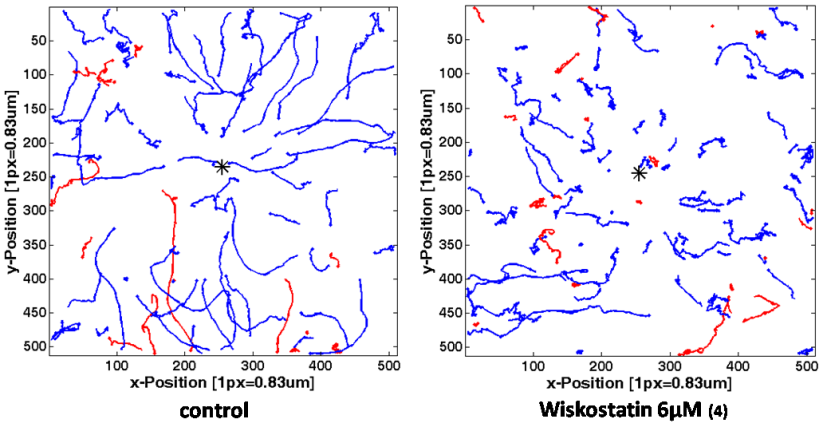
y-Position [1px=0.83um]
x-Position [1px=0.83um]
control
Wiskostatin 6µM (4)

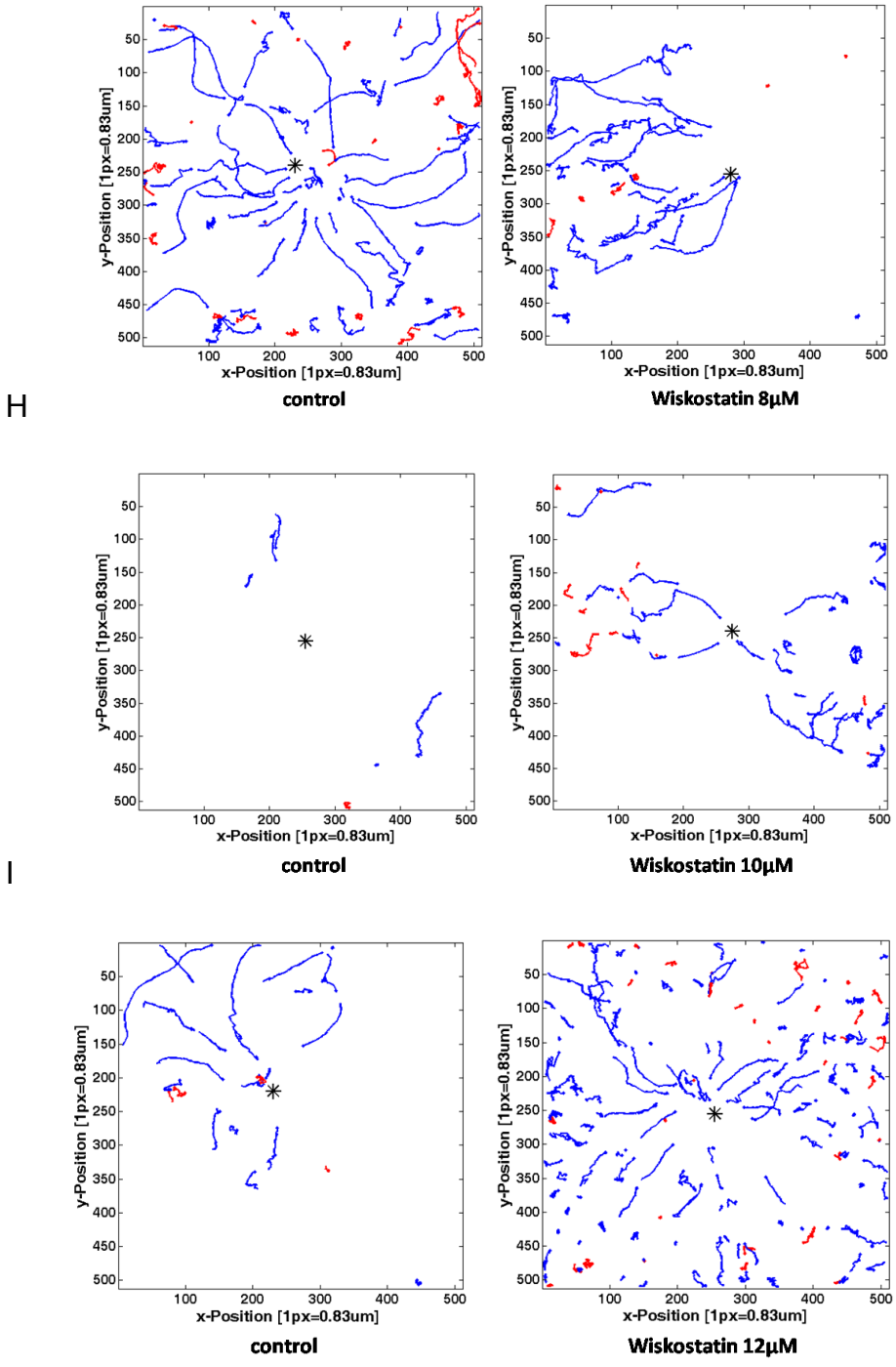

Figure 39 – Control and drug-treated trajectories of pulsed cells exposed to different concentrations of Wiskostatin. Observe how trajectories of cells treated with the drug are in general less persistent. The trajectories correspond to the ones listed in table 1: A- 2µM, B- 4µM, C- 5µM, D- 6µM$_{(1)}$, E- 6µM$_{(2)}$, F- 6µM$_{(3)}$, G- 6µM$_{(4)}$, H- 8µM, I- 10µM, and J- 12µM.

3.2 Cytoskeletal dynamics in response to intracellular release of cGMP

3.2.1 The influence of scattered light on photouncaging experiments

Photo-activatable probes are able to give precise temporal delivery control of molecules. In my photoactivation experiments, it was the aim to release cGMP inside the cell. However, it is not known how the light scattering from the uncaging laser affects the amount and the distribution of released compounds.

Because the optical properties of the cell cytoplasm are different than from buffer or medium, with small intracellular particles attenuating light and with different light scattering between the cell body and the pseudopod (135), photoactivation also depends on the amount of light reaching different cell compartments. To monitor the amount of light reaching single cells in the different experimental settings (uncaging outside and inside the cell), I used Dihydroethidium (Sigma-Aldrich Germany), a membrane permeable compound that is photo-oxidated to hydroxyethidium when exposed to UV light. The photo-oxidated component is fluorescent and membrane impermeable, permitting the quantification of the component inside the cell after light exposure (135). For the photoactivation control assay, cells (AX2-WT) were plated in glass-bottom dishes, and incubated for 2 hours in 20µM Dihydroethidium, being protected from light. A small spot of the dish (approximately 8µm^2) was then exposed for 60s to a 355nm laser, and the intensities of the fluorescence of cells before and after stimulation were measured and plotted as a function a cell's distance from the illuminated spot. All experiments were done with the assistance of Dr. Matthias Gerhardt. The results showed that not only the cells directly hit by the laser are exposed to the UV-light. Rather, all cells in the vicinity of the laser (up to 600µm) are exposed to a sufficient amount of UV-light to initiate photoactivation inside the cells. The distance to the laser source did not influence the amount of photoactivation on a micrometer scale, as can be seen in figure 40.

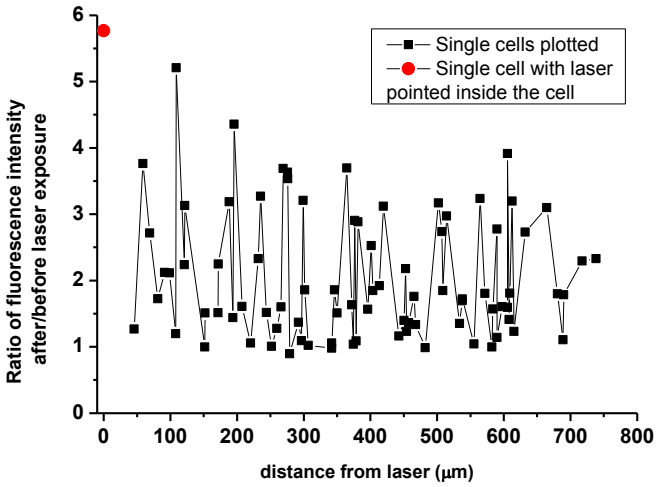

Figure 40 - Dihydroethidium photoactivation assay: each square in the plot represents a cell and the ratio between its fluorescence intensity before and after the photoactivation. Cells up to a distance of 750µm from the laser source were quantified. The red dot represents a cell with the laser focused inside the cell, that is, the distance to the laser source equals zero. 86 cells were evaluated.

3.2.2 Caged cGMP experiments: actin and myosin responses in starvation developed cells

For the uncaging experiments in a confocal microscope, two different channels (RFP for LimEΔ and GFP for Myosin II) were recorded simultaneously (figure 41) for 100s. The details on microscopy and photouncaging are shown in section 2.8.

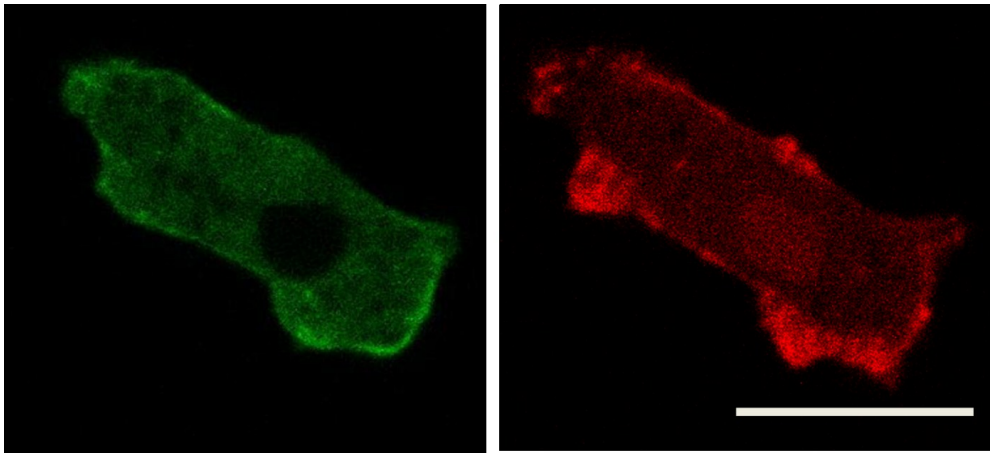

Figure 41 - Confocal images of the two labels used, and an example of a cell as visualized during the experiments: on the left, GFP-myosin II, and on the right mRFP-LimEΔ. Error bar is 10µm.

After determining the mean fluorescence intensity in the cell cortex and in the cytosol, I plotted the ratio of cortical and cytosolic fluorescence intensity as a function

of time in seconds. Many controls were performed, and the next table explains the naming of the different experiments and the settings used:

Developmental stage of the cell	Type of experiment	Settings	Fluorescent label
sta – for starvation developed cells or **veg** – for vegetative cells	**g** – for incubation in buffer + caged-cGMP (DMACM-caged-Br-cGMP) or **nog** – for incubation in buffer only	**con** – for control, no laser exposure **in** – when exposing an area inside the cell **out** – when exposing an area outside the cell	**actin – actin-mRFP** or **myosin – myo-GFP**
sta – for starvation developed cells or **veg** – for vegetative cells	**f** – for micropipette aspiration	**cc** – for control with buffer **cg** – for cGMP **cgbr** – for Br-cGMP (not the caged form) **dm** – for DMAC (correspondent of the cage molecule from DMACM-caged-Br-cGMP)	**actin – actin-mRFP** or **myosin – myo-GFP**

Table 2 - Experimental settings used for the cGMP experiments. The micropipette experiments were done with a Femtojet holder. For details of microscopy, uncaging, and micropipette experiments, see section 2.8 in Materials and Methods.

After a cAMP stimulus, the assembly of myosin II in the cell cortex takes around 20s and the actin response appears within the first 10 seconds (12). For **developed cells**, a myosin II response was detected when uncaging cGMP inside the cell (figure 42A). Surprisingly, also an actin response was observed, with a timing similar to the one found in the cAMP response of actin and myosin II (12).

When uncaging outside, next to the cell, developed cells after starvation showed both actin and myosin II response. As already stated in section 3.2.1, stray light can induce photoactivation (photouncaging) inside the cell even for distances up to 600µm. I thus assume that the signals I see when shooting with the laser outside the cell are due to uncaging via stray light inside the cell (figure 42B). Another

possibility could be due to unspecific binding of cGMP to cAMP receptors. This option is excluded in the next experiments (section 3.2.4) by the micropipette aspiration controls.

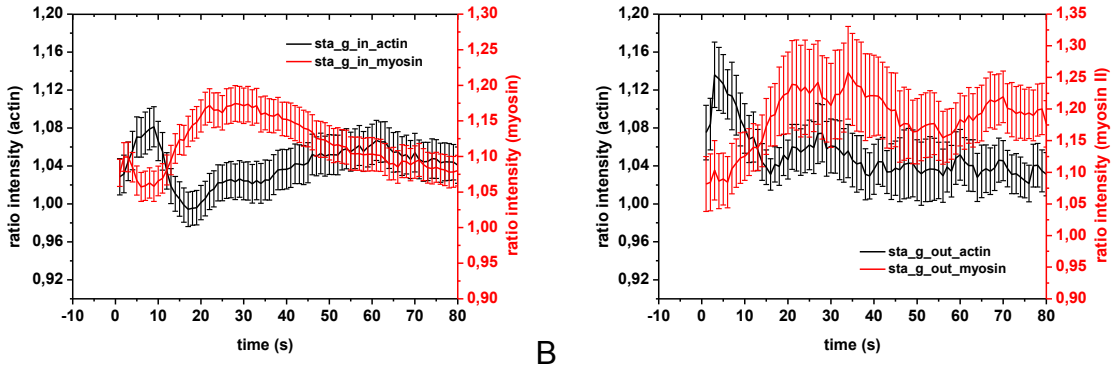

A B

Figure 42 - Actin and myosin II responses of developed cells. In A, responses after photouncaging of cGMP inside the cell are shown. The y axis on the left (black) shows the values for the actin curve, and the y axis on the right (red) the values for myosin II. Number of cells analyzed: 74 for actin and 77 for myosin. In B, responses after photouncaging of cGMP outside of the cell are plotted. The y axis on the left (black), shows the values for the actin curve, the y axis on the right (red), the values for myosin II. Number of cells analyzed: 19 for actin and 21 for myosin II. In A and B, error bars indicate the standard error.

Several controls were performed, in order to check if the actin and myosin II responses seen are not due to cellular photodamage caused by the laser, or due to the imaging process. When cells were recorded with no previously caged-cGMP incubation nor photouncaging, there is no relevant actin or myosin II response, as seen in figure 43A. Also there is no evident response when cells are pre-incubated with the caged-cGMP, but no photouncaging is done, as shown in figure 43B.

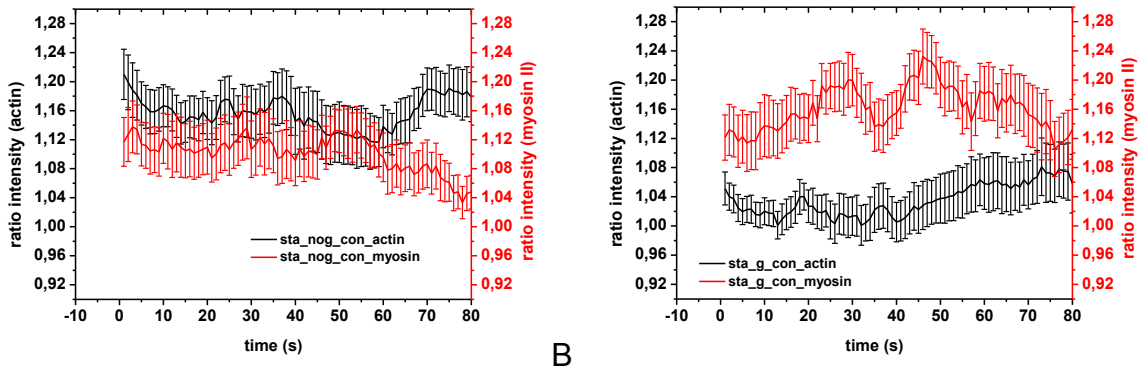

A B

Figure 43 - Actin and myosin II control curves for developed cells. In A, cells not incubated with caged-cGMP and with no exposure to an uncaging laser are shown. The y axis on the left (black) shows the values for the actin curve, the y axis on the right (red) the values for myosin II. Number of cells analyzed: 23 for both actin and myosin II. In B, control curves of cells incubated with caged-cGMP but with no exposure to the uncaging laser are displayed. The y axis on the left (black) shows the values for the actin curve, the y axis on the right (red), the values for myosin II. Number of cells analyzed: 19 for both actin and myosin II. In A and B, error bars indicate the standard error.

When cells are exposed to the 405nm laser, without incubation in caged-cGMP, I do not see an evident actin and myosin II response either (figure 44).

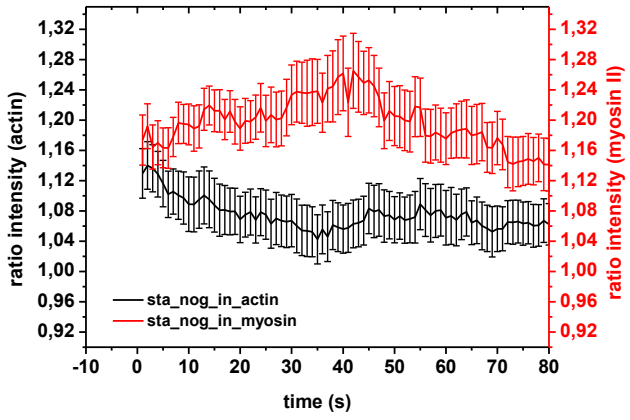

Figure 44 - Actin and myosin II control curves of developed cells, with photouncaging laser pulse in the absence of caged-cGMP. The y axis on the left (black) shows the values for the actin curve, the y axis on the right (red), the values for myosin II. Number of cells analyzed: 29 for both actin and myosin II. Error bars indicate the standard error.

Together, these results for developed cells show that:

1. Actin polymerization and myosin II filament assembly are activated by free intracellular cGMP;
2. The timing of maximal actin and myosin II accumulation in the cortex is similar to the response times to extracellular cAMP (11); and
3. Controls do not show an equivalent response, proving that the observed responses are indeed caused by photochemically released cGMP inside the cell.

3.2.3 Caged cGMP experiments: actin and myosin responses in vegetative cells

When uncaging cGMP inside **vegetative cells**, a pronounced myosin II response and, similar to the developed cells, also an actin response was observed (figure 45A). When uncaging outside the cells, vegetative cells showed no clear myosin II response, but a pronounced actin response. These curves can be seen in figure 45B.

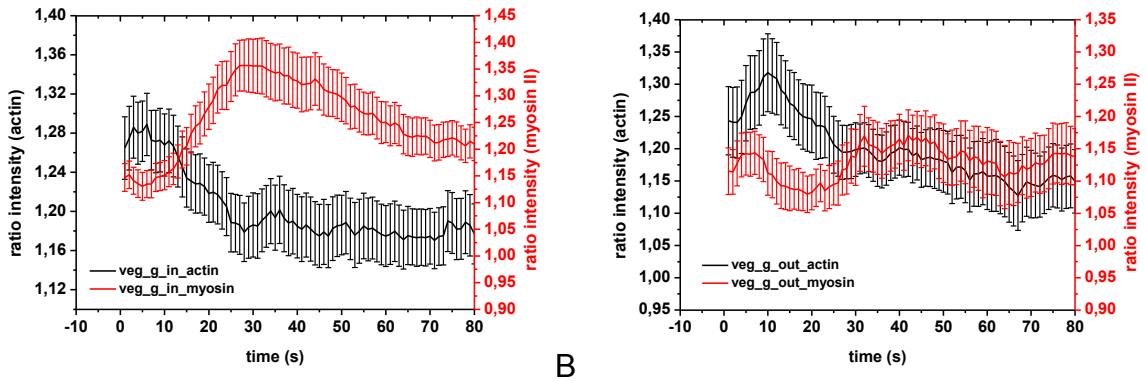

A B

Figure 45 - Actin and myosin II curves of vegetative cells. In A, cells were incubated in caged-cGMP, and exposed to a photouncaging laser pulse. The y axis on the left (black) shows the values for the actin curve, the y axis on the right (red) the values for myosin II. Number of cells analyzed: 45 for actin and 47 for myosin II. In B, curves of vegetative cells incubated in caged-cGMP, with photouncaging laser pulse outside the cell, are shown. The y axis on the left (black) shows the values for the actin curve, the y axis on the right (red) the values for myosin II. Number of cells analyzed: 25 for both actin and myosin II. In A and B, error bars indicate the standard error.

The controls for vegetative cells do not show any actin or myosin II responses (figures 46 and 47). But, in the veg_nog_in case (vegetative cells, no caged-cGMP incubation, and photouncaging inside the cell), a rise in the myosin II level could be

observed (figure 47). This rise does not match the timing of the myosin II responses seen for all other experiments. Taking a look at the individual curves, for all the 23 individual experiments with single cells, one can see that the spreading is big among the data (figures 48 and 49). We thus conclude that the slow and noisy increase in this specific data set does not indicate a myosin II response. It was rather caused by natural flucutuations and drift in the data, or eventual cellular photodamage.

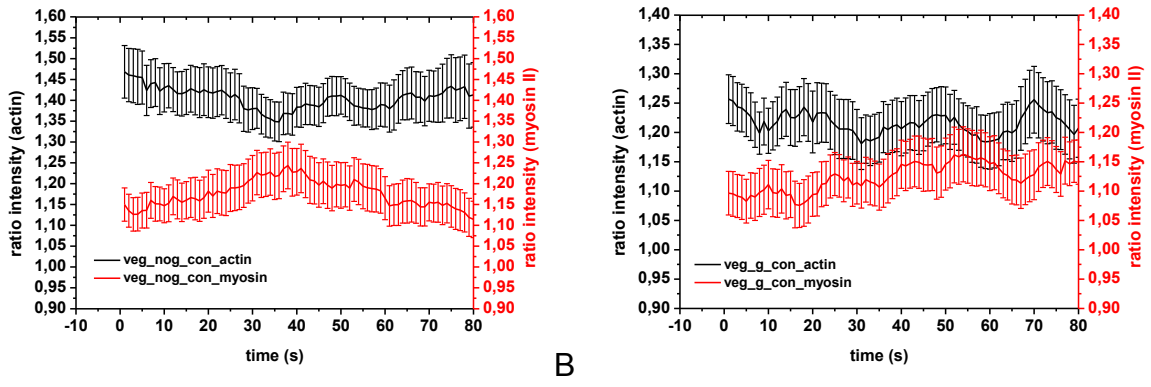

A B

Figure 46 - Actin and myosin II control curves of vegetative cells. In A, cells not exposed to a photouncaging laser pulse, and not incubated in caged-cGMP are shown. The y axis on the left (black) shows the values for the actin curve, the y axis on the right (red), the values for myosin II. Number of cells analyzed: 23 for both actin and myosin II. In B, cells not exposed to a photouncaging laser pulse, but with incubation in caged-cGMP are shown. The y axis on the left (black) shows the values for the actin curve, the y axis on the right (red), the values for myosin II. Number of cells analyzed: 22 for both actin and myosin II. In A and B, error bars indicate the standard error.

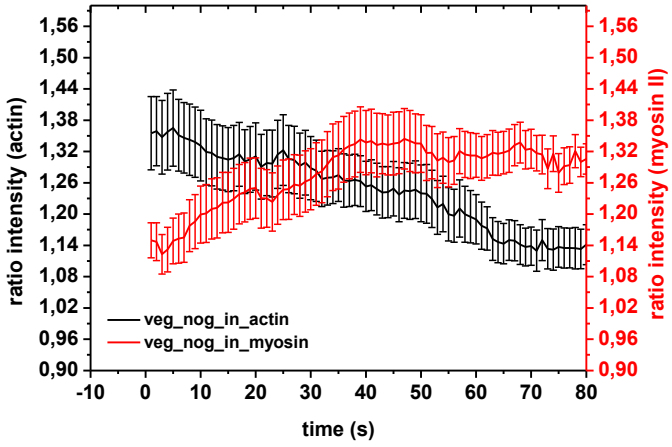

Figure 47 - Actin and myosin II control curves of vegetative cells, with photouncaging laser pulse inside the cells, but no incubation in caged-cGMP. The y axis on the left (black) shows the values for the actin curve, the y axis on the right (red) the values for myosin II. The myosin II increase seen is not interpreted as a myosin II response, see text. Number of cells analyzed: 25 for both actin and myosin II. Error bars indicate the standard error.

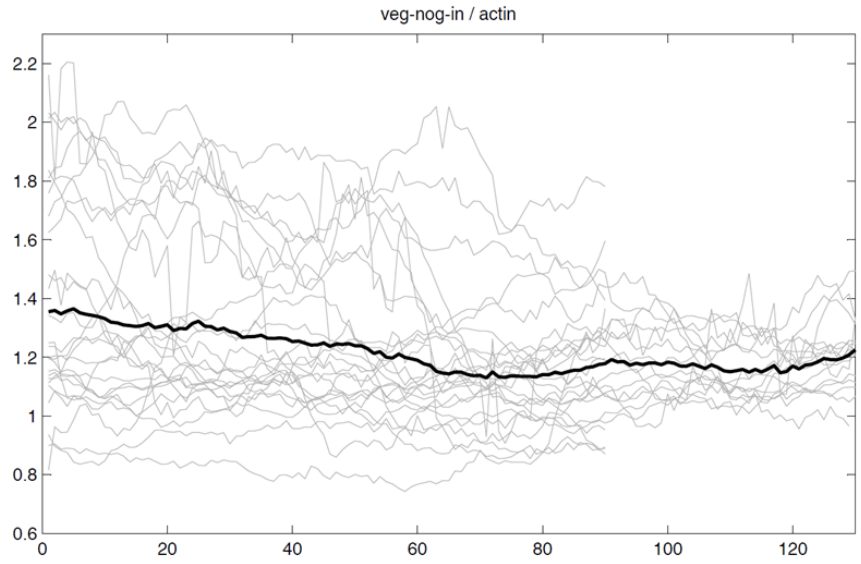

Figure 48 – Single curves for actin response in vegetative cells, not incubated in caged-cGMP but with laser stimulation inside the cell (figure 47). The x-axis represents the time (s), and the y axis the ratio of fluorescence intensities at the cortex and in the cytosol. The bold curve is the mean of all the other curves.

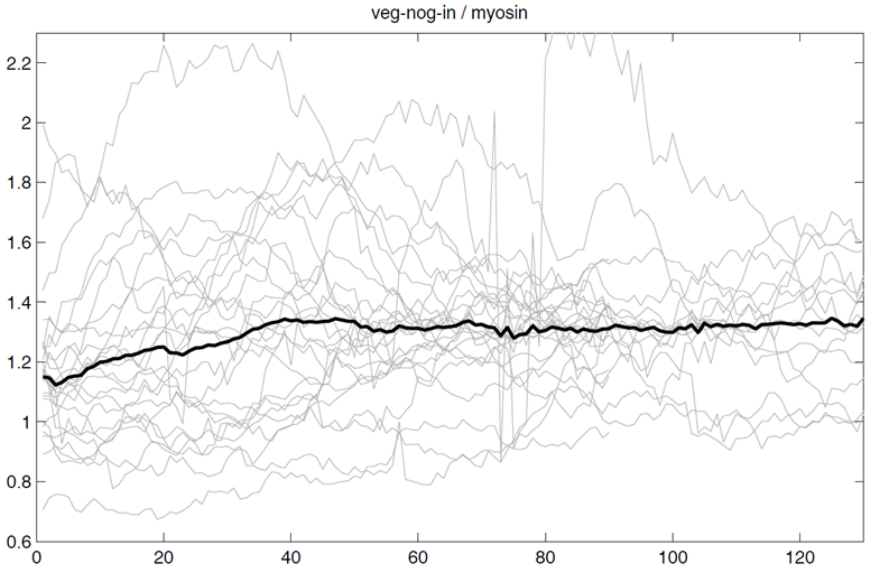

Figure 49 – Single curves for myosin II response in vegetative cells not incubated in caged-cGMP but with laser stimulation inside the cell (figure 47). The x-axis represents the time (s), and the y axis the ratio of fluorescence intensities at the cortex and in the cytosol. The bold curve is the mean of all the other curves.

As shown, for vegetative cells similar actin and myosin II responses as in the starvation developed cells case were found, with the difference that no myosin II response was seen when uncaging outside, whereas a significative actin response

was observed in that case as well. The next table presents a summary of all the photouncaging data, with the relative peak size (biggest value minus basal starting value) and the time point for all actin and myosin II curves that show a response.

	Actin		Myosin II	
	Value	Time (s)	Value	Time (s)
sta_g_in	0.0527	9	0.0404	28
sta_g_out	0.1	3	0.085	34
sta_nog_con	nr	nr	nr	nr
sta_g_con	nr	nr	nr	nr
sta_nog_in	nr	nr	nr	nr
veg_g_in	0.1099	6	0.0451	28
veg_g_out	0.1322	10	0.0556	42
veg_nog_con	nr	nr	nr	nr
veg_g_con	nr	nr	nr	nr
veg_nog_in	nr	nr	nr	nr

Table 3 - Peak size and summary of the photouncaging data. The symbol nr stands for 'no response', in the cases where no clear actin or myosin II response could be observed (including controls). See also table 2 for a summary for all data settings.

3.2.4 Micropipette aspiration controls

When photouncaging DMACM-caged-8-Br-cGMP, Br-cGMP is released, together with the cage itself, DMACM ((7-Dimethylaminocoumarin-4-yl)methyl). The actin and myosin II responses observed could be due to unspecific effects of the cage. Also, I observed pronounced effects for actin and myosin II when uncaging outside. To test whether cGMP was affecting myosin and actin responses from the outside, and to prove that the effect seen is actually due to uncaging inside the cell via stray light, I exposed cells to either cGMP, the membrane permeable equivalent Br-cGMP, the caging molecule DMAC (7-Dimethylamino-4-methyl-coumarin), and Sørensen buffer (control), using the Femtojet micropipette aspiration device (Eppendorf, Hamburg, Germany), see Materials and Methods, section 2.8 for a detailed description of the experimental settings.

Experiments were executed with vegetative and developed cells, and the actin and myosin II response was analyzed separately. When developed cells were exposed to Sørensen buffer, no actin or myosin II response was observed, as shown in figure 50A.

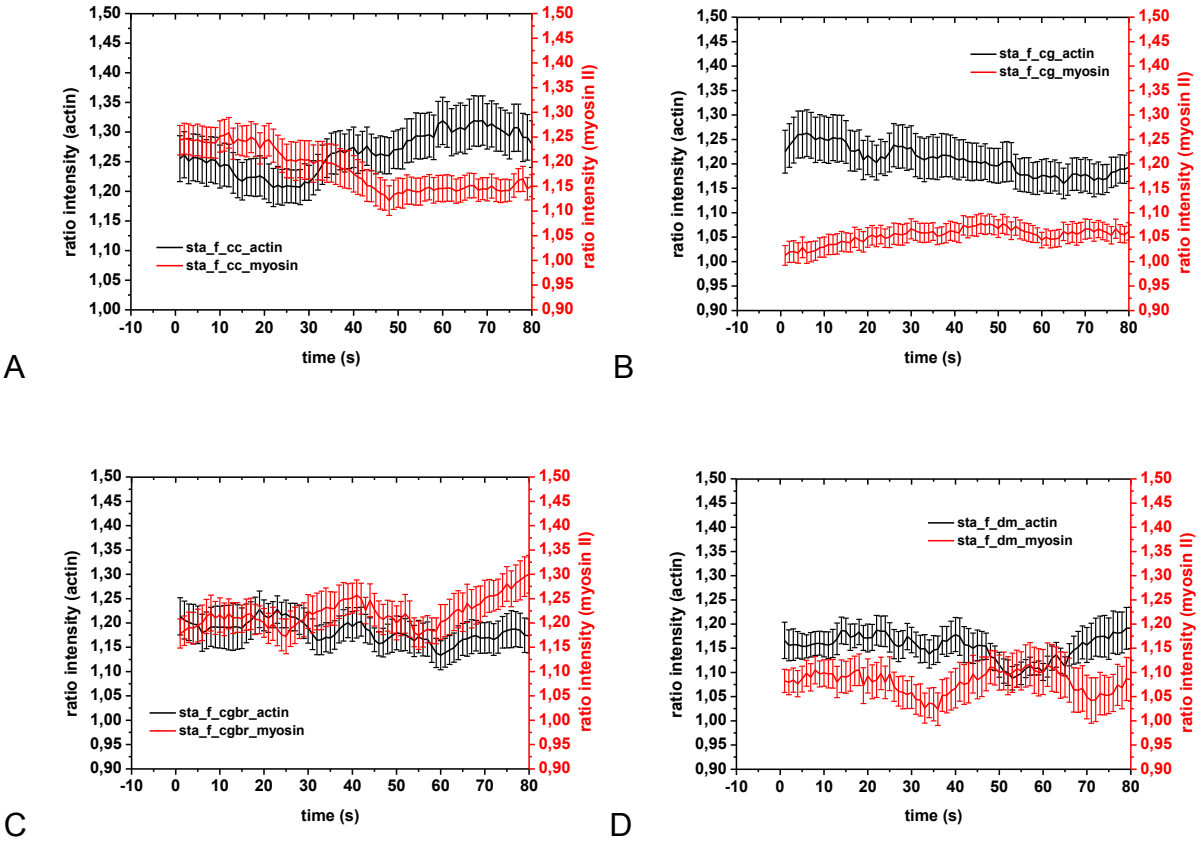

Figure 50 - Actin and myosin II control curves of starvation developed cells. In A, cells were exposed for 10s to Sørensen buffer coming out of a femtotip (Femtojet, Eppendorf). No evident actin or myosin II response was detected. Number of cells analyzed: 35 for both actin and myosin II. In B, cells were exposed for 10s to a 10µM solution of cGMP, coming out of a femtotip (Femtojet, Eppendorf). No evident actin or myosin II response was detected for this case either. Number of cells analyzed: 24 for both actin and myosin II. In C, cells were exposed for 10s to a solution of 10µM of Br-cGMP (membrane permeable cGMP), coming out of a femtotip (Femtojet, Eppendorf). Number of cells analyzed: 20 for both actin and myosin II. The increase starting around time point 55s could be due to Br-cGMP that entered the cell. In D, cells were exposed for 10s to a solution of 10µM DMAC (analogue of the cage used in the uncaging experiments), coming out of a femtotip (Femtojet, Eppendorf). No evident actin or myosin II response could be observed. Number of cells analyzed: 15 for both actin and myosin II. In all curves, the y axis on the left (black) shows the values for the actin curve, the y axis on the right (red) the values for myosin II. Also for all graphics, the error bars indicate the standard error.

Next, I exposed starvation developed cells to cGMP (non-membrane permeable), and to Br-cGMP (membrane permeable analog). These results are displayed in figures 50B and C, respectively. There, again, no significative actin or myosin II response was observed, although starting at time point 55, an increase in myosin II can be seen (figure 50C). This increase could be due the slow entry of Br-cGMP (which is membrane permeable) inside the cell.

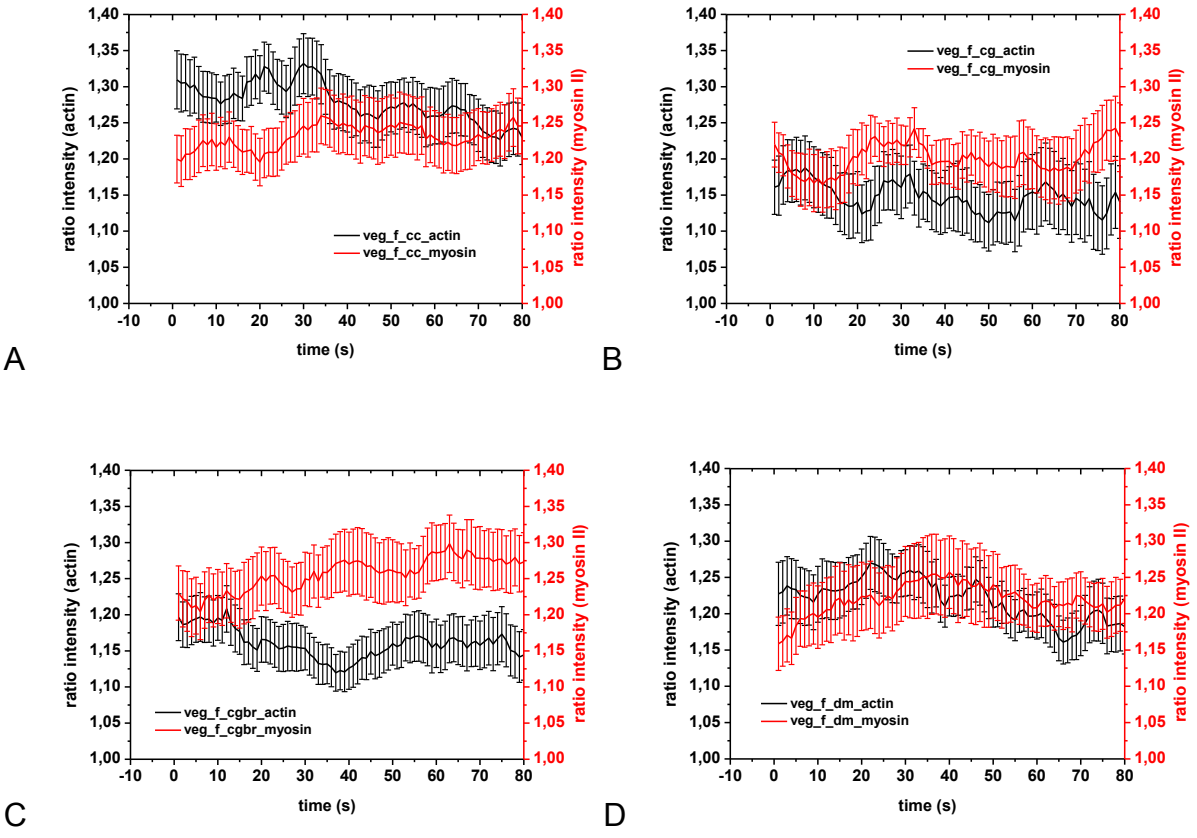

Figure 51 - Actin and myosin II control curves of vegetative cells. In A, cells were exposed for 10s to a control solution of Sørensen buffer only, coming out of a femtotip (Femtojet, Eppendorf). No evident actin or myosin II response could be observed. Number of cells analyzed: 25 for both actin and myosin II. In B, cells were exposed for 10s to a 10µM solution of cGMP, coming out of a femtotip (Femtojet, Eppendorf). No significative actin or myosin II response could be observed either. Number of cells analyzed: 24 for both actin and myosin II. In C, cells were exposed for 10s to a solution with 10µM Br-cGMP, coming out of a femtotip (Femtojet, Eppendorf). Again, no evident actin or myosin II response could be observed. Number of cells analyzed: 22 for both actin and myosin II. In D, cells were exposed for 10s to a solution containing 10µM DMAC, coming out of a femtotip (Femtojet, Eppendorf). No significative actin or myosin II response could be observed. Number of cells analyzed: 22 for both actin and myosin II. In all curves, the y axis on the left (black) shows the values for the actin curve, the y axis on the right (red) the values for myosin II. Also for all graphics, the error bars indicate the standard error.

At last, I wanted to check whether the cage itself, DMACM [((7-Dimethylaminocoumarin-4-yl) methyl)], could trigger any actin or myosin II response. For that, I used an analog of the cage, DMAC (7-Dimethylamino-4-methyl-coumarin), again with a concentration of 10μM. The results are plotted in figure 50D. As in the other control experiments, no significative actin or myosin II responses could be observed.

The same Femtojet experiments were repeated for vegetative cells. The Femtojet plots for Sørensen buffer control (veg_f_cc, fig. 51A), cGMP exposure (veg_f_cg, fig. 51B), Br-cGMP exposure (veg_f_cgbr, fig. 51C) and the cage DMAC exposure (veg_f_dm, fig. 51D) in vegetative cells are shown above.

No actin or myosin II responses were detected in those cases either, confirming that:

1. The cage itself is not responsible for the initiation of actin or myosin II response from the outside of the cell; and
2. Cyclic GMP released in the extracellular environment does not activate the responses seen in the uncaging experiments. The actin and myosin II responses seen in the case of uncaging outside of the cell were due to intracellular photouncaging by stray light.

3.3 The impact of Polyphosphoinositide-Binding Peptide (PBP10) on cell shape and dynamics

3.3.1 PBP10 suppresses pseudopod formation in D. discoideum cells

PBP10 is a peptide coupled to Rhodamine B (RhB-QRLFQVKGRR) that is supposed to bind phosphoinositides, especially PIP_2 (108). When bound to PBP10, PIP_2 should not be available for phosphorylation and conversion to PIP_3. Binding of cAMP to cAR in starvation developed cells induce the phosphorylation of PIP_2 to PIP_3, which is part of the directional sensing pathway in *D. discoideum* (136). The increase of cAMP in developed cells leads to the translocation of PH domain-proteins from the cytosol to the plasma membrane. The PH domains of many proteins specifically bind to 3-phosphoinositides, such as PIP_3. For example PH-$_{CRAC}$ is recruited to the leading edge, where it activates the ACA (136, 137). We therefore want to investigate the effect of PBP10 on cells. Phosphoinositides are not essential for chemotaxis, but are known as the internal compass of the cell (91, 136), therefore it is important to investigate how PBP10 affects *Dictyostelium* cells.

To find an adequate concentration of PBP10 (physiologically active but not lethal), I counted the ratio of living and dead cells in a control experiment (no drug treatment) and after drug treatment with different concentrations, using the exclusion dye Trypan Blue. The concentration I chose for most of the following experiments was 6µM (figure 52).

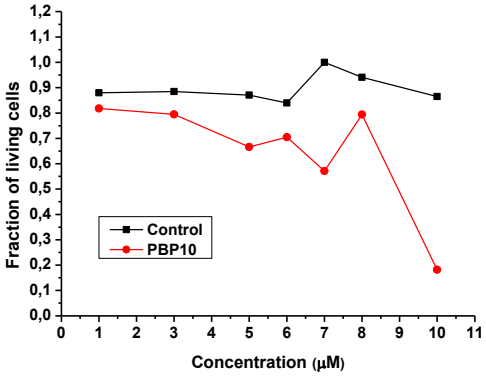

Figure 52 – Median lethal dose, Trypan Blue method. Cells (AX2-WT) were incubated for at least 30 minutes with the drug, and then dead and living cells were counted using the exclusion dye Trypan Blue. Around 15 cells were counted for each data point.

Similar to the Wiskostatin experiments, I first compared the cell morphology of untreated cells and drug-treated cells. As can be seen in figure 53, cells get rounder and show reduced pseudopod formation when PBP10 is added. In the confocal image, one can also see that PBP10 accumulates in vesicles inside the cell. Localized F-actin structures can be seen inside the PBP10-treated cells, unlike in control cells.

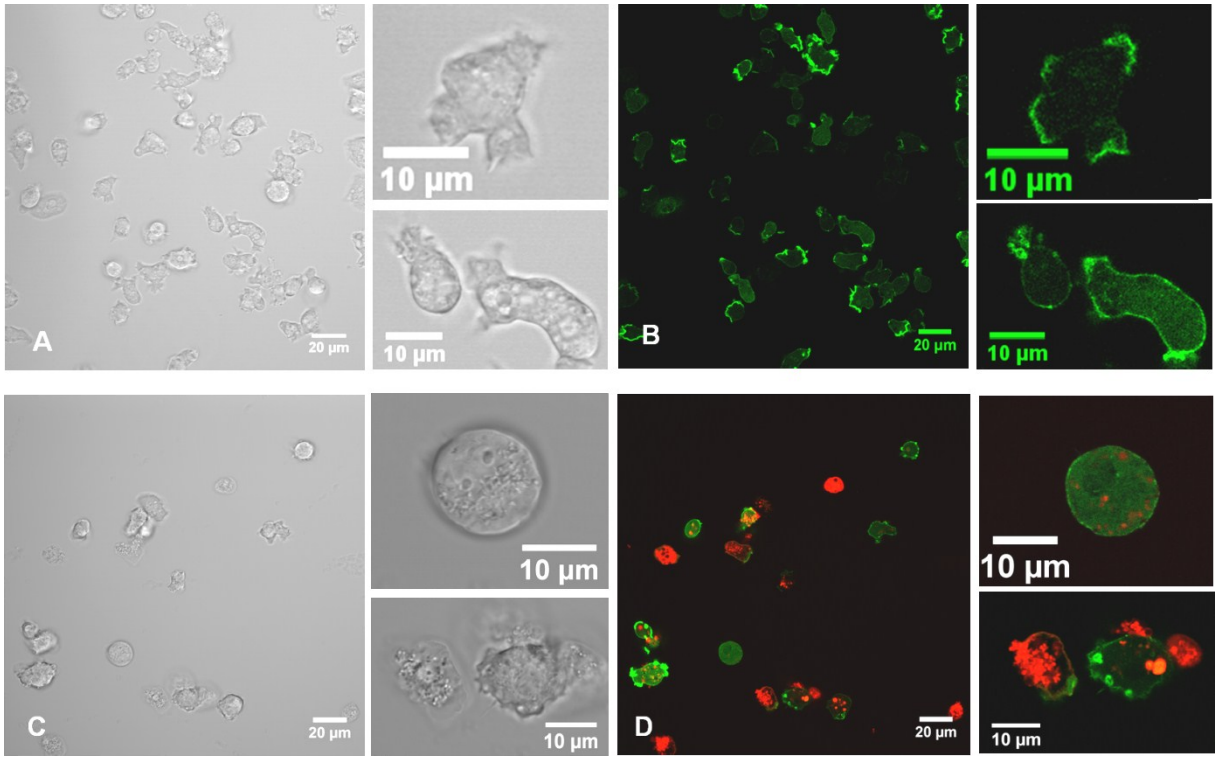

Figure 53 - Cell morphology, LSM 710 microscope (Zeiss). In A and B, brightfield and fluorescence images of vegetative LimEΔ-GFP cells (AX2) in buffer (control) are shown, respectively. In C and D, images of cells after drug treatment with 6µM PBP10 are displayed. Cells were exposed to the drug for at least 30 minutes. PBP10 can be seen in red.

To quantify the morphological changes after PBP10 exposure, I measured the cell roundness based on the isoperimetric inequality (section 2.9). The average roundness of a population of vegetative *D. discoideum* cells was calculated using a custom made Matlab program, developed with the help of Achim Quaas. The cell roundness increased around 26% after PBP10 treatment (figure 54). After washing, cells were on average 5% rounder than with the control cells.

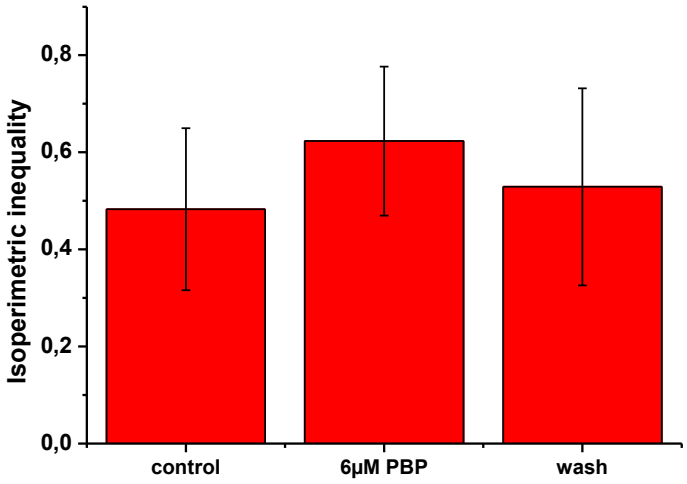

Figure 54 - Cell recovery assay. The mean isoperimetric inequality is plotted for control cells (n=24), drug treated cells (PBP10 6µM, n=21), and washed cells (recovery, n=10). Cells used were taken from the same shaking culture.

3.3.2 Cells treated with PBP10 are still able to translocate PH domains to the membrane

To image PH-domain translocation dynamics in vivo, GFP can be tagged to the pleckstrin-homology (PH) domain of the cytosolic regulator of adenylyl cyclase (CRAC). In developed cells, uniform extracellular cAMP concentrations induce transient translocation of PH-$_{CRAC}$-GFP from the cytosol to the membrane (8). I used *D. discoideum* transfected with the plasmid WF38 (a gift from Peter Devreotes, for details see section 2.14) to analyze the translocation of PH-$_{CRAC}$ to the membrane after a cAMP stimulus, with and without PBP10. Experiments were conducted as described in section 2.13. The PH-$_{CRAC}$ translocation can be seen as an increase in the fluorescence at the membrane and a simultaneous depletion of the cytosol. In the following figures, the PH-$_{CRAC}$ translocation is shown for control experiments and for cells incubated with PBP10.

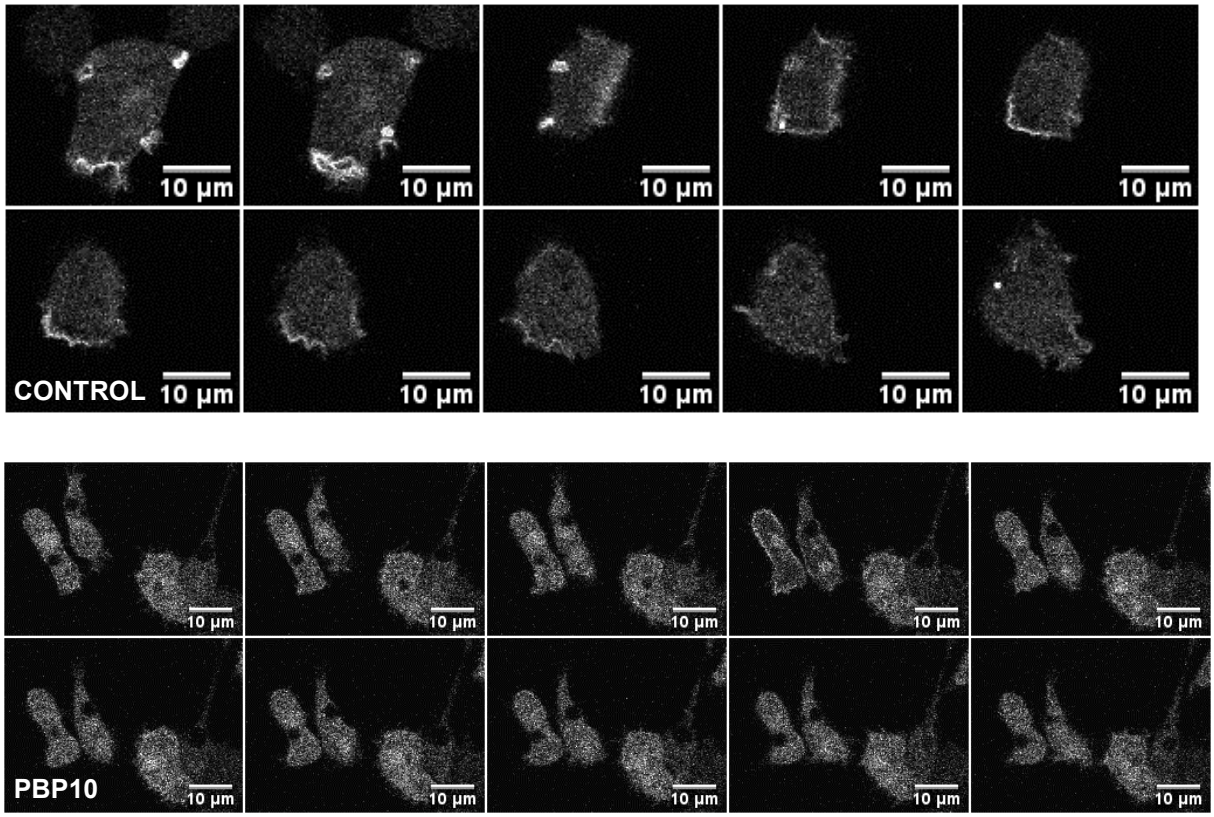

Figure 55 – PH-$_{CRAC}$ translocation, with 10nM cAMP. A time interval of 10s exists between each frame, from left to right.

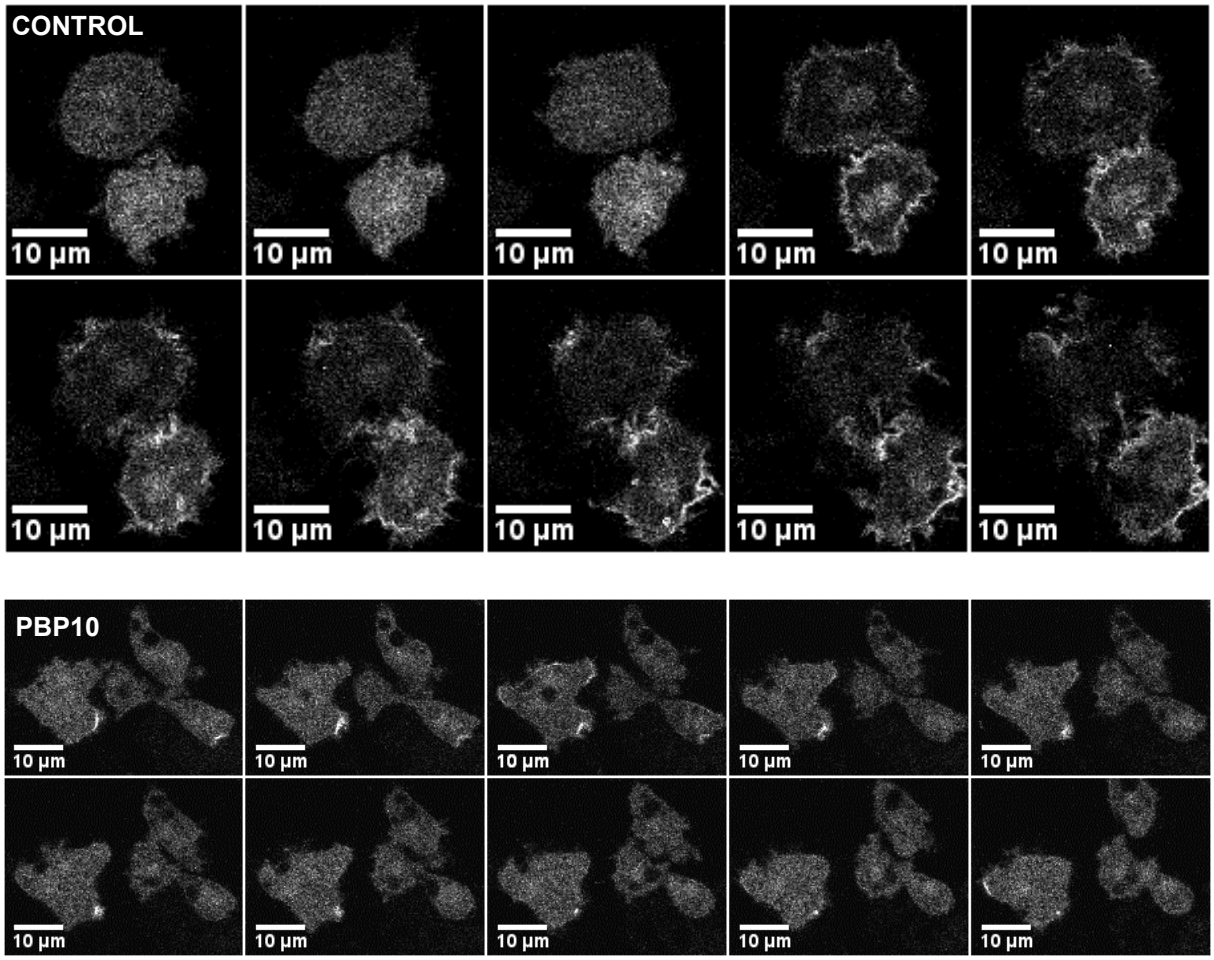

Figure 56 - PH-$_{CRAC}$ translocation, with 100µM cAMP. A time interval of 10s exists between each frame, from left to right.

As can be seen in figures 55 and 56, PH-$_{CRAC}$ translocation occurs in cells incubated with 6µM PBP10. This could either indicate that the PBP10 concentration was not sufficient to block PH-$_{CRAC}$ translocation or that PIP_2 can still be converted to PIP_3 when PBP10 is bound to it. For the example showed in figure 56 (100µM), I quantified the translocation of PH-$_{CRAC}$ to the cytosol (figure 57), using a custom made Matlab program (for details see sections 2.8 and 2.14). The PH-$_{CRAC}$ translocation in cells treated with 6µM PBP10 is delayed if compared to control cells (figure 57B), but this could be due to a delayed diffusion of cAMP into the chamber.

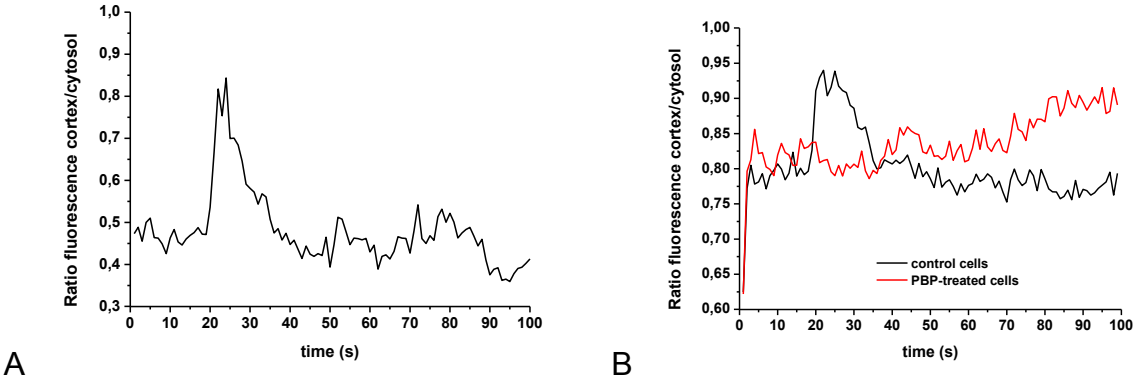

Figure 57 - PH-CRAC translocation, measured as the ratio of the fluorescence intensity in the cortex by the fluorescence in the cytosol. In A, the ratio intensity of a single control cell, exposed to 100µM cAMP, is shown. In B, the mean response calculated for 8 cells (control) and 7 cells (cells treated with 6µM PBP) is shown. Note that the ratio for PBP10-treated cells increases after second 60 in the data series.

3.3.3 Cell-substrate adhesion is reduced by PBP10

Cells changed their morphology when exposed to PBP10, as observed in section 3.3.1. Because of that, I decided to look at the cell adhesion to the substrate. I observed that cells exposed to high concentrations (12µM) of PBP10 showed reduced substrate adhesion compared to control cells (figure 58).

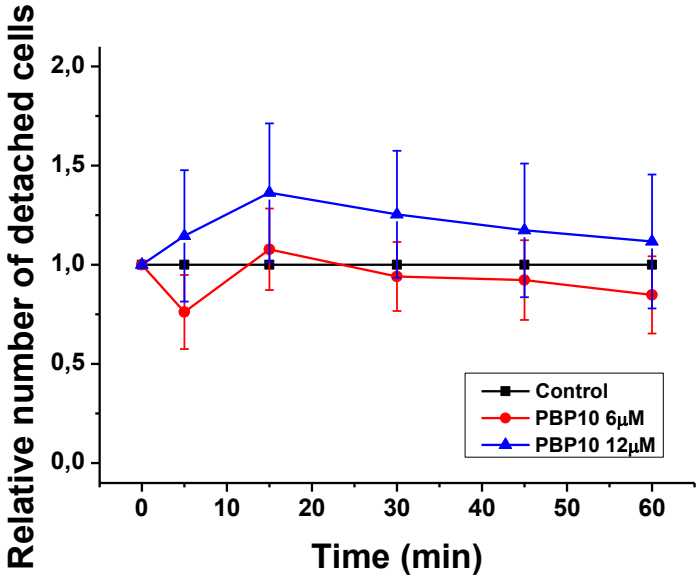

Figure 58 – Cell adhesion assay: ratio of detached cells versus control cells. Cells were incubated for 30 minutes with PBP10 before starting the experiment, control cells were incubated in phosphate buffer. The mean of 4 independent cell counts is shown.

Lower concentrations of the drug did not significantly affect cell adhesion in *Dictyostelium discoideum*.

3.3.4 Random cell motility is impaired by PBP10

It is known that PIP_3 production is not essential for chemotaxis and cell polarization. Quintuple knockouts of PI3K are still able to chemotax towards a pipette filled with cAMP (91). Since PBP10 drastically alters cell morphology and binds to phosphoinositides, the conduction of cell motility experiments proved to be essential for a deeper analysis of the effect of the peptide on cells. Cell motility is indeed negatively affected when cells are incubated with PBP10, as can be seen in figures 59, 60 and 61.

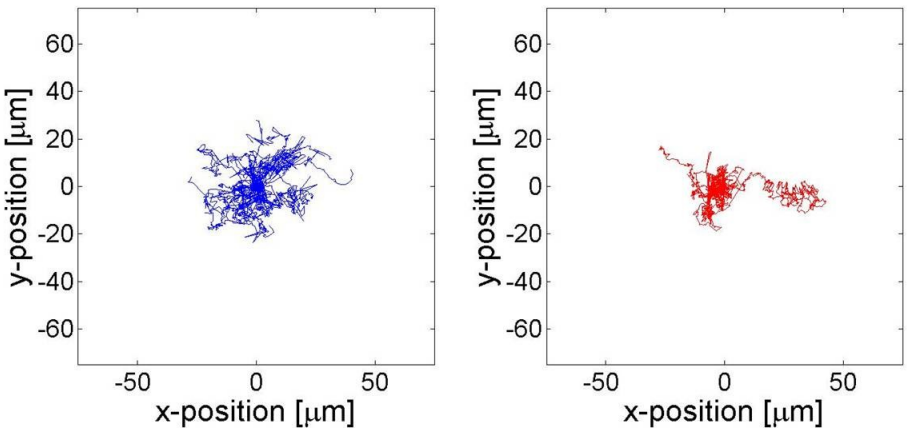

Figure 59 – Example of tracks of random motility. In blue, trajectories of control cells in HL-5 medium are showed. In red, cells incubated with 8μM PBP10 displaying impaired migration in HL-5 medium are showed. AX2-WT vegetative cells were used in this experiment.

In general, the motility of vegetative cells (figures 59 and 60) seems to be less affected than the motility of developed cells (figure 61).

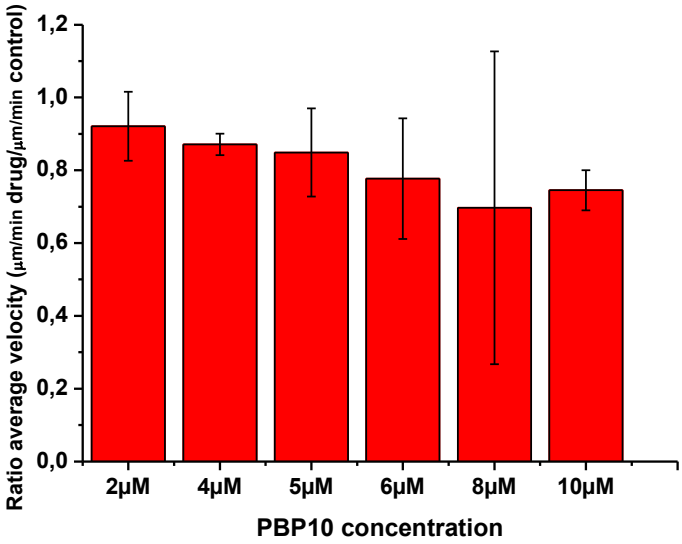

Figure 60 - Effect of different PBP10 concentrations on random cell motility of vegetative cells. Cells were incubated for one hour with the drug and images taken every 10s, during 4h. Velocity was calculated using a cell tracking program, see methods section 2.7. Cells were recorded in HL-5 medium, in the presence of PBP10 at the indicated concentrations.

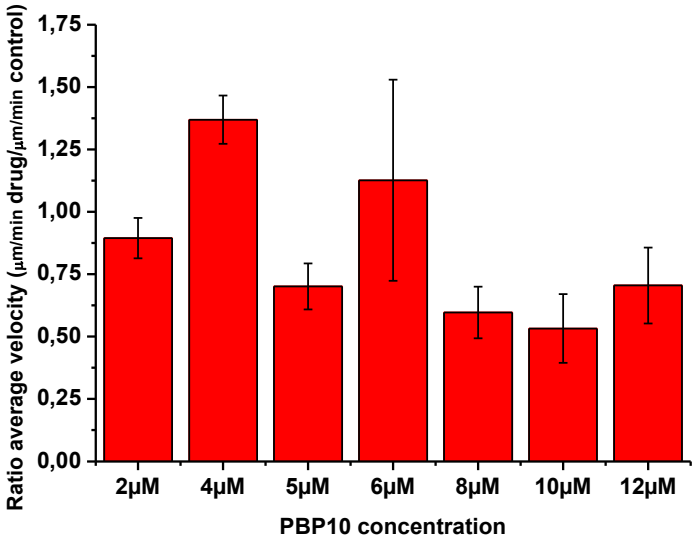

Figure 61 - Effect of different PBP10 concentrations on random cell motility of developed cells. Cells were incubated for one hour with the drug and images taken every 10s, during 4h. Before, cells were pulsed with cAMP for 5h. Velocity was calculated using a cell tracking program, see methods section 2.7. Cells were recorded in Sørensen phosphate buffer, in the presence of PBP10 at the indicated concentrations.

Although the effect of PBP10 on cell motility seems more pronounced when cells are developed, the fact that cells move faster when exposed to 4 and 6μM PBP10 (figure 61), points to deficiencies in the data analysis. When cells are developed, it is very difficult to quantify random motility over a longer time, since cells start aggregating. The control and drug experiments started at the same time, in parallel. It was observed that control cells aggregate before cells exposed to the drug, see figure 62. This could be the reason why the cells exposed to the drug have a higher average motility, since more moving single cells are counted when compared to the aggregating control cells. Another reason could be the heterogeneity in the developmental state of these cells.

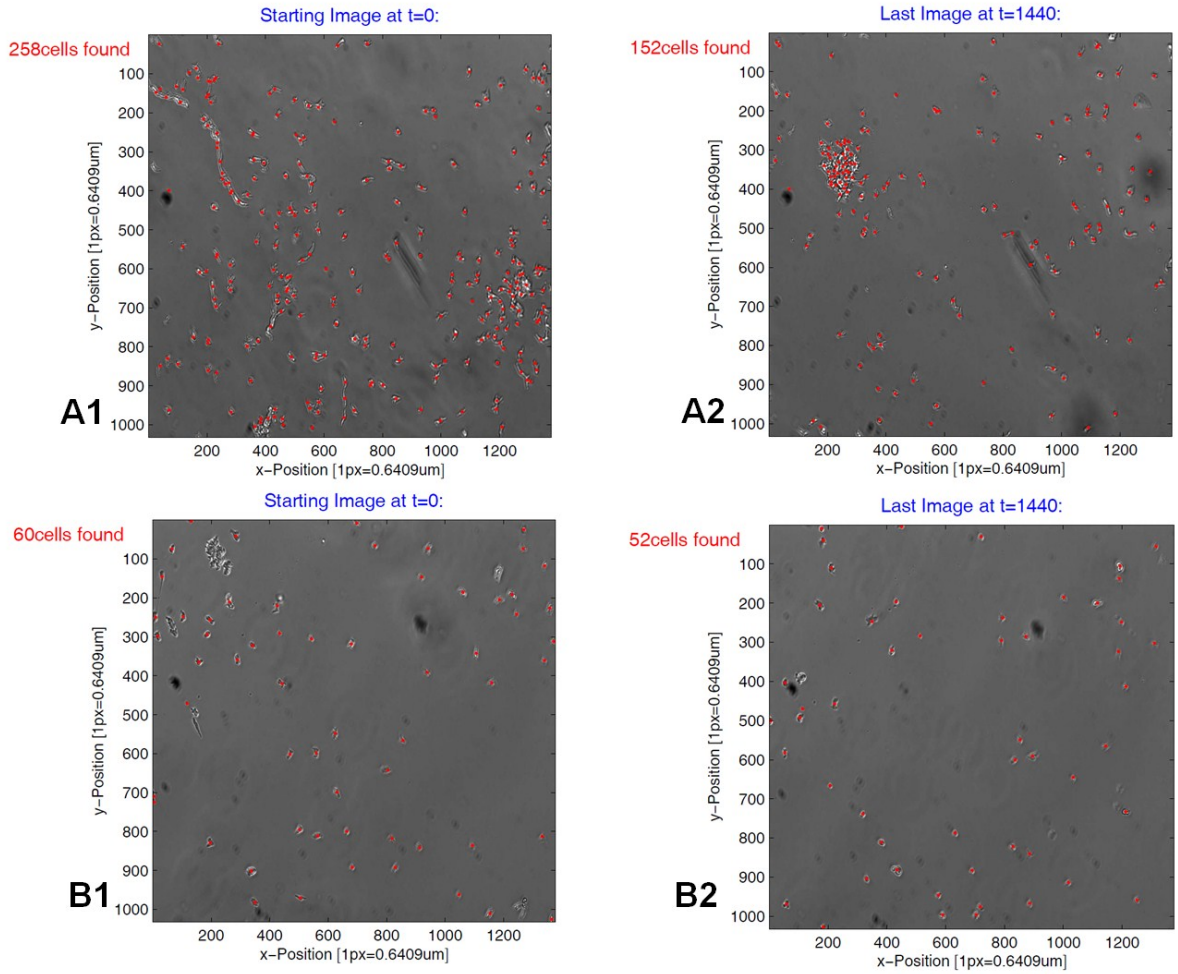

Figure 62 – Example illustrating a random motility experiment. In A1, the first frame of an experiment with control cells (including the number of cells tracked at this image) is showed. In A2, the last frame of this control experiment is displayed. Note that the aggregates affect the cell counting of the custom made Matlab code. In B1, the first frame of an experiment of cells treated with 4μM PBP10. Note that these cells do not show aggregates as compared to control cells. In B2, the last frame of the tracking of PBP10-treated cells is displayed.

3.3.5 Chemotaxis is affected by PBP10

To investigate the effect of PBP10 on chemotaxis, LimEΔ-GFP cells were pulsed and exposed to a gradient of cAMP that was generated by a pipette filled with 10^{-4}M cAMP. Confocal images were acquired on a Zeiss LSM710 microscope, and analyzed with the cell tracking program described in section 2.7. I did the chemotaxis assay using the following PBP10 ambient concentrations: 2μM, 4μM, 5μM, 6μM, 8μM, 10μM and 12μM. In most cases, the chemotactic performance was strongly impaired in the presence of PBP10. However, no systematic trend of the chemotaxis indexes (CIs) of cells treated with different PBP10 concentrations could be observed. Furthermore, cells from control experiments had different CIs. This could be due to heterogeneity in the developmental state of those cells. For 4μM and for 6μM I performed two independent experiments, because of variations of the CIs, and excluded the two first experiments, because most likely, the cells were not developed or not healthy. The controls in these cases had a smaller CI than the drug-treated cells. Table 4 summarizes the chemotactic index for control and PBP10-treated cells.

PBP10 concentration	CI control (buffer only)	CI drug
2μM	0.35	0.25
4μM (2)	0.19	0.19
5μM	0.36	0.1
6μM (2)	0.26	0.13
8μM	0.19	0.11
10μM	0.18	0.039

Table 4 – Chemotaxis indexes of control cells and cells treated with different concentrations of PBP10.

In the following images of trajectories (figure 63 A to F), control experiments are displayed next to drug experiment. Blue traces are trajectories of cells moving in the direction of the pipette (CI > 0), red traces belong to trajectories of cells moving in the opposite way of the pipette (CI < 0). The position of the pipette tip is represented by an asterisk in the images. For details on how CIs were calculated and cell trajectories analized, please see section 2.7 (Materials and Methods).

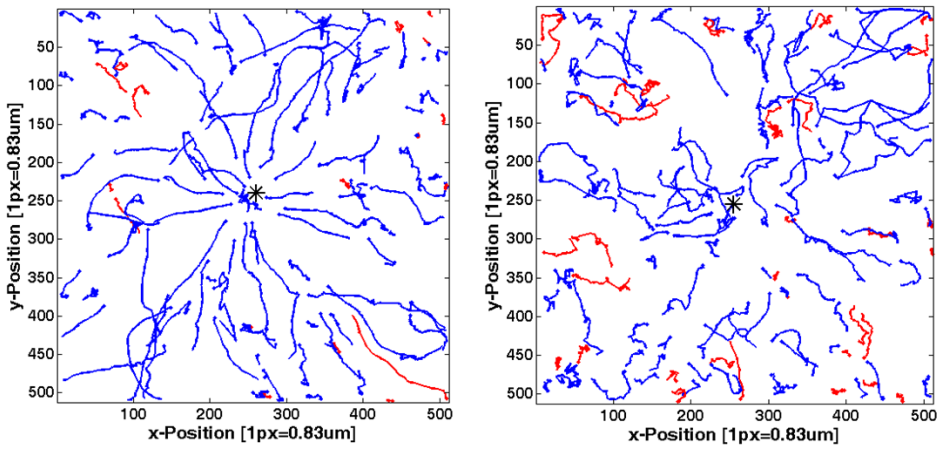
y-Position [1px=0.83um]
x-Position [1px=0.83um]
control
2 µM PBP10

A

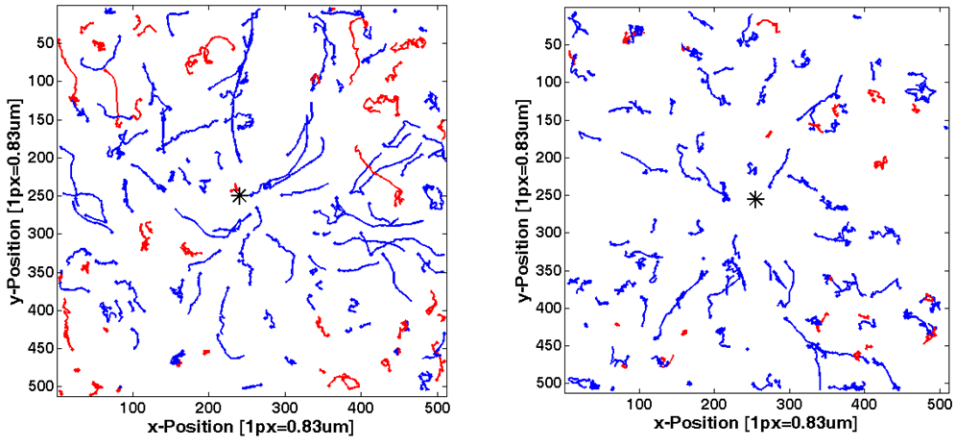
y-Position [1px=0.83um]
x-Position [1px=0.83um]
control
4 µM PBP10 (2)

B

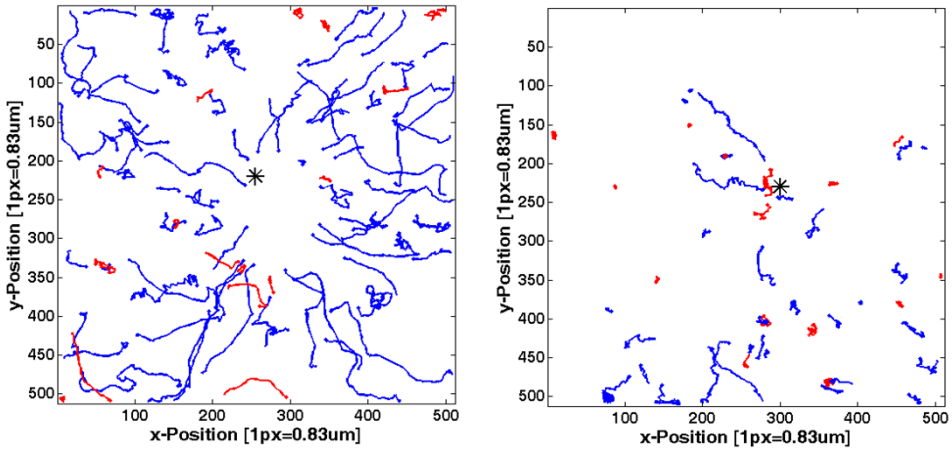
y-Position [1px=0.83um]
x-Position [1px=0.83um]
control
5 µM PBP10

C

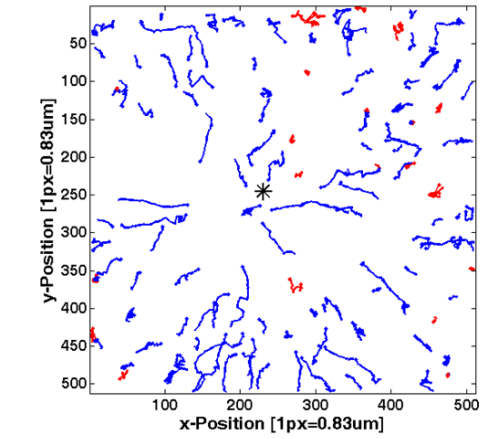

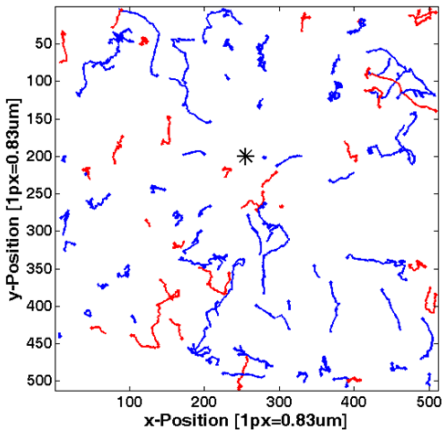

D

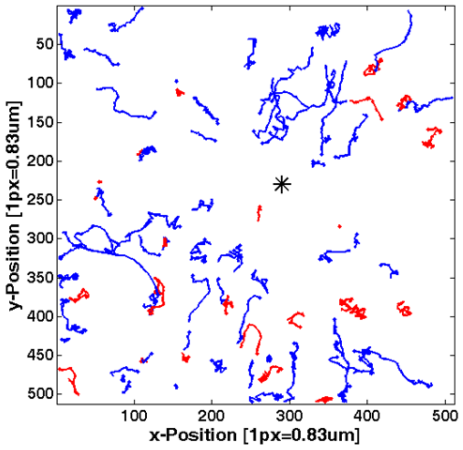

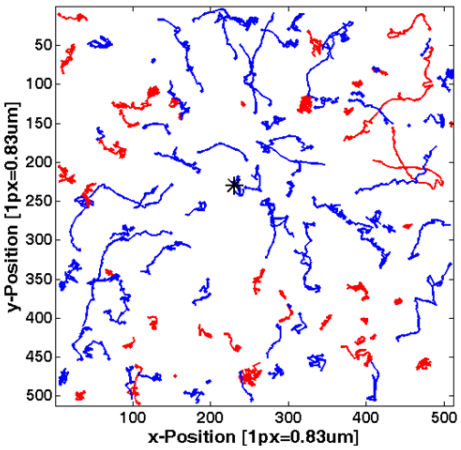

E

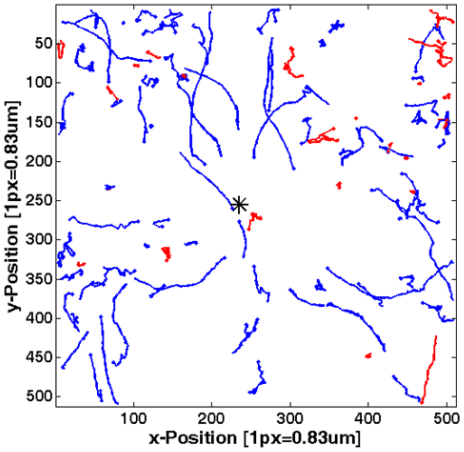

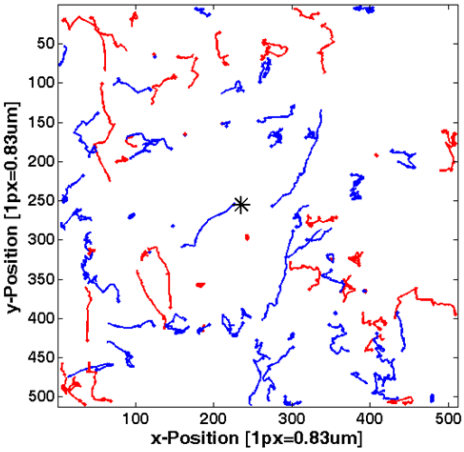

F

Figure 63 - Trajectories of control cells (left) and cells treated with different concentrations of PBP10 (right) of pulsed cells. Observe how trajectories of cells treated with the drug are less persistent. The trajectories correspond to the ones listed in table 1: A- 2µM, B- 4µM$_{(2)}$, C- 5µM, D- 6µM$_{(2)}$, E- 8µM, F- 10µM.

4 Discussion

Cell motility and chemotaxis play an important role in many essential processes, for example, the sourcing of nutrients, the formation of multicellular structures in protozoa, the tracking of bacterial infection by neutrophils, the organization of the embryo in metazoan, and tumor cell spreading from primary tumors (138, 139). It is generally accepted that actin polymerization acts via pseudopod formation as the main driving force in eukaryotic cell motility (140). However, many open questions remain about how intracellular signaling is coupled to the actin cytoskeleton (141).

In this work, I selected three signaling events involved in cytoskeleton dynamics, and investigated them using photouncaging and pharmacological tools. The influence of the actin nucleator Arp2/3 was investigated using the WASP-inhibitor Wiskostatin. The cGMP-dependent actin and myosin II responses were analyzed using uncaging of inactive caged-cGMP. Finally, the upstream effect of phospholipid signaling was studied using the phosphoinositide-binding peptide PBP10.

4.1 Wiskostatin treatment influences mechanical stability, adhesion, and dynamics of motile cells

The WASP protein family has emerged as a family of important regulatory molecules connecting signaling pathways involved in cytoskeleton dynamics (142). The effect of Wiskostatin on the morphology of the cells was clearly visible and highlighted the importance of proteins of the WASP family in cell motility and pseudopod formation. Cells exposed to Wiskostatin were round, with no or few pseudopods. Wiskostatin increases cell roundness by 30%, and this effect is mostly partially reversible.

The impact of Wiskostatin on the subcellular organization of the actin cytoskeleton was studied using total internal reflection fluorescence (TIRF) imaging. In control LimEΔ-GFP cells, the filamentous actin structures of the cell cortex are clearly visible. In Wiskostatin-treated LimEΔ-GFP cells, the overall network structure

appeared similar to the control, but the cells exhibited a reduced cell-substrate contact area. Additionally, the TIRF images of WASP A-GFP cells treated with Wiskostatin show less WASP A activity compared to the control cells. Wiskostatin also affects SCAR, as showed by the SCAR-GFP TIRF images. It is known that Wiskostatin does not bind to the VCA (*verprolin homology, central hydrophobic region, acidic region*) region of WASP (106), also named the *poly-proline region, WH2 motif, C motif and acidic region* (43). Instead, Peterson showed that Wiskostatin binds to the GBD regulatory module of N-WASP that maintains the protein in its autoinhibited conformation. Although SCAR does not have a GBD region, SCAR-GFP cells showed less wave formation in the presence of Wiskostatin. This could be due to unspecific binding of Wiskostatin to other cell targets or due to a compensation mechanism after WASP impairment as a consequence of the drug treatment. Bompard and collaborators (143) suggest that Wiskostatin might have other targets than only WASP. In their experiments, they demonstrated that the inhibition of cytokinesis by Wiskostatin is not due to the effect of the drug on WASP and consequently Arp2/3. Additionally, it was demonstrated that Wiskostatin deplete the ATP levels in cells (144), and this could be a reason for the impairment in motility in chemotactic cells.

Pseudopod formation relies on the synchronized force generation mechanisms in the actin cytoskeleton. It is strongly affected by Wiskostatin treatment, as showed in the morphological assays. The remaining F-actin rich structures could be the remnants of pseudopods, the formation of which is not completed due to the action of the drug. The mechanical properties of these cells in general should be altered. Indeed, cells treated with Wiskostatin are ‘softer’, as seen in the experiment with the fluidic *cell squeezer* device. The treatment of the cells with Wiskostatin thus resulted in a reduction of the mechanical stability as compared to fully intact wild type cells. The cell deformability is comparable to the one achieved with cells treated with Latrunculin A. However, contrary to the LatA-treated cells, no decrease in the total amount of F-actin was observed in the Wiskostatin-treated cells as compared to the control cells. Since the loss of cellular mechanical stability of Wiskostatin-treated cells is not caused by a lower F-actin content, we conclude that Wiskostatin affects Arp2/3-mediated nucleation and branching of actin filaments, leading to an altered

and less rigid micro-architecture of the actin cytoskeleton and, thus, to a change in the mechanical properties of the cells. Since the specificity of Wiskostatin is doubted (143), it can not be excluded that these effects are mediated by changes in other proteins than the Arp2/3 complex.

Cellular functions like cell adhesion and motility crucially depend on the mechanical properties of the actin cytoskeleton. They are of high medical relevance due to their central role in cancer metastasis and connective tissue disorders (145). The mechanisms of *Dictyostelium* cell-to-substrate adhesion are not known. They are probably mediated by contact sites associated with F-actin rich regions in the cell cortex (146, 147). As cell-to-substrate adhesion is not reduced under the influence of Wiskostatin, either these regions remain fully intact, or they are of only secondary importance for cell adhesion. Surprisingly, our experiments showed that an increased cell-to-substrate adhesion is observed under the influence of Wiskostatin. Generally, the formation of pseudopods induces significant fluctuations in the cell-substrate contact area (147). Such fluctuations could make the cells more susceptible for the effects of external fluid shear stress. Since Wiskostatin reduces pseudopod formation, this could explain why an increased substrate adhesion is observed in the presence of the drug.

The function of WASP in cell motility is controversial, especially in *D. discoideum* cells, but it is known that WASP is involved in clathrin-mediated endocytosis (43). Lowered expression of WASP via targeted knockdown of the gene in *Dictyostelium* impaired the ability of cells to polarize, polymerize F-actin and migrate towards cAMP (142). WASP interacting protein (WIP) interacts with human N-WASP and binds to F- and G-actin (148). Involvement of WASP in the formation of actin-based structures like lamellipodia and filopodia is controverse, as the involvement of WASP in chemotaxis and its importance in cell motility (46). To investigate this question further, the movement of both vegetative and starvation developed cells that were exposed to different concentrations of Wiskostatin was quantified. While vegetative cells were only slightly affected by Wiskostatin, the motility of developed cells showed a pronounced decrease for larger concentrations of the drug. The fact that developed cells were more affected by the drug treatment than vegetative cells can be explained by the higher basal velocity in random motility

of developed cells, and underlies the importance of WASP for the movement of developed cells. Depletion in the cellular ATP content (143) could also be a reason for the reduced motility. Chemotaxis was negatively affected by Wiskostatin. An explanation could be that the increased substrate adhesion could have as a consequence the decrease in cell motility, given by the lower average velocity of cells in random motility. However, the results show a large variation. The phase during cell cycle in which a cell finds itself when the starvation process begins is crucial for the determination of its cell fate (149). The degree of disruption of the cytoskeleton by Wiskostatin could be also dependent on the cell cycle and developmental stage. This could explain why some cells do not move at all after drug treatment whereas others do not seem much affected by Wiskostatin.

The involvement of WASP in the formation of actin-based structures is controversial (46), but the effect of Wiskostatin on cell mechanics is comparable to the effect of Latrunculin A. A simple model of the action of Wiskostatin could be based on how the drug inhibits WASP and, as a consequence, the nucleation and actin filament branching inside the cells (figure 64).

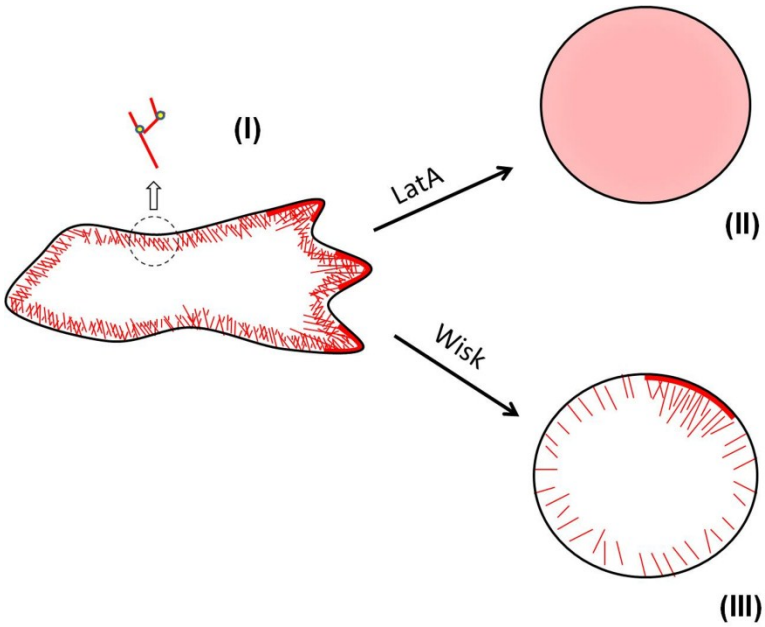

Figure 64 – Model for the action of Wiskostatin in *D. discoideum* cells. With Latrunculin A, no actin polymerization can occur and the level of F-actin drops. In Wiskostatin-treated cells, actin can still be polymerized by actin nucleators other than the Arp2/3 complex, but pseudopod formation is impaired.

In particular, dynamically changing patches of high LimEΔ-GFP concentration indicate freshly polymerized F-actin in regions of increased cytoskeletal activity, figure 64 (I). When treated with LatA, the actin cortex of the cell is rapidly disrupted and filamentous actin structures are degraded. Localization of LimEΔ-GFP in the cortex is no longer observed and cells exhibit a decreased mechanical stability (II). In contrast, cells exposed to Wiskostatin still show localization of LimEΔ-GFP close to the cell membrane, revealing the presence of a cortical actin network with patches of increased actin polymerization. However, these patches do not lead to membrane deformations, indicating that the mechanisms of force generation in the actin cytoskeleton are impaired. With Wiskostatin, there is still a partially intact actin cortex, since other actin nucleators can compensate for non-activated Arp2/3 protein complexes. We conjecture that Wiskostatin treatment, via WASP inhibition and in consequence negatively affecting Arp2/3 activity, results in a cortical actin network that is less branched and cross linked. Although the amount of F-actin is not reduced in such cells, the altered micro-architecture of the cortical network may lead to a reduced stiffness, which is insufficient to support the force generation mechanisms required for pseudopod formation, as shown in figure 64(III).

4.2 Intracellular cGMP induces myosin II association with the cytoskeleton and elicits an actin response

The second point investigated in this work was the influence of cGMP on actin and myosin II dynamics. Putnam and Pedersen (64) were the first to discover cGMP as a signaling factor in *D. discoideum*. Since then, many effects on myosin II were described. In particular, mutants defective in cGMP production cannot recruit myosin II to the cytoskeleton and show no RLC (myosin II regulatory chain) phosphorylation (55). Here, I show directly that cGMP induces the association of myosin II with the cytoskeleton, using a caged-cGMP molecule to locally release cGMP inside the cell, in a controlled manner.

It is not known how much scattered light reaches a cell when a laser is focused into a culture dish, not directly hitting the cell. In the present work I showed, using Dihydroethidium (135), that, up to a distance of about 600µm, scattered light still reaches the cell and is able to induce intracellular photoactivation (see figure 40,

section 3.2.1). This means that in the experimental setting used for the photouncaging of cGMP, the distance of the laser from the cell is only of secondary importance.

The micropipette aspiration controls (Femtojet controls) done by exposing cells to cGMP, Br-cGMP, the cage DMAC, and Sørensen buffer do not show any evident actin or myosin II responses. Based on these results, it can be concluded that all actin and myosin II responses observed are due to the uncaging of cGMP inside the cell and the consequent action of this second messenger inside the cell. I separated all the results in measurements of vegetative cells, and measurements of starvation developed cells. Usually, an increase in cGMP inside *Dictyostelium* cells happens due to cAMP receptor stimulation and cAMP production, which transiently activates the guanylyl cyclases. Cyclic GMP can bind to GbpC, regulating RLC phosphorylation and with that myosin II motor activity, as well as MHC (myosin heavy chain) phosphorylation, which in turn induce myosin II filament assembly (34). Vegetative cells do not express cAMP receptors, but intracellular cGMP can still activate the myosin II machinery. One example is the production of cGMP when cells experience an osmotic stress, which induces the activation of guanylyl cyclase and myosin II filament redistribution (81). In case of hyperosmotic stress, actin structures can also be reorganized in a myosin II-independent manner (83). I show directly that the intracellular release of cGMP is sufficient for myosin II activity in the cortex, as well as for actin polymerization, in both vegetative and developed cells.

Actin and myosin II responses were observed for developed cells when uncaging cGMP inside (sta_g_in, figure 42A), as well as when uncaging outside of the cell (sta_g_out, figure 42B). For vegetative cells, the same results were obtained (veg_g_in, figure 45A), but in the case of uncaging outside, no clear myosin II response was observed (veg_g_out, figure 45B). This result indicates that in vegetative cells, the amount of cGMP released via stray light (with the laser focused outside of the cell) is enough to elicit an actin response, but not enough to stimulate a myosin II response. All controls for vegetative cells show no responses, with the exception of the case when exposing the cell directly to the uncaging laser, with no previous caged-cGMP incubation (veg_nog_in, figure 47). In this case, the myosin II curve shows a rise. We do not relate this rise to a myosin II response, since there is

no clear peak and the subsequent decay of a typical myosin II response is missing. Analyzing the single curves for this data set (figures 48 and 49), one can see that these curves scatter over a wide range and do not show a consistent trend. We thus conclude that the observed rise in the myosin II signal is a consequence of the heterogeneity of this specific data set and cannot be interpreted as a coherent response.

Taken together, our cGMP experiments are, to the knowledge of the author, the first direct evidences that intracellular cGMP activates myosin II filament assembly and also cAMP-independent actin polymerization. It is well known that cGMP is involved in myosin II filament assembly and motor activity (34, 84), but there is no previous report on actin activity due to cGMP. My results provide a strong evidence that cGMP directly induces accumulation of actin in the cell cortex, even in non-osmotic stress conditions. In the following, I discuss possible connections of cGMP signaling and actin dynamics.

A new Rac/PAK/GC/cGMP signaling pathway was described by Guo and co-workers (150), connecting for the first time Rac and cGMP. Rac belongs to the Rho GTPases family of small GTP-binding proteins and regulates cell migration and actin polymerization. In *Dictyostelium,* there are 14 *rac*-like genes identified and only few have been characterized. Overexpression of Rac1A, 1B, and 1C in *Dictyostelium* induced the formation of filopodia and membrane ruffles. Rac1-V12 (constitutively-activated transformants with an amino acid substitution in the expressed Rac1A or Rac1C proteins) mutants have strong defects in the regulation and association of the actin cytoskeleton (151). PAK (p21-activated protein kinases) are effectors of Rac and Cdc42, from the Rho family GTPases, which can respond to receptor-mediated signals. Downstream effectors of PAK are myosin I, myosin II light chain kinase and LIM kinase. Many PAK-related kinases have been identified in *Dictyostelium*, one of them is PAKa (DPAKa). DPAKa plays a role in myosin II regulation and during cell division (34). According to Guo et al., upon ligand binding and activation, receptors would transmit the signals to Rac via guanine nucleotide-exchange factors, and Rac would activate PAK. PAK would directly activate GCs and with that the production of cGMP (150). The linking of Rac and cGMP activity thus indicates that there exists an upstream connection of cGMP and actin polymerization.

Another possible connection is that cGMP activates VASP (vasodilator-stimulated phosphoprotein), that enhances actin polymerization (152). VASP is part of the Ena/VASP family of proteins found in vertebrates, invertebrates, and *Dictyostelium* (152). VASP was first discovered as a protein phosphorylated in response to elevation of cAMP and cGMP in human platelets. In *D. discoideum* the homolog DdVASP was found (152, 153). Members of the Ena/VASP family are found in areas of dynamic actin reorganization, for example the leading edge, tips of filopodia, cell-cell contacts, and focal adhesions (154). Ena/VASP proteins are also involved in axon guidance, phagocytosis, neural tube closure, T cell activation, and attenuation of platelet aggregation (153). In *Dictyostelium*, DdVASP expression occurs in vegetative cells and increases with starvation, peaking at 8h (152). VASP phosphorylation is important for its localization and interaction with WASP and WIPa (WASP interacting protein a) (155). Lin and co-workers (155) showed that VASP phosphorylation still occurs in *Dictyostelium* null strains of the PKA catalytic domain (*pka-cat*$^{-}$) and of guanylyl cyclases (*sgc/gca*$^{-}$). My results might suggest that cGMP itself promotes VASP phosphorylation and, in consequence, VASP activity on filopodia formation, actin filament nucleation, and chemotaxis.

Furthermore, it cannot be excluded that cGMP binds in an unspecific manner to cAMP-dependent proteins when its concentration rises above the basal cellular concentration. In *Dictyostelium*, the basal cellular cGMP level is around 200nM, and it can increase up to 50-fold after stimulation with chemoattractants (156). A cAMP-dependent protein kinase (acronyms PKA or CAK) in *Dictyostelium* was first described in the beginning of the 1980s (157). It was shown that this protein has a δΔG of 13.9 for cyclic GMP (158), where δΔG is a measure of the reduction in binding of a derivative (in this case cGMP) compared to cAMP (159). In *Dictyostelium*, the PKA is composed of a regulatory and a catalytic subunit. When cAMP binds to the regulatory subunit, the latter dissociates from the catalytic subunit rendering it active (160). PKA activity is important for the formation of cAMP waves during development (160). It also affects aggregation, prespore and prestalk differentiations, and terminal differentiation (161).

Protein kinases are only moderately specific, gaining increased substrate specificity by anchor proteins (88). This means that the increase of intracellular

cGMP due to uncaging could activate cAMP-dependent protein kinases, which in turn phosphorylate proteins related to the cytoskeleton. Various kinases are involved in the parallel signaling transduction pathways that lead to cell motility and chemotaxis. Examples are the cGMP-binding protein C (GbpC), member of the Roco protein kinase family, that mediates the recruitment of myosin II to the cortex, the several proteins of the kinase B type, which have substrates in guanonucleotide exchange factors (GEFs), and the p21-activated protein kinase A (PakA) (136).

Figure 65 shows a summary of the relevant cGMP signaling in the cell, including my suggestion that VASP is activated by cGMP, thus enhancing actin polymerization. The influence of other kinases is not showed, but cannot be excluded.

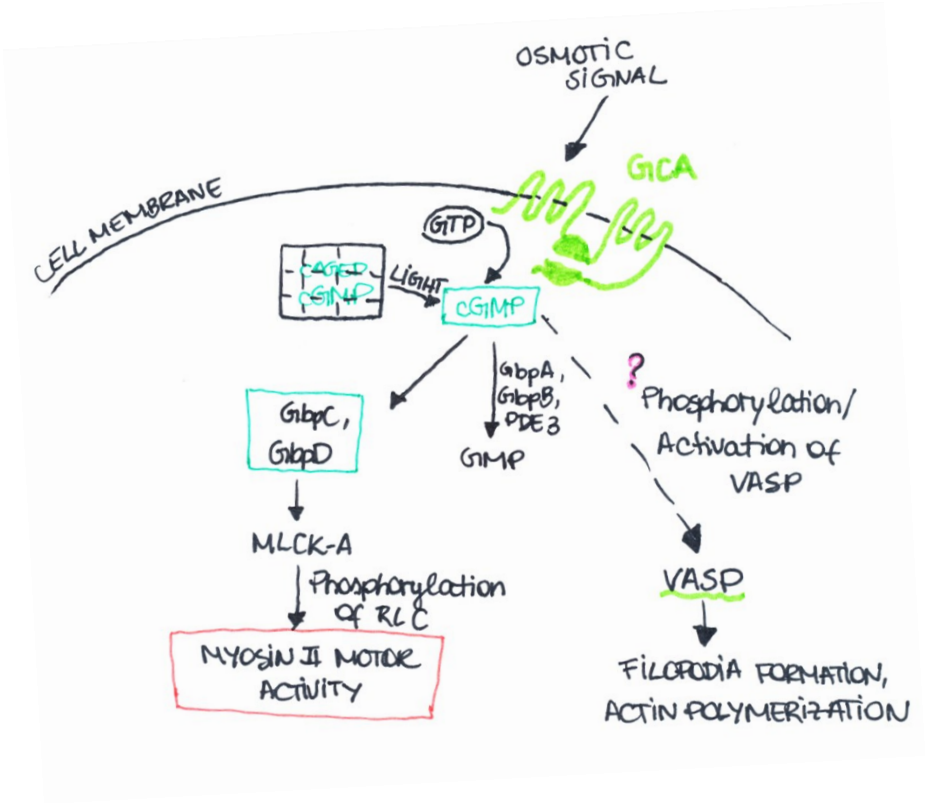

Figure 65 – Cyclic GMP signaling in *D. discoideum* cells. Here, VASP is suggested as the missing link connecting cGMP and actin polymerization independently of cAMP. Based on references (55, 73, 155).

4.3 Polyphosphoinositide binding peptide (PBP10) affects cell shape and motility but does not suppress PIP_3 formation in response to chemoattractant stimuli

Phosphoinositide signaling is involved in chemotaxis and directly affects the dynamics of actin-binding proteins. PIP_3 gradients in the plasma membrane are orientated with the external chemotactic gradient. Phosphoinositides are thus an internal compass of the cell, although PIP_3 is not essential to chemotaxis (91). In third place, I tested the rhodamine-coupled peptide PBP10 on *Dictyostelium discoideum*. I analyzed cell morphology, cell adhesion, cell motility, chemotaxis and PH-CRAC translocation.

Exposure to PBP10 led to round cells, with few or no pseudopods. However, patches of LimEΔ-GFP still accumulated in the cortex. These consequences of PBP10 treatment on the cell morphology are partially reversible (figure 53). When PIP_2 is converted to PIP_3 through the activity of PI3K, PH-$_{CRAC}$ translocates from the cytosol to the cell membrane (96, 131). PI3K is activated by the binding of cAMP to its G protein-coupled receptor. During exposure to PBP10, the PH-$_{CRAC}$ translocation still occurred, even for low concentrations of the cAMP stimulus, showing that receptor specificity, lipid dynamics and the activity of PI3K are not affected. Possibly, there is still enough PIP_2 to be converted to PIP_3 when cells are exposed to a concentration of 6µM of PBP10. Alternatively, it might be possible that PIP_2 can be still phosphorylated by PI3K even when PBP10 is bound to it. In summary, although not affecting the PH-$_{CRAC}$ translocation, it seems that binding of PBP10 to PIP_2 is responsible for the cell morphology changes and the reduction in motility of starvation developed cells.

In mammals, PIP_2 binds to gelsolin and dissociates it from the barbed ends of actin filaments, promoting actin polymerization. PBP10 prevents the binding of PIP_2 to gelsolin and as a consequence the actin cytoskeleton is depolymerized (162). Treatment of dividing *D. discoideum* cells with PBP10 causes regression of the furrow and cytokinesis failure, suggesting a function of phosphoinositides in cell division (163). Because PIP_3 promotes actin polymerization and pseudopod extension, cells must have a way to regulate the PIP_3 content. Cells that lack PIP_3

modulation have problems to reestablish their cell polarity after cytokinesis, and thus PIP_3 can be called a regulator of cell shape changes in *Dictyostelium* (163).

My results support the assumption that PIP_3 signaling is not essential for chemotaxis (91), but show that cell motility and morphology are more sensitive to changes in PIP_2 (and in consequence PIP_3) concentration, than PH-$_{CRAC}$ translocation, see figure 66. Recently, Arai Y. and co-workers (164), showed that the phosphatidylinositol lipid signaling system can self-organize in both vegetative and developed cells in the absence of chemoattractants. This would partially explain the impaired motility (visualized as short trajectories, see figure 63, section 3.3.5) observed in the chemotaxis experiments, for cells exposed to PBP10, since it is known that phosphoinositides are important regulators of *Dictyostelium* directional sensing (164).

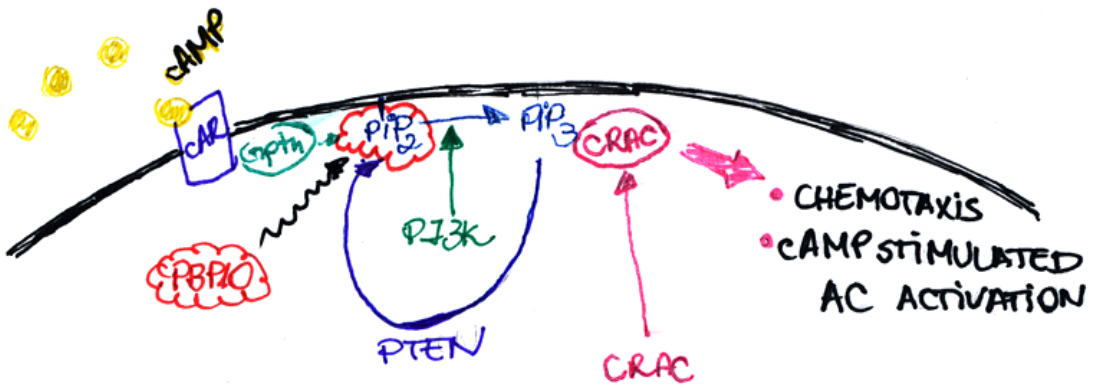

Figure 66 – Mode of action of PBP10. Developed cells usually show an increase in PIP_3 production after cAMP receptor driven activation of PI3K. CRAC, a cytosolic protein containing a PH domain, binds to PIP_3 in the membrane, and can then affect chemotaxis and induce adenylyl cyclase (AC) activation. PBP10 binds to phosphoinositides, preventing it from phosphorilation by PI3K. The results presented in this work show that PBP10 affects cell morphology, motility, and chemotaxis, but that cells are still able to translocate PH-$_{CRAC}$ to the membrane after cAMP stimulation. cAR: cAMP receptor, Gptn: G protein.

4.4 Conclusion and future experiments

In this work, I characterized three main signaling events important for cell motility. The results are summarized in figure 67. First, the importance of WASP was investigated using Wiskostatin. Wiskostatin keeps WASP in its autoinhibited form,

thus impairing Arp2/3 activation. My results showed that Wiskostatin affects cell mechanics, cell morphology, cell adhesion, and cell motility, including chemotaxis. Secondly, I analyzed the effect of cGMP on actin and myosin II dynamics. Cyclic GMP induced the translocation of both actin and myosin II to the cortex. Myosin II is activated by several cGMP binding proteins that phosphorylate the regulatory light chain of this motor. Actin responses due to cGMP release have not been reported in *Dictyostelium* before, but I show that cGMP indeed induces an increased formation of F-actin in the cortex. This response occurs in both vegetative and developed cells. I hypothesize that the actin response could be due to VASP activation (phosphorylation) by cGMP-dependent protein kinases. Third, phophoinositide signaling is responsible for fine tuning of cell polarization and chemotaxis. Here, I show that PBP10 impairs *Dictyostelium discoideum* chemotaxis and affects cell morphology, but does not prevent PH-$_{CRAC}$ translocation to the membrane in response to chemoattractant stimuli. Together, these results provide new insights into actin and myosin II dynamics, as well as cell motility and chemotaxis.

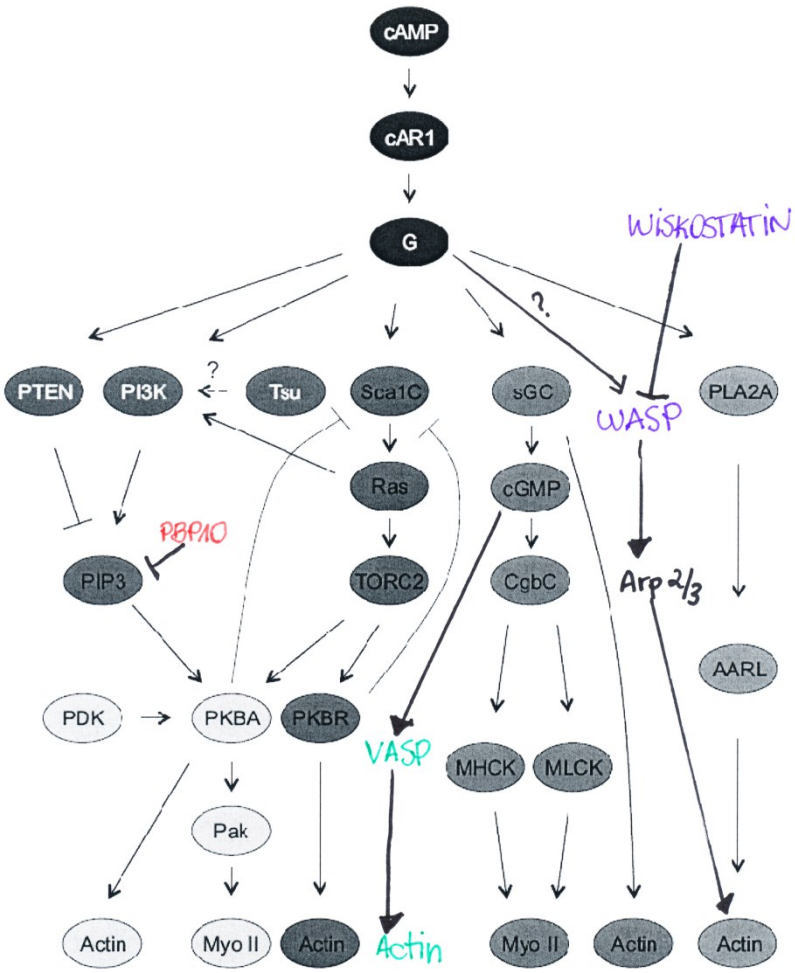

Figure 67 – Chemotactic signaling pathways. The proposed effects of Wiskostatin, cGMP release, and PBP10, investigated in this work, are inserted manually. PTEN: phosphatase and tensin homologue; Tsu: Tsunami; Sca1C: Sca1 complex; AARL: arachidonic acid-related lipid; GbpC: cGMP binding protein C; MHCK: myosin heavy chain kinase; MLCK: myosin light chain kinase; PDK: phosphoinositide dependent kinase. Adapted from reference (141).

Future experiments

For the data using Wiskostatin, future experiments should try to define with accuracy the specificity of the drug in cellular targets. This could be done by using RNAi methods, or by chemical approaches, inhibiting for example the Arp2/3 complex. Another experiment would be to determine if the effects of Wiskostatin in cell motility are due to the suggested ATP depletion (143). Controls on cell-substrate adhesion should be done using other cytoskeleton-disrupting drugs, for example Latrunculin A.

In the case of photoactivation experiments using caged-cGMP, the effect of cGMP on actin polymerization should be confirmed with biochemical assays. The results with Dihydroethidium showing photoactivation by scattered light has to be confirmed using other photoactivatable molecules. VASP mutants and VASP-labeled cells should be used with the same experimental settings as in the experiments with GFP-myosin II+mRFP-LimEΔ cells, in order to determine the target of cGMP.

Concerning the PBP10 experiments, PH-$_{CRAC}$-GFP translocation has to be quantified in a dose-dependent manner. The specificity of the peptide as well as its effects on actin should be determined.

5 References:

1. Baldauf, S. L., A. J. Roger, I. Wenk-Siefert, and W. F. Doolittle. 2000. A kingdom-level phylogeny of eukaryotes based on combined protein data. Science 290:972-977.
2. Manahan, C. L., P. A. Iglesias, Y. Long, and P. N. Devreotes. 2004. Chemoattractant signaling in *Dictyostelium discoideum*. Annu. Rev. Cell. Dev. Biol. 20:223-253.
3. Kessin, R. 2001. Dictyostelium: Evolution, Cell Biology, and the Development of Multicellularity. Cambridge University Press.
4. Chisholm, R. L., and R. A. Firtel. 2004. Insight into morphogenesis from a simple developmental system. Nature Reviews 5:531-541.
5. P.Fey, A. S. Kowald, P. Gaudet, K. E. Pilcher, and R. L. Chisholm. 2007. Protocols for growth and development of *Dictyostelium discoideum*. Nature Protocols 2:1307-1316.
6. Chisholm, R. L., P. Gaudet, E. M. Just, K. E. Pilcher, P. Fey, S. N. Merchant, and W. A. Kibbe. 2006. dictyBase, the model organism database for *Dictyostelium discoideum*. Nucleic Acids Research 34:D423–D427.
7. Saran, S., M. E. Meima, E. Alvarez-Curto, K. E. Weening, D. E. Rozen, and P. Schaap. 2002. cAMP signaling in Dictyostelium- Complexity of cAMP synthesis, degradation and detection. Journal of Muscle Research and Cell Motility 23:793-802.
8. Postma, M., J. Roelofs, J. Goedhart, H. M. Loovers, A. J. W. G. Visser, and P. J. M. V. Haastert. 2004. Sensitization of Dictyostelium chemotaxis by phosphoinositide-3-kinase-mediated self-organizing signalling patches. Journal of Cell Science 117:2925-2035.
9. Affolter, M., and C. J. Weijer. 2005. Signaling to Cytoskeletal Dynamics during Chemotaxis. Developmental Cell 9:19-34.
10. Willard, S. S., and P. N. Devreotes. 2006. Signaling pathways mediating chemotaxis in the social amoeba, *Dictyostelium discoideum*. Eur. J. Cell Biol. 85: 897-904.
11. Devreotes, P., and C. Janetopoulos. 2003. Eukaryotic Chemotaxis: Distinctions between Directional Sensing and Polarization. The Journal of Biological Chemistry 278:20445-20448.
12. Etzrodt, M., H. C. F. Ishikawa, J. Dalous, A. Muller-Taubenberger, T. Bretschneider, and G. Gerisch. 2006. Time-resolved responses to chemoattractant, characteristic of the front and tall of Dictyostelium cells. Febs Letters 580:6707-6713.
13. Swaney, K. F., C.-H. Huang, and P. N. Devreotes. 2010. Eukaryotic chemotaxis: a network of signaling pathways controls motility, directional sensing, and polarity. Annu. Rev. Biophys. 39:265-289.
14. Parent, C. A. 2004. Making all the right moves: chemotaxis in neutrophils and *Dictyostelium*. Current Opinion in Cell Biology 16:4-13.
15. Friedl, P., and K. Wolf. 2003. Tumour-cell invasion and migration: diversity and escape mechanisms. Nature Reviews Cancer 3:362-374.
16. Xiao, Z., N. Zhang, D. B. Murphy, and P. N. Devreotes. 1997. Dynamic distribution of chemoattractant receptors in living cells during chemotaxis and persistent stimulation. The Journal of Cell Biology 139:365-374.
17. Song, L., S. M. Nadkarni, H. U. Bödekera, Carsten Beta, A. Bae, C. Franck, W.-J. Rappel, W. F. Loomis, and E. Bodenschatz. 2006. Dictyostelium discoideum chemotaxis: Threshold for directed motion. Eur. J. Cell Biol. 85:981-989.
18. Janetopoulos, C., T. Jin, and P. Devreotes. 2001. Receptor-mediated activation of heterotrimeric G-proteins in living cells. Science 291:2408-2411.
19. Ueda, M., Y. Sako, T. Tanaka, P. Devreotes, and T. Yanagida. 2001. Single-molecule analysis of chemotactic signaling in *Dictyostelium* cells. Science 294:864-867.
20. Pollard, T. D., and G. G. Borisy. 2003. Cellular motility driven by assembly and disassembly of actin filaments. Cell 112:453-465.

21. Lee, E., K.-M. Pang, and D. Knecht. 2001. The regulation of actin polymerization and cross-linking in *Dictyostelium*. Biochimica et Biophysica Acta 1525:217-227.
22. Carlsson, A. E. 2010. Actin dynamics: from nanoscale to microscale. Annual Review of Biophysics 39:91-110.
23. Carlier, M. F., and D. Pantaloni. 2007. Control of Actin Assembly Dynamics in Cell Motility. The Journal of Biological Chemistry 282:23005-23009.
24. Carlier, M. F., S. Wiesner, C. L. Clainche, and D. Pantaloni. 2003. Actin-based motility as a self-organized system: mechanism and reconstitution in vitro. C. R. Biologies 326:161-170.
25. Holmes, K. C. 2009. STRUCTURAL BIOLOGY Actin in a twist. Nature 457:389-390.
26. Svitkina, T. M., and G. G. Borisy. 1999. Arp2/3 complex and actin depolymerizing factor cofilin in dendritic organization and treadmilling of actin filament array in lamellipodia. J. Cell Biol. 145:1009-1026.
27. Mitchison, T. J., and L. P. Cramer. 1996. Actin-Based Cell Motility and Cell Locomotion. Cell 84:371-379.
28. Bacac, M., and I. Stamenkovic. 2008. Metastatic cancer cell. Annu. Rev. Pathol. Mech. Dis. 3:221-247.
29. Gerisch, G., T. Bretschneider, A. Müller-Taubenberger, E. Simmeth, M. Ecke, S. Diez, and K. Anderson. 2004. Mobile actin clusters and traveling waves in cells recovering from actin depolymerization. Biophysical Journal 87:3493-3503.
30. Eichinger, L., J. A. Pachebat, G. Glockner, M. A. Rajandream, R. Sucgang, M. Berriman, J. Song, R. Olsen, K. Szafranski, Q. Xu, B. Tunggal, S. Kummerfeld, M. Madera, B. A. Konfortov, F. Rivero, A. T. Bankier, R. Lehmann, N. Hamlin, R. Davies, P. Gaudet, P. Fey, K. Pilcher, G. Chen, D. Saunders, E. Sodergren, P. Davis, A. Kerhornou, X. Nie, N. Hall, C. Anjard, L. Hemphill, N. Bason, P. Farbrother, B. Desany, E. Just, T. Morio, R. Rost, C. Churcher, J. Cooper, S. Haydock, N. van Driessche, A. Cronin, I. Goodhead, D. Muzny, T. Mourier, A. Pain, M. Lu, D. Harper, R. Lindsay, H. Hauser, K. James, M. Quiles, M. M. Babu, T. Saito, C. Buchrieser, A. Wardroper, M. Felder, M. Thangavelu, D. Johnson, A. Knights, H. Loulseged, K. Mungall, K. Oliver, C. Price, M. A. Quail, H. Urushihara, J. Hernandez, E. Rabbinowitsch, D. Steffen, M. Sanders, J. Ma, Y. Kohara, S. Sharp, M. Simmonds, S. Spiegler, A. Tivey, S. Sugano, B. White, D. Walker, J. Woodward, T. Winckler, Y. Tanaka, G. Shaulsky, M. Schleicher, G. Weinstock, A. Rosenthal, E. C. Cox, R. L. Chisholm, R. Gibbs, W. F. Loomis, M. Platzer, R. R. Kay, J. Williams, P. H. Dear, A. A. Noegel, B. Barrell, and A. Kuspa. 2005. The genome of the social amoeba Dictyostelium discoideum. Nature 435:43-57.
31. Prassler, J., A. Murr, S. Stocker, J. Faix, J. Murphyand, and G. Marriott. 1998. DdLIM Is a Cytoskeleton-associated Protein Involved in the Protrusion of Lamellipodia in *Dictyostelium*. . Molecular Biology of the Cell 9:545-559.
32. Schneider, N., I. Weber, J. Faix, J. Prassler, A. Muller-Taubenberger, J. Kohler, E. Burghardt, G. Gerisch, and G. Marriott. 2003. A LIM protein involved in the progression of cytokinesis and regulation of the mitotic spindle. Cell Motil. Cytoskeleton 56:130-139.
33. Bretschneider, T., S. Diez, K. Anderson, J. Heuser, M. Clarke, A. Muller-Taubenberger, J. Kohler, and G. Gerisch. 2004. Dynamic actin patterns and Arp2/3 assembly at the substrate-attached surface of motile cells. Current Biology 14:1-10.
34. Bosgraaf, L., A. Waijer, R. Engel, A. J. W. G. Visser, D. Wessels, D. Soll, and P. J. M. V. Haastert. 2005. RasGEF-containing proteins GbpC and GbpD have differential effects on cell polarity and chemotaxis in *Dictyostelium*. Journal of Cell Science 118:1899-1910.
35. Pantaloni, D., R. Boujemaa, D. Didry, P. Gounoun, and M. F. Carlier. 2000. The Arp2/3 complex branches filament barbed ends: functional antagonism with capping proteins. Nature Cell Biology 2:385-391.
36. Robinson, R. C., K. Turbedsky, D. A. Kaiser, J. B. Marchand, H. N. Higgs, S. Choe, and T. D. Pollard. 2001. Crystal structure of Arp2/3 complex. Science 294:1679-1684.

37. Kelleher, J. F., S. J. Atkinson, and T. D. Pollard. 1995. Sequences, Structural Models, and Cellular-Localization of the Actin-Related Proteins Arp2 and Arp3 from Acanthamoeba. J. Cell Biol. 131:385-397.
38. Goley, E. D., and M. D. Welch. 2006. The Arp2/3 complex: an actin nucleator comes of age. Nature Reviews Molecular Cell Biology 7:713-726.
39. Clainche, C. L., D. Didry, M. F. Carlier, and D. Pantaloni. 2001. Activation of Arp2/3 complex by Wiskott-Aldrich syndrome protein is linked to enhanced binding of ATP to Arp2. Journal of Biological Chemistry 276:46689-46692.
40. Li, R., and G. G. Gundersen. 2008. Beyond polymer polarity: how the cytoskeleton builds a polarized cell. Nature Reviews Molecular Cell Biology 9:860-873.
41. Goley, E. D., and M. D. Welch. 2006. The ARP2/3 complex: an actin nucleator comes of age. Nature Reviews Molecular Cell Biology 7:713-726.
42. Takenawa, T., and S. Suetsugu. 2007. The WASP-WAVE protein network: connecting the membrane to the cytoskeleton. Nature Reviews Molecular Cell Biology 8:37-48.
43. Veltman, D. M., and R. H. Insall. 2010. WASP family proteins – Their evolution and ist physiological implications. Molecular Biology of the Cell 21:2880-2893.
44. Campellone, K. G., and M. D. Welch. 2010. A nucleator arms race: cellular control of actin assembly. Nature Reviews Molecular Cell Biology 11:237-251.
45. Thrasher, A. J., and S. O. Burns. 2010. WASP: a key immunological multitasker. Nature Reviews Immunology 10:182-192.
46. Pollitt, A. Y., and R. H. Insall. 2009. WASP and SCAR/WAVE proteins: the drivers of actin assembly. Journal of Cell Science 122:2575-2578.
47. Bear, J. E., J. F. Rawls, C. L. Saxe III, and 1998. SCAR, a WASP-related protein, isolated as a suppressor of receptor defects in late *Dictyostelium* development. The Journal of Cell Biology 142:1325-1335.
48. Ibarra, N., A. Pollitt, and R. H. Insall. 2005. Regulation of actin assembly by SCAR/WAVE proteins. Biochemical Society Transactions 33:1243-1246.
49. Sweeney, H. L., and A. Houdusse. 2010. Structural and Functional Insights into the Myosin Motor Mechanism. Annu. Rev. Biophys. 39:539–557.
50. Vicente-Manzanares, M., X. Ma, R. S. Adelstein, and A. R. Horwitz. 2009. Non-muscle myosin II takes centre stage in cell adhesion and migration. Nat. Rev. Mol. Cell Biology 10:778-790.
51. Gomes, E. R., S. Jani, and G. G. Gundersen. 2005. Nuclear movement regulated by Cdc42, MRCK, myosin, and actin flow establishes MTOC polarization in migrating cells. Cell 121:451-463.
52. Clark, K., M. Langeslag, C. G. Figdor, and F. N. V. Leeuwen. 2007. Myosin II and mechanotransduction: a balancing act. Trends in Cell Biology 17:178-186.
53. Even-Ram, S., A. D. Doyle, M. A. Conti, K. Matsumoto, R. S. Adelstein, and K. M. Yamada. 2007. Myosin IIA regulates cell motility and actomyosin– microtubule crosstalk. Nature Cell Biology 9:299-309.
54. De La Roche, M. A., and G. P. Côte. 2001. Regulation of Dictyostelium Myosin I and II. Biochimica et Biophysica Acta 1525:245-261.
55. De La Roche, M. A., J. L. Smith, V. Betapudi, T. T. Egelhoff, and G. P. Côte. 2002. Signaling pathways regulating *Dictyostelium* myosin II. Journal of Muscle Research and Cell Motility 23:703–718.
56. Egelhoff, T. T., D. Croft, and P. A. Steimle. 2005. Actin Activation of Myosin Heavy Chain Kinase A in Dictyostelium. The Journal of Biological Chemistry 280:2879–2887.
57. Bosgraaf, L., and P. J. M. V. Haastert. 2006. The regulation of myosin II in Dictyostelium. Eur. J. Cell Biol. 85:969–979.
58. Kuwayama, H., S. Ishida, and P. J. M. Vanhaastert. 1993. Non-chemotactic Dictyostelium discoideum mutants with altered cGMP signal-transduction. J. Cell Biol. 123:1453-1462.

59. Ross, F. M., and P. C. Newell. 1981. Streamers - Chemotactic mutants of Dictyostelium discoideum with altered cyclic GMP metabolism. Journal of General Microbiology 127:339-350.
60. Kots, A. Y., E. Martin, I. G. Sharina, and F. Murad. 2009. cGMP: Generators, Effectors and Therapeutic Implications. Handbook of Experimental Pharmacology 191:1-14.
61. Liu, G., H. Kuwayama, S. Ishida, and P. C. Newell. 1993. The Role of Cyclic-Gmp in Regulating Myosin During Chemotaxis of Dityostelium - Evidence from a Mutant Lacking the Normal Cyclic-Gmp Response to Cyclic-Amp. Journal of Cell Science 106:591-596.
62. Nelson, D. L., and M. M. Cox. 2008. Lehninger Principles of Biochemistry. Freeman and Company.
63. Haastert, P. J. M. V., and H. Kuwayama. 1997. cGMP as second messenger during *Dictyostelium* chemotaxis. FEBS Letters 410:25-28.
64. Putnam, J. B., and L. G. Pedersen. 1975. Discovery of a 3',5'-guanosine monophosphate simulating factor in amoebae of *Dictyostelium discoideum*. Biochimica et Biophysical Acta 411:168-170.
65. Mato, J. M., P. J. M. V. Haastert, F. A. Krens, E. H. Rhijnsburger, F. C. P. M. Dobbe, and T. M. Konijn. 1977. Cyclic AMP and folic acid mediated cGMP accumulation in *Dictyostelium discoideum*. FEBS Letters 79:331-336.
66. Mato, J. M., F. A. Krens, P. J. M. V. Haastert, and T. M. Konijn. 1977. 3':5'-Cyclic AMP-dependent 3':5'-cyclic GMP accumulation in *Dictyostelium discoideum*. PNAS 74:2348-2351.
67. Mato, J. M., and D. Malchow. 1978. Guanylate cyclase activation in response to chemotactic stimulation in *Dictyostelium discoideum*. FEBS Letters 90:119-122.
68. Mato, J. M., H. Woelders, P. J. M. V. Haastert, and T. M. Konijn. 1978. Cyclic GMP binding activity in *Dictyostelium discoideum*. FEBS Letters 90:261-264.
69. Liu, G., and P. C. Newell. 1994. Regulation of Myosin Regulatory Light-Chain Phosphorylation Via Cyclic-Gmp During Chemotaxis of Dictyostelium. Journal of Cell Science 107:1737-1743.
70. Liu, G., and P. C. Newell. 1988. Evidence That Cyclic-Gmp Regulates Myosin Interaction with the Cytoskeleton During Chemotaxis of Dictyostelium. Journal of Cell Science 90:123-129.
71. Liu, G., and P. C. Newell. 1991. Evidence That Cyclic-Gmp May Regulate the Association of Myosin-Ii Heavy-Chain with the Cytoskeleton by Inhibiting Its Phosphorylation. Journal of Cell Science 98:483-490.
72. Goldberg, J. M., L. Bosgraaf, P. J. M. V. Haastert, and J. L. Smith. 2002. Identification of four candidate cGMP targets in *Dictyostelium*. PNAS 99:6749-6754.
73. Bosgraaf, L., H. Ruscher, J. L. Smith, D. Wessels, D. R. Soll, and P. J. M. V. Haastert. 2002. A novel cGMP signalling pathway mediating myosin phosphorylation and chemotaxis in *Dictyostelium*. The EMBO Journal 21:4560-4570.
74. Bosgraaf, L., and P. J. M. V. Haastert. 2002. A model for cGMP signal transduction in *Dictyostelium* in perspective of 25 years of cGMP research. Journal of Muscle Research and Cell Motility 23:781-791.
75. Veltman, D. M., and P. J. M. V. Haastert. 2006. Guanylyl Cyclase Protein and cGMP Product Independently Control Front and Back of Chemotaxing Dictyostelium Cells. Molecular Biology of the Cell 17:3921-3929.
76. Schoen, C. D., C. C. G. M. Schulkes, J. C. Arents, and R. V. Driel. 1996. Guanylate Cyclase Activity in Permeabilized *Dictyostelium discoideum* Cells. Journal of Cellular Biochemistry 60:411-423.
77. Kuwayama, H., H. Snippe, M. Derks, J. Roelofs, and P. J. M. van Haastert. 2001. Identification and characterization of DdPDE3, a cGMP-selective phosphodiesterase from Dictyostelium. Biochem. J. 353:635-644.
78. Bader, S., A. Kortholt, and P. J. M. V. Haastert. 2007. Seven *Dictyostelium discoideum* phosphodiesterases degrade three pools of cAMP and cGMP. Biochem. J. 402:153-161.

79. Mato, J. M., H. Woelders, and T. M. Konijn. 1979. Intracellular Cyclic GMP-Binding Proteins in Cellular Slime Molds. Journal of Bacteriology 137:169-172.
80. Charest, P. G., and R. A. Firtel. 2007. Big roles for small GTPases in the control of directed cell movement. Biochem. J. 401:377-390.
81. Kuwayama, H., M. Ecke, G. Gerisch, and P. J. M. V. Haastert. 1996. Protection against osmotic stress by cGMP-mediated myosin phosphorylation. Science 271:207-209.
82. Kuwayama, H., and P. J. M. Van Haastert. 1998. Chemotactic and osmotic signals share a cGMP transduction pathway in Dictyostelium discoideum. Febs Letters 424:248-252.
83. Aizawa, H., M. Katadae, M. Maruya, M. Sameshima, K. Murakami-Murofushi, and I. Yahara. 1999. Hyperosmotic stress-induced reorganization of actin bundles in *Dictyostelium* cells over-expressing cofilin. Genes to cells 4:311-324.
84. Kuwayama, H., and P. J. M. V. Haastert. 1996. Regulation of Guanylyl Cyclase by a cGMP-binding Protein during Chemotaxis in *Dictyostelium discoideum*. The Journal of Biological Chemistry 271:23718-23724.
85. Lusche, D. F., and D. Malchow. 2005. Developmental control of cAMP-induced Ca^{2+}-influx by cGMP: influx is delayed and reduced in a cGMP-phosphodiesterase D deficient mutant of *Dictyostelium discoideum*. Cell Calcium 37:57-67.
86. Lusche, D. F., H. Kaneko, and D. Malchow. 2005. cGMP-phosphodiesterase antagonists inhibit Ca^{2+}-influx in *Dictyostelium discoideum* and bovine cyclic-nucleotide-gated-channel. European Journal of Pharmacology 513:9-20.
87. Bosgraaf, L., and P. J. M. V. Haastert. 2009. Navigation of Chemotactic Cells by Parallel Signaling to Pseudopod Persistence and Orientation. Plos One 4:1-11.
88. Marks, F., U. Klingmüller, and K. M. Decker. 2009. Cellular signal processing
89. Yin, H. L., and P. A. Janmey. 2003. Phosphoinositide regulation of the actin cytoskeleton. Annu. Rev. Physiol. 65:761-789.
90. Parent, C. A., and P. N. Devreotes. 1999. A cell's sense of direction. Science 284:765-770.
91. Hoeller, O., and R. R. Kay. 2007. Chemotaxis in the absence of PIP3 gradients. Current Biology 17:813-817.
92. Weiner, O. D. 2002. Regulation of cell polarity during eukaryotic chemotaxis: the chemotactic compass. Current Opinion in Cell Biology 14:196-202.
93. Cain, R. J., and A. J. Ridley. 2009. Phosphoinositide 3-kinases in cell migration. Biology of the cell 101:13-29.
94. Zhang, P., Y. Wang, H. Sesaki, and M. Iijima. 2010. Proteomic identification of phosphatidylinositol (3,4,5) triphosphate-binding proteins in *Dictyostelium discoideum*. PNAS 107:11829-11834.
95. Janmey, P. A., and C. Chaponnier. 1995. Medical aspects of the actin cytoskeleton. Current Opinion in Cell Biology 7:111-117.
96. Parent, C. A., B. J. Blacklock, W. M. Froehlich, D. B. Murphy, and P. N. Devreotes. 1998. G protein signaling events are activated at the leading edge of chemotactic cells. Cell 95:81-91.
97. Kölsch, V., P. G. Charest, and R. A. Firtel. 2007. The regulation of cell motility and chemotaxis by phospholipid signaling. Journal of Cell Science 121:551-559.
98. Kortholt, A., P. Bolourani, H. Rehmann, I. Keizer-Gunnink, G. Weeks, A. Wittinghofer, and P. J. M. Van Haastert. 2010. A Rap/Phosphatidylinositol 3-Kinase Pathway Controls Pseudopod Formation Molecular Biology of the Cell 21:936-945.
99. Janmey, P. A., and U. Lindberg. 2004. Cytoskeletal regulation: Rich in lipids. Nat Rev Mol Cell Biol. 5:658-666.
100. Allingham, J. S., V. A. Klenchin, and I. Rayment*. 2006. Actin-targeting natural products: structures, properties and mechanisms of action. Cellular and Molecular Life Sciences 63:2119-2134.

101. Spector, I., F. Braet, N. R. Shochet, and M. R. Bubb. 1999. New anti-actin drugs in the study of the organization and function of the actin cytoskeleton. Microsc. Res. Tech. 47:18-37.
102. Morton, W. M., K. R. Ayscough, and P. J. McLaughlin. 2000. Latrunculin alters the actin-monomer subunit interface to prevent polymerization. Nature Cell Biology 2:376-378.
103. Yarmola, E. G., T. Somasundaram, T. A. Boring, I. Spector, and M. R. Bubb. 2000. Actin-latrunculin A structure and function - Differential modulation of actin-binding protein function by latrunculin A. Journal of Biological Chemistry 275:28120-28127.
104. Peterson, J. R., and T. J. Mitchison. 2002. Small molecules, big impact: a history of chemical inhibitors and the cytoskeleton. Chemistry & Biology 9:1275-1285.
105. Leung, D. W., D. M. Morgan, and M. K. Rosen. 2006. Biochemical properties and inhibitors of N-WASP. Methods in Enzymology 406:281-296.
106. Peterson, J. R., L. C. Bickford, D. Morgan, A. S. Kim, O. Ouerfelli, M. W. Kirschner, and M. K. Rosen. 2004. Chemical inhibition of N-WASP by stabilization of a native autoinhibited conformation. Nat. Struct. Mol. Biol. 11:747–755.
107. Janmey, P. A., J. Lamb, P. G. Allen, and P. T. Matsudaira. 1992. Phosphoinositide binding Peptides Derived from the Sequences of Gelsolin and Villin. The Journal of Biological Chemistry 267:11818-11823.
108. Cunningham, C. C., R. Vegners, R. R. Bucki, M. Funaki, N. Korde, J. H. Hartwig, T. P. Stossel, and P. A. Janmey. 2001. Cell Permeant Polyphosphoinositide-binding Peptides That Block Cell Motility and Actin Assembly. The Journal of Biological Chemistry 276:43390–43399.
109. Guck, J., F. Lautenschläger, S. Paschkeb, and M. Beil. 2010. Critical review: cellular mechanobiology and amoeboid migration. Integrative Biology 2:575-583.
110. Gardel, M. L., J. H. Shin, F. C. MacKintosh, L. Mahadevan, P. Matsudaira, and D. A. Weitz. 2004. Elastic Behavior of Cross-Linked and Bundled Actin Networks. Science 304:1301-1305.
111. Weibel, D. B., and G. M. Whitesides. 2006. Applications of microfluidics in chemical biology. Current Opinion in Chemical Biology 10:584–591.
112. Sia, S. K., and G. M. Whitesides. 2003. Microfluidic devices fabricated in poly(dimethylsiloxane) for biological studies. Electrophoresis 24:3563–3576.
113. Whitesides, G. M. 2006. The origins and the future of microfluidics. Nature 442:368-373.
114. Walker, J. W., G. P. Reid, J. A. McCray, and D. R. Trentham. 1987. Photolabile 1-(2-nitrophenyl)ethyl phosphate esters of adenine nucleotide analogues. Synthesis and mechanism of photolysis. Physiol. Rev. 67:583-617.
115. Hagen, V., J. Bendig, S. Frings, B. Wiesner, B. Schade, S. Helm, D. Lorenz, and U. B. Koupp. 1999. Synthesis, photochemistry and application of (7-methoxycoumarin-4-yl)methyl-caged 8-bromoadenosine cyclic 39,59-monophosphate and 8-bromoguanosine cyclic 39,59-monophosphate photolyzed in the nanosecond time region. J. Photochem. Photobiol. B: Biol. 53:91-102.
116. Hagen, V., J. Bendig, S. Frings, T. Eckardt, S. Helm, D. Reuter, and U. B. Kaupp. 2001. Highly efficient and ultrafast phototriggers for cAMP and cGMP by using long-wavelength UV/vis-activation. Angew. Chem.-Int. Edit. 40:1046-1048.
117. Ishihara, A., K. Gee, S. Schwartz, K. Jacobson, and J. Lee. 1997. Photoactivation of caged compounds in single living cells: an application to the study of cell locomotion. Biotechniques 23:268-274.
118. Hagen, V., S. Frings, B. Wiesner, S. Helm, U. B. Kaupp, and J. Bendig. 2003. [7-(dialkylamino)coumarin-4-yl]methyl-caged compounds as ultrafast and effective long-wavelength phototriggers of 8-bromo-substituted cyclic nucleotides. Chembiochem 4:434-442.
119. Wegner, C. 2010. Untersuchung einer mikrofluidischen Methode zur Charakterisierung der mechanischen Eigenschaften von Zellen. In Mathematisch-Naturwissenschaftliche Fakultät, Institut für Physik und Astronomie. Universität Potsdam, Potsdam.

120. Braunmüller, S., L. Schmid, and T. Franke. 2011. Dynamics of red blood cells and vesicles in microchannels of oscillating width. J. Phys.: Condens. Matter 23:184116 184111-184118.
121. Schnitzler, W. 2004. Abbildung von Biomolekülen im kontinuierlichen Fluss. Universität Ulm.
122. Noguchi, H., G. Gompper, L. Schmid, A. Wixforth, and T. Franke. 2010. Dynamics of fluid vesicles in flow through structured microchannels. EPL 89:28002 p28001-p28006.
123. Beta, C. 2009. Spatiotemporal stimulation of single cells using flow photolysis. In Chemotaxis: Methods and Protocols. T. Jian, and D. Hereld, editors. Humana Press. 321-331.
124. Ridler, T. W., and S. Calvard. 1978. Thresholding using an iterative selection method IEEE Trans. System, Man and Cybernetics SMC-8:630–632.
125. Theves, M. 2009. Quantitative Study of Eukaryotic Chemotaxis with Microfluidic Devices. In Max-Planck Institut für Dynamik und Selbstorganisation. Georg-August Universität Göttingen Göttingen
126. Crocker, J. C., and D. G. Grier. 1996. Methods of digital video microscopy for colloidal Studies. Journal of Colloid and Interface Science 179:298–310.
127. Olympus. Olympus Microscopy Resource Center. http://www.olympusmicro.com/primer/techniques/fluorescence/tirf/olympusaptirf.html.
128. Osserman, R. 1978. The isoperimetric inequality. Bulletin of the American Mathematical Society 84:1182-1238.
129. Bradford, M. M. 1976. Rapid and sensitive method for quantitation of microgram quantities of protein utilizing principle of protein-dye binding. Analytical Biochemistry 72:248-254.
130. Roth, U., S. Müller, and F.-G. Hanisch. 2006. Proteomic Analysis of *Dictyostelium discoideum*
131. Dormann, D., G. Weijer, C. A. Parent, P. N. Devreotes, and C. J. Weijer. 2002. Visualizing PI3 kinase-mediated cell-cell signaling during Dictyostelium development. Current Biology 12:1178-1188.
132. Eichinger, L., and F. Rivero. 2006. *Dictyostelium discoideum* protocols.
133. Diez, S., G. Gerisch, K. Anderson, A. Muller-Taubenberger, and T. Bretschneider. 2005. Subsecond reorganization of the actin network in cell motility and chemotaxis. Proceedings of the National Academy of Sciences of the United States of America 102:7601-7606.
134. Kepp, O., L. Galluzi, M. Lipinski, J. Yuan, and G. Kroemer. 2011. Cell death assays for drug discovery. Nature Reviews Drug Discovery 10:221-237.
135. Brasen, J. C., S. Dewitt, and M. B. Hallett. 2010. A Reporter of UV Intensity Delivered to the Cytosol during Photolytic Uncaging. Biophysical Journal 98:L25-L27.
136. Swaney, K. F., C.-H. Huang, and P. N. Devreotes. 2010. Eukaryotic Chemotaxis: A Network of Signaling Pathways Controls Motility, Directional Sensing, and Polarity. In Annual Review of Biophysics, Vol 39. 265-289.
137. Comer, F. I., and C. A. Parent. 2002. PI 3-kinases and PTEN: How opposites chemoattract. Cell 109:541-544.
138. Haastert, P. J. M. V., and P. N.Devreotes. 2004. Chemotaxis: Signalling The Way Forward. NATURE REVIEWS MOLECULAR CELL BIOLOGY 5:626-634.
139. Condeelis, J., R. H. Singer, and J. E. Segall. 2005. The great escape: When cancer cells hijack the genes for chemotaxis and motility. Annual Review of Cell and Developmental Biology 21:695-718.
140. Kay, R. R., P. Langridge, D. Traynor, and O. Hoeller. 2008. Changing directions in the study of chemotaxis. NATURE REVIEWS MOLECULAR CELL BIOLOGY 9:455-463.
141. Wang, Y., C. L. Chen, and M. Iijima. 2011. Signaling mechanisms for chemotaxis. Development Growth & Differentiation 53:495-502.
142. Myers, S. A., J. W. Han, Y. Lee, R. A. Firtel, and C. Y. Chung. 2005. A *Dictyostelium* homologue of WASP is required for polarized F-actin assembly during chemotaxis. Molecular biology of the cell 16:2191-2206.

143. Bompard, G., G. Rabeharivelo, and N. Morin. 2008. Inhibition of cytokinesis by wiskostatin does not rely on N-WASP/Arp2/3 complex pathway. Bmc Cell Biology 9.
144. Guerriero, C. J., and O. A. Weisz. 2007. N-WASP inhibitor wiskostatin nonselectively perturbs membrane transport by decreasing cellular ATP levels. American Journal of Physiology-Cell Physiology 292:C1562-C1566.
145. Harwood, A., and J. C. Coates. 2004. A prehistory of cell adhesion. Current Opinion in Cell Biology 16:470–476.
146. M Buenemann, H. L., W-J Rappel and LM Sander. 2010. The Role of Cell Contraction and Adhesion in *Dictyostelium* Motility. Biophysical Journal 99:50-58.
147. Schindl, M., E. Wallraff, B. Deubzer, W. Witke, G. Gerisch, and E.Sackmann. 1995. Cell-Substrate Interactions and Locomotion of Dictyostelium Wild-Type and Mutants Defective in Three Cytoskeletal Proteins: A Study Using Quantitative Reflection Interference Contrast Microscopy. Biophysical Journal 68:1177-1190.
148. Myers, S. A., L. R. Leeper, and C. Y. Chung. 2006. WASP-interacting protein is important for actin filament elongation and prompt pseudopod formation in response to a dynamic chemoattractant gradient. Molecular biology of the cell 17:4564-4575.
149. Jang, W., and R. H. Gomer. Initial Cell Type Choice in Dictyostelium. Eukaryotic Cell 10:150-155.
150. Guo, D., J. J. Zhang, and X.-Y. Huang. 2010. A new Rac/PAK/GC/cGMP signaling pathway. Molecular and Cellular Biochemistry 334:99-103.
151. Dumontier, M., P. Hocht, U. Mintert, and J. Faix. 2000. Rac1 GTPases control filopodia formation, cell motility, endocytosis, cytokinesis and development in Dictyostelium. Journal of Cell Science 113:2253-2265.
152. Han, Y. H., C. Y. Chung, D. Wessels, S. Stephens, M. A. Titus, D. R. Soll, and R. A. Firtel. 2002. Requirement of a vasodilator-stimulated phosphoprotein family member for cell adhesion, the formation of filopodia, and chemotaxis in *Dictyostelium*. Journal of Biological Chemistry 277:49877-49887.
153. Kwiatkowski, A. V., F. B. Gertler, and J. J. Loureiro. 2003. Function and regulation of Ena/VASP proteins. Trends in Cell Biology 13:386-392.
154. Krause, M., E. W. Dent, J. E. Bear, J. J. Loureiro, and F. B. Gertler. 2003. ENA/VASP proteins: Regulators of the actin cytoskeleton and cell migration. Annual Review of Cell and Developmental Biology 19:541-564.
155. Lin, W. H., S. E. Nelson, R. J. Hollingsworth, and C. Y. Chung. 2010. Functional Roles of VASP Phosphorylation in the Regulation of Chemotaxis and Osmotic Stress Response. Cytoskeleton 67:259-271.
156. Wanner, R., and B. Wurster. 1990. Cyclic GMP-activated protein kinase from *Dictyostelium discoideum*. Biochimica et Biophysica Acta 1053:179-184.
157. Degunzburg, J., D. Part, N. Guiso, and M. Veron. 1984. An unusual adenosine 3',5'-phosphate dependent protein kinase from Dictyostelium discoideum. Biochemistry 23:3805-3812.
158. De Wit, R. J. W., J. C. Arents, and R. Van Driel. 1982. Ligand binding properties of the cytosplamic cAMP-binding protein of *Dictyostelium discoideum*. FEBS Letters 145:150-154.
159. Vanmentscohen, M., and P. J. M. Vanhaastert. 1989. The cyclic nucleotide specificity of 8 cAMP-binding proteins in Dictyostelium discoideum is correlated into 3 groups. Journal of Biological Chemistry 264:8717-8722.
160. Zhang, H., P. J. Heid, D. Wessels, K. J. Daniels, T. Pham, W. F. Loomis, and D. R. Soll. 2003. Constitutively active protein kinase A disrupts motility and chemotaxis in Dictyostelium discoideum. Eukaryotic Cell 2:62-75.
161. Loomis, W. F. 1998. Role of PKA in the timing of developmental events in Dictyostelium cells. Microbiology and Molecular Biology Reviews 62:684-+.

162. Beaulieu, V., N. Da Silva, N. Pastor-Soler, C. R. Brown, P. J. S. Smith, D. Brown, and S. Breton. 2005. Modulation of the actin cytoskeleton via gelsolin regulates vacuolar H+-ATPase recycling. Journal of Biological Chemistry 280:8452-8463.
163. Janetopoulos, C., and P. Devreotes. 2006. Phosphoinositide signaling plays a key role in cytokinesis. J. Cell Biol. 174:485-490.
164. Arai, Y., T. Shibata, S. Matsuoka, M. J. Sato, T. Yanagida, and M. Ueda. 2010. Self-organization of the phosphatidylinositol lipids signaling system for random cell migration. Proceedings of the National Academy of Sciences of the United States of America 107:12399-12404.

6 Acknowledgements

I would like to thank first Prof. Dr. Carsten Beta for the good advices and support while doing this work, and for all the freedom while choosing and accomplishing the project.

Many thanks to Katharina Schneider and the Laboratory for Fluid Dynamics, Pattern Formation and Nanobiocomplexity (Prof. Dr. Eberhard Bodenschatz) for showing me everything I needed to start working with Dictys.

I thank Prof. Dr. Ralph Gräf and his group, for the constant help and support. I also thank Prof. Dr. Bernd Walz and apl. Prof. Dr. Otto Baumann for providing the access to their microscopy facilities, and helping me with the imaging. I would also like to thank Dr. Christian Fiedler and Prof. Dr. Robert Seckler, for helping with the F-actin assay.

Special thanks to Douwe Veltman from Robert Insall's group, for the discussion and the WASP and SCAR plamids, and Hellen Ishikawa-Ankerhold for the hints and discussions concerning my data. I thank Dr. Günther Gerisch for discussions, suggestions on the cGMP data and the cAMP-dependent protein kinases, and for providing many *Dictyostelium* cell lines to my research.

I thank all the people from the Biological Physics Group for the nice working atmosphere, especially Matthias Theves, Christian Wegner, Alexander Anielski, Achim Quaas, Matthias Gerhardt and Kirsten Krüger for helping in many experimental and data analysis steps.

I would like to give my gratitude to all my friends in Germany, Europe and Brazil, new and old ones. Thanks also to all my friends from theatre and acting classes, for giving me the equilibrium I needed for the PhD. I could not forget to cite Prof. Beirão, Anita, Éder, Diogo Galan, Flaviana, Rafaela, Iva, Diogo Sampaio, Graci Almeida, Natália Fadel, Lylla, Maria Luiza, and Ivana for always being there for me. I thank Matti for making the hard days in Germany special and very funny.

Finally, I would like to thank the unconditional support from my family, especially from my father, for just being the best father in the world, and my sister Claudia ('Siiiis'), for the long skype chats across the ocean and for being my best

friend. This work, from the beginning until the end, I dedicate to my mother, and in memory of her. I know she would be delighted to see the result of what she encouraged me to do from the beginning on. *Essa é pra você Ida!*